

PRELIMINARY EVALUATION OF A NONDESTRUCTIVE ULTRASONIC
TECHNIQUE FOR ASSESSING STABILITY OF EXTERNAL SKELETAL
FIXATION PINS

A Thesis

by

JAMES ROBERT DICKENS

Submitted to the Office of Graduate Studies of
Texas A&M University
in partial fulfillment of the requirements
for the degree of

MASTER OF SCIENCE

August 1992

Major Subject: Mechanical Engineering

TEXAS A&M UNIVERSITY LIBRARY

PRELIMINARY EVALUATION OF A NONDESTRUCTIVE ULTRASONIC
TECHNIQUE FOR ASSESSING STABILITY OF EXTERNAL SKELETAL
FIXATION PINS

A Thesis

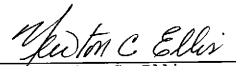
by

JAMES ROBERT DICKENS

Approved as to style and content by:


Don E. Bray
(Chair of Committee)


Malur N. Srinivasan
(Member)


Newton C. Ellis
(Member)


Ross H. Palmer
(Member)


for Walter L. Bradley
(Head of Department)

August 1992

ABSTRACT

Preliminary Evaluation of a Nondestructive Ultrasonic
Technique for Assessing Stability of External Skeletal
Fixation Pins. (August 1992)

James Robert Dickens, A.A., North Harris County College;
B.S., Texas A&M University

Chairman of Advisory Committee: Dr. Don E. Bray

The purpose of this study was to determine the existence and strength of a functional relationship between ultrasonic attenuation measurements and axial pin extraction forces.

Femora were collected from five adult canine cadavers weighing 15 to 25 kg each. Two or four nonthreaded fixation pins were implanted into each of seven femoral diaphyses ($n = 22$). Four implantation methods and four implantation sites were used to create a range of bone-pin interface bonding conditions. Each pin was independently tested using two ultrasonic probes (2.48 and 3.87 MHz). Signal response waveforms were digitized and stored in a computer for later analysis. Immediately following ultrasonic testing, axial extraction forces were measured with a universal testing machine.

After detailed analysis of the digitized waveforms, ultrasonic and extraction data were graphically represented. Scatter plots, linear regression analyses, and means testing

were relied upon for identifying the relationships between variables.

A strong relationship was observed between extraction forces of fixation pins implanted in cadaveric femur and an acoustic attenuation parameter obtained with a simple ultrasonic pulsed-wave excitation technique. Statistical analysis verified this relationship while showing weak or near-zero relationships for most other experimental factors.

A prediction model was selected using the minimum mean squared error (MSE) method. Minimum MSE was achieved with an R^2 of 0.8270 using four inputs (Pin Number, Implantation Site, and Pulse Energy Time Shift data from Probe 1 and Probe 2). Scatter plots of residual force variables showed reasonably random data patterns using this model. Ninety-five percent confidence intervals were calculated and showed that extraction forces were predictable to within about 180 N (40 lb) based on the above model.

With further development, it is believed that the technique presented in this paper could become a clinically viable method for detecting the onset of pin loosening.

DEDICATION

This work is dedicated to my parents.

ACKNOWLEDGEMENTS

I would like to extend my thanks to all those who contributed to the completion of this work, directly or indirectly. In particular:

Dr. John Calvin, for lending a critical statistical eye and helping with the data analysis.

Dr. Clarence Hough, for introducing me to experimental design and analysis, and for helping me see a much better way to do it.

Tom Wilson, Mike Walker, and the staff of the machine shop. Whenever I needed a widget they had the know-how to make it.

Toby Selcer, Carl Frederickson, and Jeff in the structures lab, for guidance in operation of the Instron machine. They were all very helpful in answering questions and providing instructions.

Scott Cronauer in the metallurgy lab, for his many insights into the complexities and subtleties of metallography.

The Texas Veterinary Medical Center, for providing funding for my research.

The Small Animal Clinic at Texas A&M University, for providing fixator hardware and bone specimens, and Diana Farley for preparing my specimens.

A special thanks to the members of my advisory committee for a challenging and rewarding experience:

Dr. Don Bray in Mechanical Engineering, for his support, guidance and even temper; he has been a neutralizing factor in times of certain crisis.

Dr. Malur Srinivasan in Mechanical Engineering, for his general agreeability on all major points.

Dr. Ross Palmer in Small Animal Medicine, for the opportunity to work on this project and for all the support that goes with it. I feel fortunate that he introduced me to the world of veterinary orthopedics.

Dr. Newton Ellis in Industrial Engineering, for his enthusiastic willingness to sign on to a short-handed committee, and for his knowledge of human factors.

A special thanks is in order for Dr. Don Hulse in Small Animal Medicine, for offering a critical evaluation and for sitting in for Dr. Palmer. It is my hope that we will have the opportunity to collaborate in future projects.

I would also like to thank the following people for their friendship, kinship, and tutelage:

Joe Mulvey, for teaching me the art and discipline of flying.

Mark Smith and Steve Poprik, for many years of pizza, movies, mischief, and generally goofing off.

Tommy Armstrong, for being the rare kind of friend who helps you get to know yourself better.

Dr. Joyce Sutliff, for a strong and lasting friendship, many kind words, and encouragement in times of despair. As much as anyone, she has always believed in my abilities.

My sisters Kristie Dickens Knoll, Kathy Dickens Haines, Karol Dickens Whitlow, Kimmie Dickens Browning and all their families (too many people to name!). I don't know how they've all put up with having such an educated brother (and uncle). Just wait; in a few more years they'll have to call me "doctor."

Most especially, my parents Ferman A. Dickens and Doris Coan Dickens, for their continued love and support which has put my goals within reach and made all my success over the years possible.

TABLE OF CONTENTS

	Page
ABSTRACT.	iii
DEDICATION.	v
ACKNOWLEDGEMENTS.	vi
TABLE OF CONTENTS	viii
LIST OF TABLES.	xi
LIST OF FIGURES	xiii
CHAPTER	
I INTRODUCTION	1
External Skeletal Fixation.	1
Pulsed Ultrasonic Materials Evaluation.	2
Clinical Application of Ultrasound.	4
Research Objective and Goals.	4
II EXTERNAL SKELETAL FIXATION	6
Biomechanical Principles.	6
Fixator Strength and Stiffness.	11
History	12
Indications for Usage	13
Medical Capabilities.	13
Research Methodologies.	14
Pin Insertion	16
Pin Design.	20
Implantation Site	23
Mechanical Influences	23
Complications	24
Utility of Experimentation.	27
Stress Distribution	29
III ULTRASONIC MATERIALS EVALUATION.	33
Ultrasonic Testing Principles	33
Ultrasonic Inspection Systems	35
Elastic Wave Propagation.	35
Transmission and Reflection	39
Pulse Attenuation	42
Fourier Transformation.	43
Ultrasonic Techniques for Adhesive Bonds.	46
An Ultrasonic Technique for Dental Implants	48

CHAPTER	Page
IV LAMB WAVES	49
Definition.	49
Theory of Lamb Waves.	49
Plate Equation Derivation	56
Bar Wave Propagation.	63
Discussion and Summary.	64
V EXPERIMENTAL TECHNIQUES.	66
Ultrasonic and Computer Hardware.	66
Probe Characteristics	66
Probe Holder.	70
Axial Extraction.	72
Pin Preparation	72
Bone Specimens.	74
Pin Insertion	76
Experimental Design	76
Data Collection	77
Ultrasonic Attenuation Parameter.	79
Reference Values.	82
Additional Ultrasonic Parameters.	82
Statistical Analysis.	83
VI RESULTS.	85
Ultrasonic Data	85
Other Experimental Factors.	85
Statistical Analysis.	100
Repeatability	110
Microstructure.	114
Hardness Testing.	115
VII DISCUSSION	117
Ultrasonic Data	117
Other Experimental Factors.	119
Statistical Analysis.	122
Repeatability	126
Mechanism of Pulse Attenuation.	126
Attenuation Parameter	127
Effect of Probe Frequency	131
Probe Holder.	132
Axial Extraction.	132
Pulse Velocity and Arrival Times.	133
Microstructure.	136
Sources for Experimental Error.	136

CHAPTER	Page
VIII SUMMARY AND CONCLUSIONS.	138
Strengths and Limitations	138
Areas for Future Research	141
Future Application.	142
Improving Accuracy and Sensitivity.	143
Conclusions	144
REFERENCES.	147
APPENDICES	
I GLOSSARY OF MEDICAL TERMINOLOGY.	152
II PCDS SIGNAL ANALYSIS SOFTWARE	156
III PROBE HOLDER	174
IV PROPERTIES AND MICROSTRUCTURE OF 316L STAINLESS STEEL.	177
V DATA TABLES.	187
VITA.	200

LIST OF TABLES

	Page
Table 5.1	Pulsar-receiver and PCDAS settings . . . 68
Table 5.2	Probe characteristics. 69
Table 5.3	Pin dimension data 75
Table 5.4	Sample of FFT data before primary reduction. 80
Table 5.5	Sample of FFT data after primary reduction. 81
Table 6.1	Individual variables and paired ultrasonic data 101
Table 6.2	Worst and best in each category. . . . 102
Table 6.3	Results of means testing (d.f. = 9, α = 0.05) 109
Table 6.4	Error in Pulse Energy Cutoff Point, by Pin 113
Table 6.5	Hardness data (Rockwell C scale) . . . 116
Table 7.1	Results of analysis of variance testing for the optimal prediction model 124
Table A-2.1	Listing of subroutines 167
Table A-2.2	Function subroutines with no available source code. 171
Table A-2.3	Subroutines with available source codes and their respective tasks 172
Table A-4.1	Composition of 316L stainless steel. . 182
Table A-5.1	Individual variables and paired ultrasonic data 188
Table A-5.2	Models containing no ultrasonic data . 189
Table A-5.3	Paired ultrasonic data with one other factor. 191

	Page
Table A-5.4	Paired ultrasonic data with two other factors 192
Table A-5.5	Paired ultrasonic data with three other factors 194
Table A-5.6	Paired ultrasonic data with more than three other factors. 196
Table A-5.7	Baseline reference values. 197
Table A-5.8	Summary data sheet 198

LIST OF FIGURES

	Page
Figure 2.1	A simple 6 pin external skeletal fixation frame. 7
Figure 2.2	Threaded and nonthreaded fixation pins. 8
Figure 2.3	Frame configurations for external skeletal fixation 9
Figure 3.1	Hardware associated with an ultrasonic pulse-echo inspection system. 36
Figure 3.2	Illustration of the principles of reflection and refraction at an interface (Snell's Law). 41
Figure 3.3	Idealized power spectrum display showing peak (F_{peak}), center (F_{cen}), and half-power frequencies (F_{low} and F_{high}) 45
Figure 4.1	Exaggerated representation of macroscopic displacements for various modes of Lamb waves traveling in a plate 51
Figure 4.2	Phase speed curves for Lamb waves traveling in a steel plate 52
Figure 4.3	Group speed curves for Lamb waves traveling in a steel plate 54
Figure 5.1	Experimental test setup showing computer display screen (top), pulser-receiver unit (middle), and computer keyboard (bottom) 67
Figure 5.2	Plexiglas probe holder with probes mounted inside and connecting cable attached to Probe 1 71
Figure 5.3	Axial extraction jig 73
Figure 6.1	Probe 1 Pulse Energy Cutoff Point vs Extraction Force. 86

	Page
Figure 6.2	Probe 2 Pulse Energy Cutoff Point vs Extraction Force. 87
Figure 6.3	Probe 1 Pulse Energy Time Shift vs Extraction Force. 88
Figure 6.4	Probe 2 Pulse Energy Time Shift vs Extraction Force. 89
Figure 6.5	Probe 1 Percent Time Shift vs Extraction Force. 90
Figure 6.6	Probe 2 Percent Time Shift vs Extraction Force. 91
Figure 6.7	Implantation Method vs Extraction Force 92
Figure 6.8	Bone Number vs Extraction Force. . . . 93
Figure 6.9A	Averaged Femoral Diameter vs Extraction Force. 94
Figure 6.9B	Averaged Femoral Diameter vs Extraction Force, excluding data for Implantation Method 4 95
Figure 6.10A	Implantation Site vs Extraction Force 96
Figure 6.10B	Implantation Site vs Extraction Force, excluding data for Implantation Method 4 97
Figure 6.11A	Pin Number vs Extraction Force 98
Figure 6.11B	Pin Number vs Extraction Force, excluding data for Implantation Method 4. 99
Figure 6.12	Observed Force vs Predicted Force. . . 108
Figure 6.13	Extraction Force vs Probe 1 Coefficient of Variance. 111
Figure 6.14	Extraction Force vs Probe 2 Coefficient of Variance. 112
Figure 7.1	Pin Number vs Averaged Femoral Diameter 121

	Page
Figure 7.2	Plots of Averaged Center Frequency as a function of position along the time-domain scale. 128
Figure 7.3	Illustration of the extreme effects of circuit noise 129
Figure 7.4	Comparison of the baseline response of two pins tested with Probe 2 130
Figure 7.5	Group speed curves for Lamb waves traveling in a steel plate and showing points corresponding to Probe 1 (6.9 MHz mm) and Probe 2 (10.8 MHz mm). 134
Figure A-2.1	Simplified schematic of PCDAS program. 161
Figure A-2.2	PCDAS main program and subroutine calls 162
Figure A-2.3	SETMD subroutine 163
Figure A-2.4	MMI subroutine showing UPDATE, INWAVE, and OUTWAVE. 165
Figure A-3.1	Plexiglas probe holder placed onto a fixation pin inserted through a plastic pipe 176
Figure A-4.1	Photomicrograph of Pin 2 at a magnification of 400 times 186

CHAPTER I
INTRODUCTION

External Skeletal Fixation

External skeletal fixation (ESF) is a fracture treatment technique which was originally suggested with a crude device invented during the mid-19th century. Since about 1900 the technique has advanced considerably but has not always found wide acceptance. In spite of its many applications, ESF is perhaps known best for its tendency to result in clinical complications. Foremost is premature loosening of the percutaneous fixation pins. Pin loosening is widely regarded as the most serious complication of ESF, and preventing its occurrence has proven quite elusive. Even when the most advanced materials, techniques, and aftercare are employed, pin loosening still may develop. Presently, the best solution is reducing rather than eliminating pin loosening.

Unfortunately the onset of pin loosening is generally not detectable. Radiographic examination can be used to detect a ring sequestra, or halo, surrounding the pin. This is often an indication of pin loosening, but is a subjective evaluation at best. In most instances pin loosening is not detected until the time of removal of the fixation device or

The citations on the following pages follow the style of *Ultrasonics*.

when side effects begin to appear in the patient. Pin loosening can cause severe pain which leads to poor limb function. It can result in fracture instability, delayed union, or nonunion. In addition, pin loosening is considered a significant contributor to the development of pin tract infection.

A simple and quantifiable technique of determining the stability or holding power of a pin is to perform an extraction test using a universal testing machine. The measured resistance to extraction is an indication of the pin stability. Extraction is used extensively in research settings, but is practical only after the animal has undergone euthanasia and necropsy. For the clinical treatment of fractures, extraction measurements are not possible. In addition, extraction has limited usefulness in research settings by virtue of the inability to repeat measurements for a given pin or to take successive measurements over time.

Pulsed Ultrasonic Materials Evaluation

The circuitry associated with pulsed ultrasonics began to develop during World War II with the use of the first sonar devices in submarines. This technology led to applications in thickness testing of materials shortly thereafter. Since then ultrasound has come into its own as a diagnostic tool in industry and the medical profession

alike. Ultrasound is used to "look" inside a material to search for defects or to create a two-dimensional image of the interior of the testpiece. This is accomplished in most cases without impairing the integrity of the testpiece in any way.

The basic principle of pulsed ultrasonic evaluation is to excite a transient acoustic stress wave into the material of interest. This stress wave propagates by causing successive local particle (atomic) displacements according to the laws of elasticity. As the stress wave passes a point in space, the particles are displaced in a harmonic fashion and then return to their original (equilibrium) positions soon after the stress wave passes. In the course of propagation, energy is gradually dissipated from the pulse. This can be due to material properties, geometric constraints, or abnormalities which the pulse comes in contact with. After travelling some distance, the pulse will contact an opposing boundary and be reflected. If the reflecting boundary is normal to the ultrasonic beam path, the pulse will travel back along its original path to the source. When it reaches the source, the pulse signal is captured and displayed on-screen. Abnormalities existing within the material are interpreted by an operator based on the appearance of the reflected pulse on the display screen.

Clinical Application of Ultrasound

If a clinical pin stability evaluation method were available, it could be used for constructing time histories of pins to assess maximum rigidity, trends, and differences between the many types and sizes of pins. In addition, it could be used for identifying the point where pin loosening becomes a clinical problem, i.e., begins to cause observable complications.

Since a clinically applicable method for evaluating external fixation pins is not available, the present study explores the possibility of utilizing a simple pulsed ultrasonic technique for this purpose.

Research Objective and Goals

The objective of this study was to determine the existence and strength of a functional relationship between ultrasonic test measurements and the axial extraction forces of nonthreaded 2.78 mm (0.1094 inch) stainless steel fixation pins implanted into cadaveric femur specimens of mature canines. The specific goals of the research were as follows:

- Simulate several different levels of pin fixation quality in order to produce a wide range of extraction forces, from the very lowest (zero) to the highest
- Propose several methods for presenting an ultrasonic parameter and determine which might be most suitable

- Assess repeatability of the experimental technique and identify sources which may contribute to variability
- Using statistical analysis, quantify the strength of the relationships between ultrasonic test parameters, extraction forces, and other experimental factors
- Suggest a method for estimating the quality of pin fixation based on data gathered in the experiment
- Assess the advantages and limitations of the proposed technique and suggest ways in which the accuracy and sensitivity of the test might be improved
- Discuss areas for future research

CHAPTER II

EXTERNAL SKELETAL FIXATION

Biomechanical Principles

The purpose of External Skeletal Fixation (ESF) is to immobilize the fragments of fractured bones by implanting them with transcutaneous fixation pins which are clamped rigidly in an external frame (*Figure 2.1*). Typically ESF devices consist of four to eight fixation pins, the same number of clamps, and one to three connecting rods for clamping the pins together¹. Currently there is a wide variety of pin designs (threaded and nonthreaded, *Figure 2.2*), fixation frames (unilateral, bilateral, and ring-type, *Figure 2.3*), and techniques of application (direct implantation, predrilling, pretapping, pin angling, pin placement, etc.). Although standard techniques are applied whenever possible, each patient's needs will vary according to the injuries, and the operating surgeon must choose which device and method of application is most suitable.

Once in place, the fixation device prevents relative motion between bone fragments which allows healing to proceed^{2,3}. Additionally, loads applied to the limb are transmitted around the site of the injury by the fixation frame. Loads arise from normal ambulatory activity and generally take on a combination of three forms: axial (compression or tension parallel to the longitudinal bone

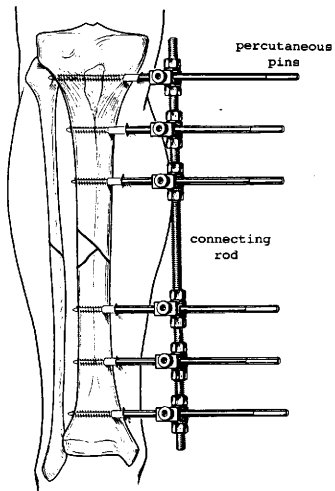


Figure 2.1 A simple 6 pin external skeletal fixation frame [Adapted from Weber, B.G., and Magerl, F. The External Fixator Springer-Verlag, Berlin (1985) 79]

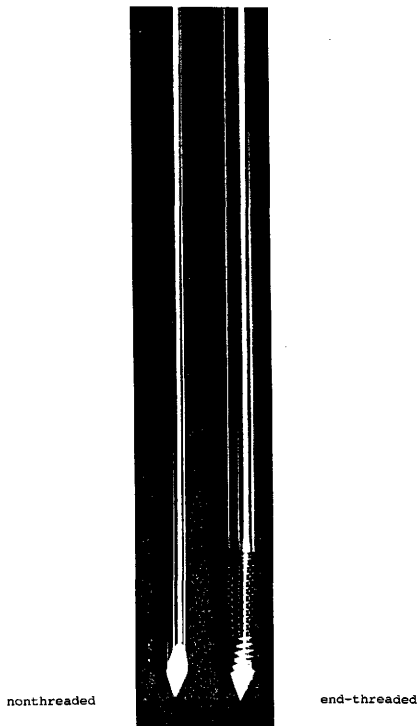


Figure 2.2 Threaded and nonthreaded fixation pins [Adapted from IMEX Veterinary, Inc., 1227 Market Street, Longview, Texas 75604]

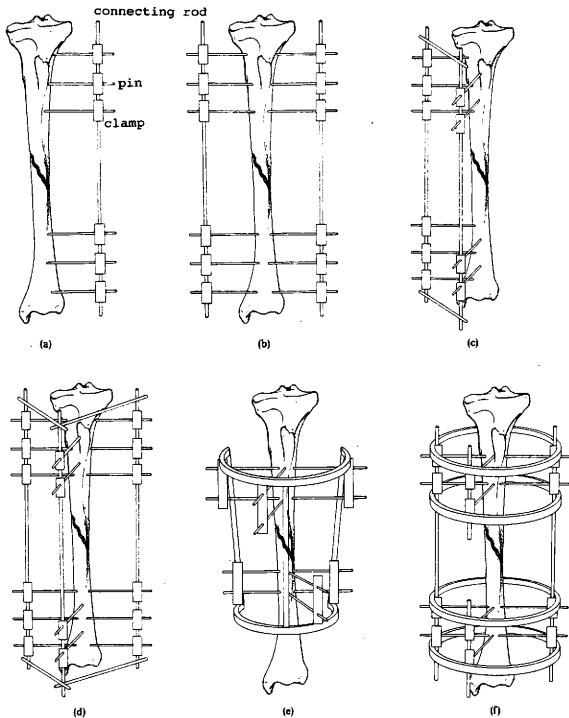


Figure 2.3 Frame configurations for external skeletal fixation.
 (a) Unilateral, uniplanar; (b) Bilateral, uniplanar; (c) Unilateral, biplanar; (d) Bilateral, biplanar; (e) semicircular ring; (f) full ring
 [Adapted from Coombs, R., Green, S.A., and Sarmiento, A. External Fixation and Functional Bracing Orthotext, London (1989) 82]

axis), bending (flexing about the longitudinal bone axis), and torsion (twisting about the longitudinal bone axis). With simple transverse fractures, axial compression loads can be distributed between the fixation frame and the fracture site. However, the fracture site cannot support axial tension loads, bending loads, or torsional loads. The fixation device carries these loads instead. In cases where the fracture cannot be adequately reconstructed, or when ESF is used for limb-lengthening procedures, the fixation device must carry 100% of loads applied to the limb⁴.

Loads transmitted between the fixator apparatus and the bone must pass through the bone-pin interface (the point of contact between fixation pins and bone fragments). In order to maintain rigid fixation, the bone-pin interface must remain mechanically intact and biologically stable. The success of fracture fixation depends largely on how stable the bone-pin interface remains during the healing period⁵.

Pin holding power (or pullout force) describes the force necessary to extract a fixation pin from the bone. It is a standardized, quantifiable measure of pin stability. This force is usually found by applying an axial tensile load to the pin. A load-displacement curve is plotted and the maximum tensile load needed to produce failure is found^{6,7,8,9}. Unfortunately, this technique cannot be applied to clinical situations but is used only in research. Even as an aid to research, holding power measurements are limited

in their use to a single measurement per pin. This requires the use of many more experimental animals than would be required if a repeatable (nondestructive) technique were available to characterize the pin fixation quality. A goal of future research should be to develop a nondestructive technique that could be used to clinically diagnose the fixation quality of a pin without interfering with the functioning of the fixation device⁶.

Fixator Strength and Stiffness

The most important mechanical characteristics of the fixation device are strength and stiffness. Factors affecting strength and stiffness of the fixator include: (1) the proportion of compressional loads carried by the fracture site, (2) the number of fixation pins, (3) pin diameter, (4) pin design, (5) pin spacing, (6) pin implantation angle, (7) frame configuration, (8) the number of connecting rods, (9) the lateral distance between connecting rods and bone, and (10) the mechanical properties of the pin and frame construction material⁴.

For a given material, only geometry affects stiffness. Strength is derived from material properties and the manufacturing process. Geometry largely determines the magnitude of stresses generated within the component. Exceeding the yield stress within an ESF component results in permanent, plastic deformation. Stresses higher than

yield may produce breakage. Stresses within the component can be reduced by increasing its dimensions. In the case of a pin or a connecting rod, this generally means using one with a larger diameter.

History

ESF had its origins in the mid-1800's when the first crude fixation device was employed for stabilizing patellar fractures in human patients. Around 1900 the first forebear of the modern fixator was used in a clinical application. Since that time significant advances in technology have been made. Nevertheless, ESF has only recently begun to see widespread application. The high incidence of medical complications has discouraged many practitioners from using ESF⁸.

ESF was originally aimed at applications in human patients. Due to the high rate of complications experienced in treating injuries (particularly after World War II), the technique was all but abandoned in the U.S. although it found continued use in Europe. During the period immediately following WWII, a fixation frame was designed for use in animal patients. This frame and others like it have seen increasing use in veterinary orthopedics over the last 40 years⁸.

Indications for Usage

Many common clinical situations are well-suited to ESF. These include: (1) open or contaminated fractures, (2) highly comminuted fractures, (3) limb lengthening procedures or major alignment/length deficits, (4) severe traumatic musculoskeletal injuries, particularly ones involving significant bone loss, (5) delayed unions, nonunions, or treatment requiring extended healing time, (6) application of compressional forces across the fracture site, (7) corrective osteotomies, (8) injuries where internal fixation would require unacceptable exposure or could not be covered by soft tissue, (9) operating conditions that do not permit formal, clean osteosynthesis, and (10) patients in need of urgent stabilization or transportation^{1-3,6,8,10}.

Medical Capabilities

There are a number of important characteristics of ESF that make its use particularly advantageous:

- ESF allows for skeletal stabilization away from the site of the injury which gives better access to the injuries. There is no hardware directly in the fracture site. Contamination at the fracture site is more easily isolated (other types of fixation may spread contamination throughout the limb)
- ESF is versatile enough to accommodate a large variety of injuries including those which extend across adjacent joints. Or, fixtures can be configured to provide minimal interference with adjacent joints
- ESF can be applied either with open or closed fracture reduction

- ESF provides a rigid environment which promotes healing of traumatized and infected tissues
- The fixation device can be adjusted (both in length and alignment) as needed following the initial application
- ESF can be used to enhance the effectiveness of other methods of fracture fixation such as intramedullary nails, lag screws, and cerclage wire
- ESF allows the limb to be used for weight-bearing during the postoperative fracture rehabilitation period

The mobility and weight-bearing afforded by ESF improves blood circulation to promote faster healing, applies some stress to the fracture site which stimulates bone growth, reduces muscle and bone atrophy, and results in an early return to function^{1-3,8,10}.

Research Methodologies

A great deal of research has been performed with regard to fixation of implants into the bony skeleton. Of course, there are many different types of implants, fixation pins being only one example. Others include artificial joints, plates, rods, screws, and wires. These are the devices which come into direct contact with the bone. Interactions between the implant and bone are the focus of research aimed at determining the causes of premature loosening.

For any given investigation, there are a variety of experimental approaches available. Most of these experiments fall into one of two categories: *in vivo* or *in vitro*. An *in*

vivo study utilizes live patients, whereas *in vitro* studies use bone specimens obtained from cadavers. In most cases an *in vivo* study is completed by euthanizing the patient, harvesting bones containing implants, and performing mechanical tests to determine the holding power of the implant. In addition, histologic evaluation can be performed to determine structural changes in the bone caused by the implant. These results can be compared to radiographic films taken postoperatively and at successive intervals prior to euthanasia.

Within the scope of both *in vivo* and *in vitro* methods, the implants can either be subjected to some kind of loading or they can be left undisturbed until pullout testing or histologic evaluation is performed. The experimental approach will vary according to the parameters under study. No completely standardized method has been adopted. However, a popular method of *in vivo* investigation is to divide a study into two sections, referred to as *acute* and *chronic*. An acute study involves euthanasia shortly after the operative procedure (one or two days). The chronic study involves euthanasia at a later point in time (typically eight weeks postoperatively). The acute and chronic studies can be compared to see what changes have taken place over time.

As mentioned earlier, the implant system under investigation may either be unloaded, statically loaded, or

dynamically loaded, depending on the wishes of the experimenter. An unloaded system is one in which the implants are placed directly into the bone but are not attached to a frame or other load-carrying device. A statically loaded system is one in which, for example, adjacent fixation pins have been deflected slightly toward each other and then held in this position by an external connecting rod. A dynamically loaded system involves placing the fixation device under the conditions typically seen in clinical applications. This is done by performing an osteotomy prior to applying the fixation device. The fixator now supports loads imposed by the patient during normal postoperative fracture rehabilitation. Sometimes a small gap is maintained across the site of the osteotomy. In this case the fixation device must support all loads incurred by the limb.

Pin Insertion

Of the many factors influencing implant stability, insertion technique is one of the most important. Many researchers have found that insertion technique determines in large part the quality of the initial bond between implant and bone, which in turn influences whether the implant ultimately remains stable or becomes loosened. Unfortunately, controversy over the most effective technique still abounds. This is due in part to conflicting research

results. The best conclusion may be that implant bonding is such a complex phenomenon that no single factor can determine its final outcome. Some explanation of the complexities of introducing an implant into the bony skeleton follow.

There are several basic facts to consider. The fixation of any implant depends initially on the establishment of a good mechanical interlock between the implant and the bone. However, trauma associated with implantation (due to frictional heating, mechanical damage, etc.) makes it impossible to insert an implant without producing a local region of bone death (necrosis). A thin glycoproteinaceous interface conversion film forms on the surface of the implant in a matter of seconds. Subsequent tissue attachment to the implant is through this film. Tissues in contact with the implant immediately following insertion include dead bone, shattered bone trabeculae, marrow, tissue debris, and clotted blood. Living bone will not be in direct contact with the implant. The insertion technique determines what amounts of each tissues are present, in addition to influencing the extent of initial bone trauma and necrosis. Excessive necrosis may prevent the implant from becoming integrated into the bone over time¹¹.

Hand chuck insertion of nonthreaded pins has been favored over high speed power drill insertion for forty years. Experience has shown that high speed power drill

insertion results in greater thermal damage, more frequent pin loosening, and lower extraction forces compared to low speed or hand chuck insertion techniques⁷.

Pullout results of studies aimed at determining the effect of pin (or bone screw) insertion technique have been mixed. In one study the pullout forces between acute and chronic cases were compared, based on insertion technique. For the hand chuck technique, the average pullout force was 25 N (5.62 lb) lower, the coefficient of variance was 13% higher, and the incidence of pin loosening was five times higher than for the slow speed hand drill⁷.

In an investigation utilizing two types of fixation pins and five insertion methods, an acute and chronic study were conducted in an unloaded pin system. The study showed that low speed power drill insertion produced the highest initial holding power while maintaining temperatures below 55°C (131°F). It has been shown that above 55°C (131°F) bone tissue is destroyed due to thermal necrosis¹².

One study found that pin tip design was a more significant factor than drill speed in determining maximum bone temperatures, the extent of heating, and the duration for localized areas of the bone to remain above 55°C (131°F)¹³.

In a study of the pullout resistance of bone screws, self-tapping and non-self-tapping implants of similar material and size were found to maintain comparable holding

power at all intervals tested in an unloaded pin system *in vivo*. No histological differentiation could be made with regard to necrosis or tissue reaction around the implant, between implant materials, nor between the self-tapping and non-self-tapping insertion methods⁹.

In a study using 5.5 mm (0.217 inch) and 6.5 mm (0.256 inch) bone screws, insertion after pre-tapping threads into the bone resulted in a greater holding power than insertion by a self-tapping method. The difference was especially marked for the 6.5 mm (0.256 inch) screw where pre-tapping produced a higher pullout force in all trials¹⁴.

One *in vitro* study utilized self-tapping and non-self-tapping bone screws which were cyclically loaded in shear. The study concluded that self-tapping screws were more difficult to insert and created more damage to the cortex (macroscopic chipping and microscopic cellular trauma)¹⁵.

It is interesting to note that in some cases, self-tapping implants showed no difference in pullout resistance when compared to non-self-tapping implants. There is no clear consensus, based on pullout studies, that non-self-tapping screws are preferable. However, the studies do tend to agree that non-self-tapping screws are less subject to alignment problems and undue bone damage during insertion. For these reasons alone, it seems reasonable to choose a non-self-tapping insertion method. Although no guarantee of greater stability is evidenced, the fact that bone damage is

reduced seems certain to increase the likelihood of achieving stable implantation. The chief drawback to pretapping is an increase in required surgical time. This can lead to complications resulting from anesthesia or extended biological exposure.

Pin Design

Many factors related to pin design will substantially affect the holding power of the implant. These factors include pin material, geometry, dimensions, thread parameters, and characteristics of the bone-penetrating point. Studies have consistently shown that threaded pins have much higher holding power than nonthreaded pins, particularly after several weeks of fracture stabilization. Furthermore, pins whose threads engage both cortices have greater holding power than those whose threads engage only one cortex. However, this difference is generally less than a factor of two for any given thread profile. At this time, the specific role of thread parameters (such as profile and pitch) on holding power is not completely understood^{4,6}.

An acute and chronic study were performed using four pin designs with the intent of evaluating the pullout resistance of different types of pins. The study concluded that one-cortex partially threaded pins were better at maintaining holding power than nonthreaded pins, while two-cortex threaded pins maintained better holding power than

both nonthreaded and one-cortex threaded pins¹⁶.

In a recent study, the differences in holding power between nonthreaded and two types of end-threaded pins were investigated. Both an acute and chronic study were performed. It is clear from the results that the threaded pins demonstrated the greatest advantage in holding power immediately following insertion as well as eight weeks after insertion, particularly the two-cortex threaded pins⁴.

A study mentioned in the previous section found that pin tip design was a more significant factor than drill speed in determining maximum bone temperatures, the extent of heating, and the duration localized areas of the bone remained above 55°C (131°F). This study concluded that pin tips which provide for effective chip elimination are associated with much lower cortical temperatures¹³.

In a preliminary study of the effect of a porous titanium coating on pin holding power, researchers found that after eight weeks of fracture fixation, pin holding power was significantly improved over the non-titanium-coated pins (by a factor of greater than two to one) in one of their earlier experiments. However, the rate of pin loosening (8.3%) of titanium-coated pins was similar to that of the non-titanium-coated pins. All pins were implanted at approximately 70° to the longitudinal axis of the bone¹⁷. One drawback to this study was that it did not include acute pullout data, so no indication of initial pin holding power

was obtained.

In a more detailed study of the effects of porous titanium coatings and implantation methods, holding power was evaluated at three different times postoperatively (one day, two weeks, and five weeks) in an unloaded system. The holding power afforded by the titanium-coated pins five weeks after insertion was greater than for uncoated pins, but only when inserted using a hand chuck. Insertion by slow-speed power drill resulted in loss of holding power regardless of whether a titanium coating was present. Threaded pins which had been coated with titanium appeared to show a reduction in holding power compared to threaded pins which had not been coated. In all cases tested, the uncoated pins lost only a small percentage of their one day holding power after two and five weeks. However, the pins were not subjected to loading⁸.

Using two-cortex end-threaded pins, an *in vitro* evaluation of the differences between the holding power of the near and far cortex demonstrated that the far cortex showed substantially greater holding power (factor of 1.6) than the near cortex. With the aid of scanning electron microscopy, greater microstructural damage and debris was observed in the near cortex compared to the far cortex, suggesting that the near cortex experiences greater damage upon pin insertion and less direct bone-pin contact¹⁸.

Implantation Site

There is little conclusive evidence that pin loosening occurs more frequently at any given implantation site in the bone. Loosening depends on many related factors which are not all known or understood. Therefore, inferences should be made with caution.

One study showed that mean holding power of nonthreaded pins did not vary with implantation site in canine tibiae⁶.

In a study cited earlier⁷, all loose pins were located in the proximal pin positions of the tibia. The authors suggested that proximal pins may carry a greater share of the load which results in a higher incidence of loosening.

In another study cited earlier¹⁷, researchers found that loose pins in two different experiments were located in the proximal tibia.

Mechanical Influences

From an engineering standpoint, living bone tissue is a poor material. This is because the local stress-strain environment determines whether or not bone is capable of becoming integrated with an implant. In the presence of low-to-moderate stresses and strains, bone is strong and remains so. In fact, stress stimulates the growth of strong bone, but only up to a point. Past a certain threshold corresponding to about two percent strain, bone behaves in an unstable manner by forming a structurally inferior

material. The process is known as cell differentiation, indicating that certain bone cells are capable of forming fundamentally different structures (mechanically strong or weak) based on the local stress-strain environment. These undifferentiated cells are in many ways the key to implant stability. The stress field surrounding an implant should not be in excess of that which favors stable cell differentiation^{11,19,20}.

Complications

The popularity of ESF has been increasing over the years in spite of numerous complications associated with the technique. Pin tract seepage, pin tract infection, implant breakage, and premature pin loosening all contribute to patient morbidity through loss of fracture reduction, delayed fracture union or nonunion, severe pain, and loss of limb function^{4,6}. Other difficulties can result from faulty pin placement, obstruction of the injury site, inadequate strength or improper application of ESF, unrealistic expectations, lack of experience, and lack of long-term planning¹⁰. A few of the more common complications are presented in greater detail.

Pin tract seepage is not generally serious. In most cases it can be minimized or prevented. Common causes of seepage include: (1) pin insertion prior to fracture reduction (resulting in excessive distortion of soft tissues

around the pin), (2) pin insertion through large muscle masses, (3) pin insertion through the fracture hematoma or through a large blood vessel, (4) pin insertion through the injury incision line rather than through individual stab incisions, (5) improper bandaging, (6) contact between soft tissue and the fixation clamp, and (7) insufficient restriction of activity during postoperative recovery¹.

Pin tract infection affects nearly all external fixation splints to some degree, some seriously enough to require removal of the pin. The factors believed to contribute to pin tract infection include bone and soft tissue necrosis, excessive stress at the bone-pin interface, thermal damage occurring during pin insertion, soft tissue motion around the pin, and pin loosening²¹. In addition, any departure from aseptic surgical techniques can lead to contamination and subsequent infection.

Implant breakage is a rare but significant occurrence. It is generally caused by improper use of pins (improper sizing or insertion) or overstressing the fixation device. In addition, the effect of stress concentration at the thread roots is significant. Shock loads may be responsible for breakage of a component, but fatigue failure is more common⁴.

Premature pin loosening is not only one of the most common complications of ESF, but it is also one of the most serious^{4,6,7}. It is predisposed by the fact that the bone-pin

interface is the most highly-stressed component of the fixation system⁶. Pin loosening is also largely determined by the implantation technique. Excessive bone trauma at the time of implantation is a contributor to pin loosening^{1,2}. Placement of the pins in close proximity to the fracture site or through a crack in the bone will lead to a higher incidence of premature loosening, as will failure to fully penetrate both cortices or improper selection of pin size¹.

The term "pin loosening" is not strictly defined. However, it can generally be thought as having occurred when the pin is loose to the touch (it wobbles or tends to slide out). This applies to both threaded and nonthreaded pins. A loose nonthreaded pin can be removed from the bone by hand and will be measured with a universal testing machine as having zero extraction force. A loose threaded pin, however, cannot necessarily be removed by pulling straight out (without unscrewing it) and could register several hundred newtons (or pounds) of extraction force. This difference is due to the fact that threaded pins physically engage the bone cortices. Therefore even standardized testing methods such as extraction force measurements should be approached with some skepticism. One cannot always make the correct conclusion based simply on a pullout force. Judgement is required to interpret test results properly.

Due to the role of cellular differentiation in the loosening process, the fixation device should be protected

from unnecessary loads for the first few weeks post-operatively. Excessive loads must be avoided at all times. This provides an opportunity for rigid fixation to take place between the bone and the implant, thereby reducing the incidence of loosening^{1,19}.

There is an important point to make regarding implant stability. The fixation quality is not wholly determined at the time of insertion, nor is it determined after cell differentiation begins. Although a localized high stress environment can lead to pin loosening, the process appears to be reversible. That is, when stresses are reduced, biological processes again favor formation of a stable environment. Local conditions continuously affect the formation of new tissues²⁰. One of the reasons stability reversal is possible is that bone turnover is an ongoing process¹¹. Old cells are replaced with new ones, the formation of which are governed by the current level of stress.

Utility of Experimentation

Many of the factors affecting fixation of implants to the skeleton revolve around the conditions created at the moment of implantation. However, biological events following implantation are what ultimately determine whether the implant maintains its utility. In a study cited earlier⁹, no significant difference was found in pullout resistance of

screws implanted using two different methods in an *in vivo* model. However, the screws were not subjected to loading and there is no way to predict what effect different implantation methods would have had under the action of loads. Likewise with the latter study of titanium-coated pins⁸, inferences about the behavior of coated pins in a loaded model should not be made. There is a possibility that the rough surface of titanium-coated pins results in additional microstructural bone trauma during insertion. This in turn may lead to premature loosening in a dynamically loaded model.

Due to the unpredictable effect of dynamic loading on a fixation pin, it cannot be considered appropriate to speculate how pins will behave based on data obtained with experiments using statically loaded or unloaded pins *in vivo*. Likewise, the erratic interactions between implants and living tissues makes the use of *in vitro* studies questionable. Pins having different design, material, thread configuration, and insertion technique will show different responses depending on the conditions of the experiment. The only sure way to determine the response of an implant to a dynamically loaded system is to test it under those conditions. One cannot conclude, based on acceptable results in an unloaded model, that a given pin or insertion method will work well in a dynamically loaded model. On the other hand, unacceptable results in a statically loaded model

imply that unacceptable results will occur in a dynamically loaded model as well. Ambulatory loads have proven to play a critical and inseparable role in the pin loosening process. Therefore, unloaded pin models and *in vitro* pin models should be reserved for investigations of a general or preliminary nature.

Stress Distribution

As mentioned earlier, loads transmitted through the fixation pins produce high stresses at the bone-pin interface. One of the major objectives in external skeletal fixation should be to minimize these stresses to the extent possible. For a given applied force, stress depends on the surface area over which the force acts:

$$\sigma_{AVG} = \frac{Force}{Area} \quad (2.1)$$

In addition, when the applied force and reaction force are not collinear, a bending component is introduced according to the relation:

$$Moment = Force \times Distance \quad (2.2)$$

If conditions do not allow the applied force to be reduced, the surface area must be increased if stresses are to be reduced. This can be achieved in one of three ways: (1) by using pins having a larger diameter, (2) by incorporating a greater number of pins into the fixator, and (3) by inserting the pins at oblique angles. Also, positioning the

connecting rod as close to the bone as possible will reduce bending moments. Of course, there are practical limits to all of these methods. The question then remains: Are further reductions in stress necessary? Probably so.

The problem is not one of total pin surface area in contact with the bone. The area over which the greatest proportion of stresses are transmitted between pin and bone is a fraction of the total contact area. Stresses are unevenly distributed. The net effect is a several-fold increase in the average stress value. Unfortunately the bone does not behave as if under the action of an average stress. The bone responds based on highly localized, concentrated stresses. Maximum stresses at points of concentration can be many times in excess of the average stress, and well in excess of the material strength. An insidious danger is that high stress concentrations can occur even when applied loads are in a reasonable range. This is due to forces being concentrated over a limited surface area. Necrosis-producing stresses are likely to occur even in patients whose physical activity is carefully restricted.

With respect to unilateral frames, the outer near cortex appears to be the location of the highest stresses and strains, and therefore is probably the point where pin loosening originates. After its original onset, pin loosening is a self-perpetuating process. Once a portion of the bone becomes damaged from high stress and can no longer

support a share of the pin loads, the bone directly adjacent to it will carry the additional load. This results in an increasingly higher stress concentration as the pin progressively loosens and also tends to enlarge the pin tract.

A significant property of bone has to do with its strain-rate sensitivity, also known as viscoelasticity. Research indicates that statically applied loads are quite benign compared to dynamically applied loads. This suggests that the rate at which a stress is applied to the bone (slowly versus suddenly) is as important in some cases, or more so, than the magnitude or duration of the stress.

Inserting pins at oblique angles increases the effective area over which forces act (by increasing the effective thickness of the bone) and also resolves stress into a component acting perpendicular to the pin (compressive stress) and a component acting parallel to the pin (shear stress). Thus pin angling results in better distribution of stress throughout the bone-pin interface. Several researchers have concluded that angling pins about 70° significantly reduces the incidence of pin loosening and is an optimal method^{1,2,7,17}. This is an interesting statement in light of the fact that only a 6.4% gain in interfacial surface area is obtained when a pin is angled at 70° compared to a pin inserted at 90°. The theoretical reduction in average compressive stress at the interface is 12%. This

would not seem to be significant enough to account for the gain in pin stability. There are likely other factors at work which at this point have not been recognized. Certainly one consideration is that pins angled away from each other become mechanically locked once clamped by a connecting rod. There is much less opportunity for axial motion of the pins due to transverse loading of the frame. When pins are inserted parallel to one another, transverse loading is more likely to result in axial motion.

Calculating an average stress is an oversimplified exercise that can easily lead one into a false sense of well-being. In real-world situations, average stresses generally do not cause components to fail. Maximum stresses at the points of highest stress concentration and stresses at vulnerable areas of a component are what ultimately lead to failure. Stress concentrations can self-perpetuate and accelerate the failure process.

CHAPTER III
ULTRASONIC MATERIALS EVALUATION

Ultrasonic Testing Principles

Mechanically generated acoustic waves are applied in a variety of situations to characterize the properties or conditions of materials or components. The sound waves are introduced directly into the material where they become subject to the influence material properties. Any irregularities can be discriminated by displaying a portion of the sound echoes on a viewing screen. Ultrasonic tests are benign to the material being inspected since no permanent changes are induced and there is no effect on useful life. Ultrasonics can be used to detect internal flaws, inspect welds or adhesive bonds, measure thickness, or detect changes in the material properties. It should be noted that the presence of flaws does not indicate an unserviceable component. Accept-reject criteria must be established for flaws based on the type, magnitude, location, and number for each component being tested²².

Flaws can be detected with ultrasound in one of several ways: by reflection, travel time, attenuation, or frequency analysis. Reflection occurs when the propagating pulse impinges on a discontinuity within its path. This will reflect energy back toward the source, and/or scatter some of the pulse energy. The travel time of ultrasonic pulses

can be measured to within a few nanoseconds using highly sensitive ultrasonic inspection equipment. Changes in the length of the travel path or a change in the material properties will often result in an observable change in the travel time. Gradual attenuation occurs as sound waves travel through the material. Changes in the observed attenuation can be related to variations in the length of the travel path or in properties of the material through which the pulse passes. Lastly, frequency content of the signal, or changes in the frequency content, can be analyzed to determine whether material conditions along the travel path differ from some known standard²².

Ultrasonic inspection has many advantages over other types of nondestructive material evaluation, namely: (1) it has high penetrability, sensitivity, and accuracy, (2) inspection usually requires access to only one surface, (3) real-time results lead to immediate interpretation, automation, rapid scanning, production monitoring, or process control, (4) a permanent record of inspection can be made, (5) it can scan over a volume, (6) there is no hazard to personnel or materials, (7) it can be portable, and (8) output can be processed with a digital computer. There are also several disadvantages to using an ultrasonic inspection method, including: (1) the operator must be skilled and properly trained, (2) technical knowledge is required for process development, (3) inspection of irregular, rough,

small, or thin parts may be difficult, (4) detection of near-surface defects may be inconsistent, (5) couplants are required, and (6) established standards must be adopted²².

Ultrasonic Inspection Systems

The essential elements of an ultrasonic inspection system include the following (*Figure 3.1*): (1) a signal generator to produce electrical spikes, (2) one or more transducers (also called probes or search units) for converting electrical signals to mechanical waves, and vice versa, (3) liquid couplant to aid in the transmission of ultrasonic energy between probe and testpiece, (4) a signal amplifier and processor, (5) a display screen, and (6) an electronic clock. The electronic circuitry and display are often integrated into a single control unit. Also, depending on the type of inspection, separate transducers may be used for sending and receiving pulses (pitch-catch). In pulse-echo systems the same probe serves both functions²².

Elastic Wave Propagation

Wave propagation takes place when a particle within an elastic material is displaced away from its equilibrium position by some transient disturbance. Interatomic forces between the displaced particle and its undisplaced neighbor will tend to displace the neighboring particle, and so on through the material. In this manner the disturbance can be

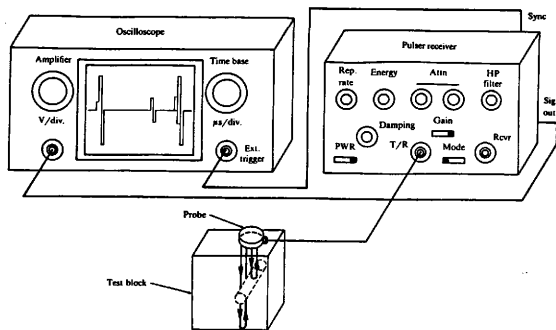


Figure 3.1 Hardware associated with an ultrasonic pulse-echo inspection system [Adapted from Bray, D.E., and Stanley, R.K. Nondestructive Evaluation: A Tool for Design, Manufacturing, and Service McGraw-Hill, New York (1989) 103]

propagated over long distances, and is referred to as a wave front. The same basic principle of propagation applies to solids, liquids and gases. However, wave behavior is considerably different in each of these mediums owing to the differences in interatomic forces and interatomic spacing.

In any medium the wave is observed to have a specific velocity, frequency, and wavelength. Velocity is the speed of the advancing wave front. Frequency is the number of repetitions of the periodic displacement cycle in a given time. Wavelength is the distance between identical points on the periodic cycle. These quantities are related according to the equation:

$$C = f\lambda \quad (3.1)$$

where C = wave speed (m/s)
 f = frequency (Hz)
 λ = wavelength (m)

Two basic cases of wave propagation are recognized: plane wave propagation and bulk wave propagation. Plane wave (one-dimensional) propagation is the simpler form. It assumes that displacements within an advancing wave front all occur in the same plane. In general, this holds when the lateral dimensions of the testpiece are much smaller than the wavelength of the pulse. Bulk wave (three-dimensional) propagation takes into account motion of particles along a hemispherically-shaped advancing wavefront and entails considerably more mathematical complexity. Bulk waves are the ones most often encountered in ultrasonic testing. They

occur when material dimensions are much larger than the wavelength of the pulse. Development of the wave propagation equations is left to the reader for further investigation. The references include plane wave derivations^{23,24} and bulk wave derivations²⁴.

Several distinct types of wave propagation can occur, classified according to the manner in which the particles are displaced by the wavefront. They can occur separately or in certain combinations. The four basic types are: (1) longitudinal waves (also called compressional or dilatational waves), (2) transverse waves (also called shear or torsional waves), (3) Rayleigh waves (also called surface waves), and (4) Lamb waves (also called plate waves). Longitudinal waves produce particle displacements within the bulk material along the direction of propagation. Transverse waves produce particle displacements within the bulk material perpendicular to the direction of propagation. Rayleigh waves produce elliptical particle displacements at the surface of a material and penetrate to a depth of $0.5-1.5\lambda$. Lamb waves produce complex elliptical particle displacements which are similar to Rayleigh waves, but penetrate through the entire material thickness. In ultrasonic inspection, each type of wave has specific applications to which it is well-suited. Bulk longitudinal and shear waves are the types most frequently encountered²². Utilization of Rayleigh and Lamb waves is increasing, particularly with the greater use

of layered materials in engineering structures. Lamb waves are discussed in greater detail in Chapter 4.

Transmission and Reflection

When a pulse encounters a boundary between two materials, several things can occur. Part of the wave energy may be transmitted across the boundary into the second material, while part of it may be reflected back. In addition, both transmitted and reflected wave energy may undergo mode conversion if the incident beam is at an oblique angle to the boundary.

Transmission refers to energy passing across the boundary. Reflection refers to energy which does not cross the boundary, but remains in the same material. Transmission and reflection coefficients for normally incident waves can be calculated based on the material properties on either side of the boundary. The characteristic of interest is the impedance ratio between the two materials. Impedance is the product of material density and longitudinal wave velocity:

$$Z = \rho C \quad (3.2)$$

where Z = acoustic impedance ($\text{kg/m}^2 \text{ s}$)
 ρ = material density (kg/m^3)
 C = bulk longitudinal wave speed (m/s)

If the values of Z are identical for both materials, then all pulse energy will be transmitted and none will be reflected. On the other hand, if there is a large difference between the Z values, all pulse energy will be reflected and

none will be transmitted. An example of poor impedance matching is the boundary between steel (high impedance) and air (low impedance). This results in almost complete reflection of an incident pulse travelling either in the air or the steel. Impedance ratio is an important underlying principle of flaw detection. Volumetric discontinuities within a component result in a highly mismatched impedance. An impinging ultrasonic beam will be strongly reflected from such a discontinuity²³.

Mode conversion is the process by which a wave transforms from one type to another. For instance, incident longitudinal waves can be used to excite longitudinal and/or shear waves, Rayleigh waves, or Lamb waves, depending upon the angle at which the pulse energy impinges on the boundary. This is a particularly useful principle of ultrasonics and is known as Snell's Law (*Figure 3.2*). The relationships between incident, reflected, and refracted components of the pulse are given by:

$$\frac{\sin\theta_1}{C_1} = \frac{\sin\theta_1''}{C_1} = \frac{\sin\theta_2''}{C_2} = \frac{\sin\theta_1'}{C_1'} = \frac{\sin\theta_2'}{C_2'} \quad (3.3)$$

The angle θ_1 represents longitudinal waves while the angle θ_2 represents shear waves. The unprimed angle indicates an impinging wave. A prime is used to indicate propagation across the material boundary, while a double prime indicates reflection. In the same way, the speeds C_1 and C_2 indicate longitudinal and shear wave speeds respectively, with primes

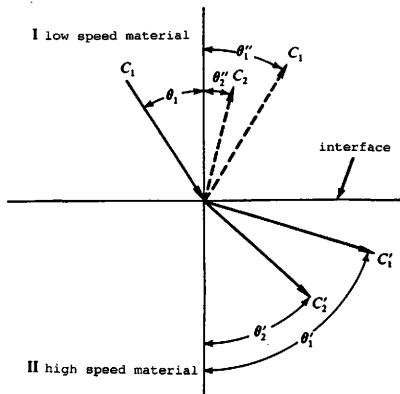


Figure 3.2 Illustration of the principles of reflection and refraction at an interface (Snell's Law) [Adapted from Bray, D.E., and Stanley, R.K. Nondestructive Evaluation: A Tool for Design, Manufacturing, and Service McGraw-Hill, New York (1989) 66]

again indicating propagation in the second material. Note that acoustic velocities are lower in material one (top) than in material two (bottom). For mode conversion to occur, the incident beam must strike a mismatched impedance boundary at an oblique angle²²⁻²⁴.

Pulse Attenuation

As any pulse travels through a material, it undergoes attenuation. That is, it gradually loses its original strength and after some time is completely dissipated. This is due to the combined effects of beam spreading, scattering, and absorption. Beam spreading results in loss of pulse intensity due to the increasing surface area of an advancing wave front. Scattering is a wavelength-dependent phenomenon that occurs when material inhomogeneities deflect portions of the beam energy away from its original path. Absorption results from conversion of pulse energy into heat as the wave propagates. Attenuation coefficients have been measured for many materials and serve as a guide to the depth to which inspections can be performed effectively. However, attenuation depends strongly on the material structure, heat treatment, and manufacturing process, in addition to being influenced greatly by the frequency of the ultrasonic pulse^{22,23}.

Special forms of energy loss are associated with Rayleigh and Lamb waves. Rayleigh wave energy is highly

concentrated at the surface and is easily attenuated, propagating long distances only on a smooth, clean air-metal boundary. Contamination or surface roughness (grease, dirt, pits, tool marks) will rapidly attenuate Rayleigh waves. In contrast, Lamb waves are subject to a phenomenon known as dispersion. This involves distortion of the pulse shape as it travels through the material and takes the form of a gradual pulse elongation or selective attenuation of frequency components. For this reason the characteristics of the original pulse are undergoing constant change. Dispersion results in more rapid energy attenuation than that found in bulk wave propagation²³. Chapter 4 contains further discussion.

Fourier Transformation

Fourier transformation is the means by which a signal in the time domain (an ultrasonic pulse signal) is transformed into the frequency domain. The purpose in doing so is to break down the time-domain waveform into its constituent waves. Typical ultrasonic pulses consist of a complex superposed band of discrete frequencies. Using Fourier transformation allows one to obtain a distribution for these frequencies. In this way, the dominant frequency can be identified, in addition to other parameters such as bandwidth and minor frequency components. Reference 24 contains a brief discussion of the theory and mathematics

associated with Fourier analysis²⁴.

In more practical terms, the information calculated by a Fourier transformation algorithm includes the following: (1) a power spectrum display, (2) peak frequency, (3) half-power frequencies, (4) center frequency, (5) spectral bandwidth, and (6) spectral skew. A power spectrum display shows the relative distribution of pulse energy as a function of frequency. Peak frequency is where the power spectrum reaches its peak (in some cases this is referred to as a resonant frequency). Half-power frequencies are at the points where power spectrum height is one-half its maximum value, on opposite sides of the peak frequency. Center frequency is the midpoint between half-power frequencies. Spectral bandwidth is the difference between half-power frequencies and is often expressed in percent. Lastly, skew describes a measure of symmetry of the power spectrum. A value of unity indicates symmetry about the peak. Of the six spectral parameters just described, only four are independent. Bandwidth and skew are computed values²³. *Figure 3.3* shows the spectral frequencies where the power curve has been idealized as a normal distribution of frequencies about a mean of 4 MHz. In this case, skew is equal to unity due to symmetry, and center frequency is equal to peak frequency. When skew is not equal to unity, peak and central frequencies will have different values.

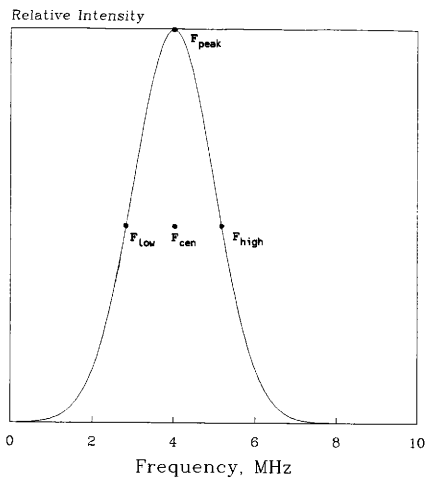


Figure 3.3 Idealized power spectrum display showing peak (F_{peak}), center (F_{cen}), and half-power frequencies (F_{low} and F_{high})

Ultrasonic Techniques for Adhesive Bonds

A number of researchers have addressed the problem of detecting adhesive disbonding in layered material or lapped joints²⁵⁻³¹. Much of the earlier work has centered around simply locating an area which had become disbanded. This is not of great interest in this paper. Instead, studies are considered in which the physical strength of the bond was correlated to an ultrasonic parameter. This has been done to determine the feasibility of predicting an ultimate bondline shear strength based on a nondestructive ultrasonic inspection. Research has shown that several measurable ultrasonic parameters can be used to predict bond strength. These parameters include signal amplitude ratios^{25,26}, signal bandwidth²⁶, characteristic Lamb wave velocity²⁷, attenuation coefficient²⁸, and wave velocity in the adhesive layer²⁸. Further, the adhesive layer thickness and modulus have been measured using ultrasound²⁹. In more general cases, ultrasound has been used to predict acceptable bond performance³⁰ and to detect variations in the interface bond quality³¹⁻³⁴.

Immersion techniques utilizing signal amplitude ratios have been used as a nondestructive method for characterizing and predicting the shear strength of adhesively bonded panels. One example of signal amplitude ratio compares the strength of signals reflected from the water-metal interface to the signals reflected from the metal-adhesive interface²⁵.

A similar technique compares the signals reflected from each of the two adhesive-metal interfaces while ignoring reflections from the outer panel surfaces, and also measures the signal bandwidth²⁶. In all cases, a reasonable correlation was observed between ultimate shear strength and ultrasonic parameters.

Using numerical techniques, the velocity of waves propagating along two bonded surfaces was calculated. The technique showed that theoretical Lamb wave phase velocity was strongly correlated to adhesive bond strength. Thus, dispersive properties of Lamb waves could be useful for predicting adhesive bond strength²⁷.

An immersion technique similar to the one described earlier sought to characterize the properties of the adhesive layer and its interfaces. Sound velocity and attenuation measurements were used for this purpose. Sound velocity in the adhesive layer was measured and correlated to maximum bond strength. This relationship appeared to be linear in nature. In addition, attenuation was calculated using signal amplitude ratios and bondline thickness which showed a distinctly nonlinear relationship with maximum bond strength. The study found that relationships between ultrasonic parameters and maximum bondline strength suggest that bond strength should be predictable from an ultrasonic test²⁸.

More recent investigation has shown that an immersion

method of ultrasonic testing which utilizes Lamb waves has proven quite sensitive to the detection of minute changes in the adhesive layer of bonded panels³²⁻³⁴. In principle, it appears that the elastic properties and thickness of the adhesive layer can be determined through careful analysis of this data.

An Ultrasonic Technique for Dental Implants

Recent experimentation has been conducted in which the interfacial rigidity of dental bone implants was evaluated using ultrasonic techniques³⁵⁻³⁸. The studies included extensive implant simulation as well as some testing *in vivo*. The results showed that good bonding produces substantial changes in both signal amplitude and frequency content over a range of 10 to 150 kHz.

CHAPTER IV

LAMB WAVES

Definition

Lamb waves were described briefly in *Chapter 3* as a type of wave mode having complex elliptical particle motions. In general, Lamb waves are induced when the distance between at least one set of opposing lateral boundaries in a test specimen is similar to the wavelength of the pulse. As the distances between any remaining lateral boundaries approach the wavelength, particle motion continues to increase in complexity.

There is still controversy over the exact mechanism for Lamb wave propagation. It has been suggested that complex internal reflections within a restricted dimensional space account for the particle motion³⁹. In any case, the behavioral characteristics of Lamb waves have been thoroughly studied and are well understood. The unique behavior of Lamb waves is well-suited to many ultrasonic testing tasks which cannot be performed using bulk pulse-echo waves.

Theory of Lamb Waves

Consider first the case of a plate, or a pair of large parallel surfaces separated by a thickness. If a wave is propagated between the surfaces, only plate thickness

directly influences the wave behavior. The nature of this behavior can be determined from the wave frequency and plate thickness, expressed as a product, $f \times t$. At a low frequency (and/or using a thin plate), the pulse wavelength is much greater than the plate thickness and a plane wave is generated. At a high frequency (and/or using a thick plate), two forms of energy are seen. Bulk waves travel through the interior while Rayleigh waves travel at the plate surfaces. All intermediate values of $f \times t$ result in multi-modal Lamb wave propagation. Individual modes are classified according to their particle motions. In the vertical plane, symmetric modes have opposing particle displacements on opposite sides of the thickness centerline, while asymmetric modes have comparable particle displacements on opposite sides²³. *Figure 4.1* illustrates this concept.

As seen in *Figure 4.1*, Lamb waves are represented by the symbol L . The first subscript indicates symmetry (1) or asymmetry (2). The second subscript denotes the rank order (1, ..., n) of the Lamb wave mode corresponding to increasing excitation frequencies. The arrows shown on this illustration represent particle vector displacements at various locations²³.

Lamb wave notation is convenient for use when plotting phase speed (dispersion) curves. *Figure 4.2* shows the dispersion curves for Lamb waves traveling in steel. For a single fixed frequency and plate thickness, a number of wave

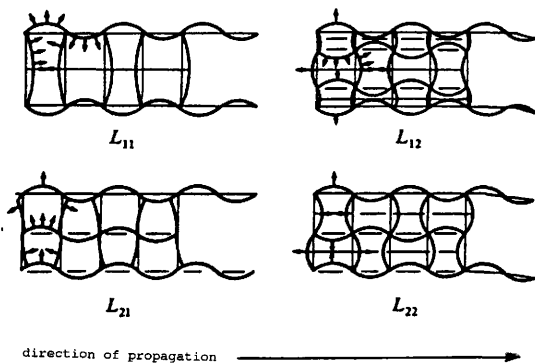


Figure 4.1 Exaggerated representation of macroscopic displacements for various modes of Lamb waves traveling in a plate. Propagation is from left to right. L_{11} and L_{12} are the fundamental and first higher-order symmetric waves, while L_{21} and L_{22} are the fundamental and first higher-order asymmetric waves. Arrows indicate displacement vectors for several individual particles [Adapted from **Lehfeldt, W.** Ultrasonic testing of sheets with Lamb waves Materialpruf (1962) 4 331-337]

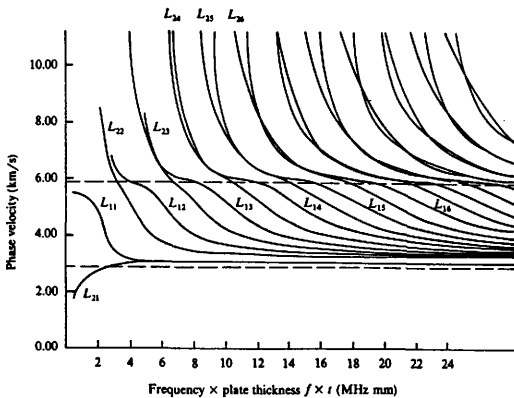


Figure 4.2 Phase speed curves for Lamb waves traveling in a steel plate [Adapted from Egle, D.M., and Bray, D.E. Nondestructive Measurement of Longitudinal Rail Stresses Federal Railroad Administration FRA-ORD-76-270 (1975)]

modes are expected to be present, each traveling at a unique velocity. Since ultrasonic pulses consist of a spectrum of frequencies, the wave modes excited within the plate will propagate over a range of velocities. This characteristic of Lamb waves often results in a cluttered arrival pattern which can be difficult to interpret. Nevertheless, Lamb waves can provide important information about the layers through which they travel²³.

Two extreme situations were mentioned earlier, and these can be observed on the phase velocity diagram. For very low values of $f \times t$, the fundamental symmetric Lamb wave speed (L_{11}) approaches the plane wave speed (shown by the upper dashed line), indicating that wave motion becomes planar. Conversely, as $f \times t$ approaches infinity, the fundamental Lamb wave speed approaches the surface wave speed (shown by the lower dashed line), while the remaining wave modes travel through the interior of the plate at bulk speeds without being affected by the surfaces of the plate. Another significant observation made from the dispersion plot is that all Lamb wave modes with the exception of L_{11} have lower bounds of existence. For a given value of $f \times t$, the phase velocity approaches infinity indicating that at a slightly lower $f \times t$, the wave mode does not exist²³.

Figure 4.3 shows the group speed curves for individual Lamb wave modes. Each curve exhibits a characteristic peak. Near the top of this peak, there are no appreciable changes

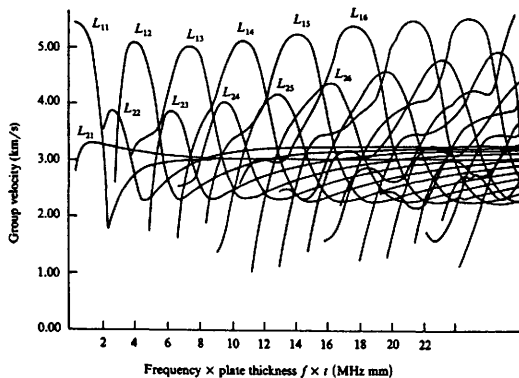


Figure 4.3 Group speed curves for Lamb waves traveling in a steel plate [Adapted from Egle, D.M., and Bray, D.E. Nondestructive Measurement of Longitudinal Rail Stresses Federal Railroad Administration FRA-ORD-76-270 (1975)]

in the group velocity over a narrow range of $f \times t$, while to the left and right of the peak, group velocities change rapidly. At increasingly higher values of $f \times t$, all group speeds appear to approach the Rayleigh wave speed.

To help understand the importance of *Figure 4.3*, first consider a wave pulse traveling in an unbounded medium. The pulse will consist of a dominant band of frequencies distributed around a peak (resonant) frequency (previously illustrated by *Figure 3.3*) where most of the wave energy is concentrated. In an unbounded medium, wave energy components at different frequencies will travel at the same velocity, and the pulse maintains its original shape (the pulse is non-dispersive). By contrast, each frequency component of a Lamb wave travels at a unique velocity determined by the product of its frequency and the plate thickness. A band of frequencies which falls at the peak of a group speed curve will travel with little distortion since all components travel at approximately the same speed. On the other hand, if the band falls to one side of the peak, a wide range of velocities is produced and causes the pulse to rapidly lose its original shape. The degree of total dispersion will be determined by the pulse's location on the curve and its bandwidth. Narrow bandwidth at the peak of a curve results in the least dispersion, whereas wide bandwidth away from the peak results in the greatest dispersion.

Comparing *Figures 4.2* and *4.3*, it is seen that peaks of

the group velocity curves correspond to points on the phase velocity curve near the bulk longitudinal wave speed. Along these points a pulse will travel undistorted. To the left of a peak, group velocity approaches zero while phase velocity approaches infinity and the wave mode vanishes (except for L_{11}). To the right of a peak, both group and phase velocity approach the Rayleigh wave speed²³.

Plate Equation Derivation

Now that the essential characteristics of Lamb waves have been established, the derivation of Lamb wave equations for plates will be described. The equations will be solved for the two extreme cases of frequencies approaching zero and infinity. Equations governing wave propagation in bars are similar and will be covered only briefly. The following derivations are excerpted from References 39 and 40.

To begin, several assumptions must be made: (1) the plate material is homogeneous and isotropic, (2) the plate has stress-free boundaries of infinite extent, (3) particle displacements are periodic in time and space with zero component in the plane of the plate perpendicular to the direction of wave propagation. In deriving the equations of motion for an acoustic wave, it is convenient to express the displacements in terms of the potential functions ϕ and ψ , where ϕ is a scalar function and ψ is a vector function with

three components. The corresponding wave equations in terms of the potential functions are given by:

$$\nabla^2 \phi = \frac{1}{c_d^2} \frac{\partial^2 \phi}{\partial t^2} = \frac{\rho}{\lambda + 2\mu} \frac{\partial^2 \phi}{\partial t^2} \quad (4.1)$$

$$\nabla^2 \psi_i = \frac{1}{c_t^2} \frac{\partial^2 \psi_i}{\partial t^2} = \frac{\rho}{\mu} \frac{\partial^2 \psi_i}{\partial t^2} \quad (4.2)$$

where c_d is the dilatational (longitudinal) wave velocity, and c_t is the transverse (shear) wave velocity, and $i = x, y, z$. The quantities λ and μ represent Lamé constants where μ is the shear modulus. These two constants are the only ones needed to characterize any isotropic elastic solid. Material density is given by ρ .

For this analysis, the solutions to the wave equations when y -displacements are zero are the ones of interest. This describes wave motion in the longitudinal mode. The potential functions ϕ and ψ_i must satisfy the boundary conditions

$$[\tau_{xz}]_{x=+b} = 0$$

$$[\tau_{xx}]_{x=+b} = 0$$

where b is the half-plate thickness. A solution can be found if ϕ and ψ_y have finite values.

Solutions to Eqs. (4.1) and (4.2) may be written in the following form:

$$\phi = [A_1 \cos k_d x + A_2 \sin k_d x] e^{-ik_0 z} e^{i\omega t} \quad (4.3)$$

$$\psi_y = [B_2 \cos k_c x + B_1 \sin k_c x] e^{-ik_0 z} e^{i\omega t} \quad (4.4)$$

where

$$k_d^2 = \left(\frac{\omega}{C_d} \right)^2 - k_0^2 \quad (4.5)$$

$$k_c^2 = \left(\frac{\omega}{C_c} \right)^2 - k_0^2 \quad (4.6)$$

and ω = angular frequency. Eqs. (4.3) and (4.4) can be separated into their respective symmetric and asymmetric components as follows:

$$\phi_{\text{symmetrical}} = A_1 \cos(k_d x) e^{-ik_0 z} e^{i\omega t} \quad (4.7)$$

$$\psi_{y \text{ symmetrical}} = B_1 \sin(k_c x) e^{-ik_0 z} e^{i\omega t} \quad (4.8)$$

$$\phi_{\text{asymmetrical}} = A_2 \sin(k_d x) e^{-ik_0 z} e^{i\omega t} \quad (4.9)$$

$$\psi_{y \text{ asymmetrical}} = B_2 \cos(k_c x) e^{-ik_0 z} e^{i\omega t} \quad (4.10)$$

Now boundary conditions are applied to the corresponding pairs of symmetric and asymmetric equations. For symmetric modes,

$$2ik_0k_d A_1 \sin k_d b + (k_0^2 - k_c^2) B_1 \sin k_c b = 0 \quad (4.11)$$

$$\begin{aligned} & - [(\lambda + 2\mu)k_d^2 + \lambda k_0^2] A_1 \cos k_d b \\ & + 2i\mu k_0 k_c B_1 \cos k_c b = 0 \end{aligned} \quad (4.12)$$

and for asymmetric modes,

$$-2ik_0k_d A_2 \cos k_d b + (k_0^2 - k_c^2) B_2 \cos k_c b = 0 \quad (4.13)$$

$$\begin{aligned} & - [(\lambda + 2\mu)k_d^2 + \lambda k_0^2] A_2 \sin k_d b \\ & - 2i\mu k_0 k_c B_2 \sin k_c b = 0 \end{aligned} \quad (4.14)$$

Eliminating A_1 and B_1 from Eqs. (4.11) and (4.12) results in the frequency equation for the symmetric modes:

$$\frac{\tan k_d b}{\tan k_c b} = \frac{\tanh i k_d b}{\tanh i k_c b} = -\frac{k_0^2 - k_c^2}{4k_0^2 k_d k_c} \quad (4.15)$$

Similarly, eliminating A_2 and B_2 from Eqs. (4.13) and (4.14) results in the frequency equation for the asymmetric modes:

$$\frac{\tan k_d b}{\tan k_c b} = \frac{\tanh i k_d b}{\tanh i k_c b} = -\frac{4k_0^2 k_d k_c}{k_0^2 - k_c^2} \quad (4.16)$$

The solutions of Eqs. (4.15) and (4.16) determine the possible phase velocities at any frequency and the form of the displacements for any mode. An equivalent form of the equation for symmetric modes is given by:

$$\frac{\tanh(\alpha_t b)}{\tanh(\alpha_d b)} = \frac{4k_0^2 \alpha_d \alpha_t}{(k_0^2 + \alpha_t^2)^2} \quad (4.17)$$

This is the same as Eq. (4.15), inverted, with the following parameters:

$$k_0 = \frac{\omega}{c}$$

$$\alpha_d^2 = -k_d^2 = k_0^2 - \left(\frac{\omega}{c_d}\right)^2$$

$$\alpha_t^2 = -k_t^2 = k_0^2 - \left(\frac{\omega}{c_t}\right)^2$$

To put the equation into a more useful form, it can be rewritten as a function of the phase velocity and frequency. This is done by defining the following:

$$\epsilon = \left(\frac{c_t}{c_d}\right)^2$$

$$\Gamma = \left(\frac{c}{c_t}\right)^2$$

$$W = \frac{2b}{\lambda}$$

Then α_d and α_t can be expressed as:

$$\alpha_d^2 = \left(\frac{\pi W}{b}\right)^2 (1 - \epsilon \Gamma)$$

$$\alpha_t^2 = \left(\frac{\pi W}{b}\right)^2 (1 - \Gamma)$$

where $\left(\frac{\pi W}{b}\right)^2 = k_0^2$

Now substituting into the frequency equation,

$$\frac{\tanh \pi W \sqrt{1 - \Gamma}}{\tanh \pi W \sqrt{1 - \epsilon \Gamma}} = \frac{4 \sqrt{1 - \epsilon \Gamma} \sqrt{1 - \Gamma}}{(2 - \Gamma)^2} \quad (4.18)$$

Define T and R to represent the left and right sides of Eq. (4.18):

$$T = \frac{\tanh \pi W \sqrt{1 - \Gamma}}{\tanh \pi W \sqrt{1 - \epsilon \Gamma}}$$

$$R = \frac{4 \sqrt{1 - \epsilon \Gamma} \sqrt{1 - \Gamma}}{(2 - \Gamma)^2}$$

An alternate way of expressing Eq. (4.18) is:

$$\Gamma^4 - 8\Gamma^3 + \left[24 - \frac{16\epsilon}{T^2}\right]\Gamma^2 + 16\left[\frac{1 + \epsilon}{T^2} - 2\right]\Gamma + 16\left[1 - \frac{1}{T^2}\right] = 0 \quad (4.19)$$

which yields a unique phase velocity for any frequency determined by W . For low frequencies, $W \rightarrow 0$ and

$$T = \frac{\sqrt{1 - \Gamma}}{\sqrt{1 - \epsilon \Gamma}}$$

The limiting expression is

$$[\Gamma - 4(1 - \epsilon)]\Gamma = 0 \quad (4.20)$$

The solutions to this quadratic expression are

$$\Gamma = 0$$

$$\Gamma = 4(1 - \epsilon)$$

The zero solution is trivial since it results in a zero phase velocity. Therefore the unique solution is given by

$$\Gamma = 4(1 - \epsilon) = 4 - 4\epsilon \quad (4.21)$$

Similarly, at high frequencies, $W \rightarrow \infty$ and the limiting expression becomes

$$[\Gamma^3 - 8\Gamma^2 + (24 - 16\epsilon)\Gamma + 16(1 - \epsilon)]\Gamma = 0 \quad (4.22)$$

The trivial solution is again discarded leaving

$$\Gamma^3 - 8\Gamma^2 + (24 - 16\epsilon)\Gamma + 16(\epsilon - 1) = 0 \quad (4.23)$$

Taking, for example, steel, the corresponding value of ϵ is 0.296, which gives $\Gamma = 2.816$. From this solution the phase speed $c = 5420$ m/s is calculated for low frequencies. At high frequencies, the equation produces a pair of complex roots and one real root. The complex solutions are discarded which results in a phase velocity $c = 2981$ m/s for high frequency waves. This is approximately the Rayleigh wave speed on a semi-infinite medium.

The same procedure is applied to the solution of the asymmetric wave frequency equation and results in a 4th-order polynomial in Γ as before. At low frequency, the single solution is $\Gamma = 0$. However, it has been shown that low frequency asymmetric wave propagation is governed by the equation

$$\Gamma = \frac{4}{3}k_0^2 b^2 (1 - \epsilon) \quad (4.24)$$

At high frequencies, the phase velocity again approaches the Rayleigh wave speed.

Bar Wave Propagation

The discussion so far has centered around a flat plate having two boundaries which affect wave propagation. The mathematical development can be extended to include materials with additional constraints. The next logical step would be to examine the behavior of waves traveling in a bar of arbitrary cross section. This type of wave propagation is more representative of the type observed in the present study of external skeletal fixation pin stability evaluation, namely, wave propagation in a cylindrical bar.

The theoretical development for rectangular bars is considerably more difficult than for plates. One of the obstacles is that boundary conditions cannot be completely satisfied. Phase velocity curves demonstrate two branches corresponding to wave motion along the differing width and height dimensions. For a square bar these branches coincide³⁹.

An approximation must be introduced before proceeding to a solution of the wave equations. This is done by writing the boundary stress components as products of their sine functions. This theoretical approximation agrees with experimental results when the height/width ratio is about 1/8. The frequency equation, after applying the first set of boundary conditions, looks similar to the frequency equation for a plate:

$$\frac{\tan k_2 b}{\tan k_1 b} = -\frac{4k_1 k_2 (h^2 + k_0^2)}{(h^2 + k_0^2 - k_2^2)^2} \quad (4.25)$$

where the second set of boundary conditions determines h .

Experimental investigation has shown that for a bar with a height/width ratio of 1/8, phase velocities are within a few percent of those for an infinite plate. Similarly, square cross-sections have phase velocities within a few percent of those for a circular cylindrical rod.

Discussion and Summary

These derivations illustrate several concepts introduced earlier in the chapter regarding extremes of frequency. Note that in the case of low frequency waves, phase velocity approaches the speed of plane longitudinal waves. Conversely, at high frequencies, phase velocity approaches the Rayleigh wave speed. This is an indication that at low frequencies, wave energy travels within the interior of the medium in the form of plane waves. At high frequencies, the fundamental Lamb wave mode energy (L_{11}) travels at the surface in the form of Rayleigh waves with the remainder of the energy propagating as bulk waves on the interior of the plate.

At intermediate frequencies, the wave energy is distributed between the interior and the surface and takes the form of numerous higher-order modes of both symmetric

and asymmetric waves. Energy also propagates such that particle motion is parallel to the plate surfaces. This is referred to as a shear horizontal (SH) wave which propagates at the bulk shear (transverse) wave speed and is independent of frequency⁴⁰.

Although the equations governing wave behavior in plates assumes an isotropic material, this is rarely the case in practice. Most metal plates and bars have a strong preferred orientation. Similarly, properties of composite materials vary considerably over short distances. Fortunately, these material property variations do not degrade the utility of an inspection using plate waves.

CHAPTER V

EXPERIMENTAL TECHNIQUES

Ultrasonic and Computer Hardware

The ultrasonic hardware consisted of a Panametrics 5058 ultrasonic pulser-receiver, two Gamma HP Aerotech ultrasonic transducers and a computer-based display and analysis system. The pulse waveform was captured with a Texas Instruments personal computer equipped with a PCTR-160 analog-to-digital transient recorder board. PCDAS software was subsequently used for displaying and analyzing the pulse signals. Brand names of equipment are provided for clarification and are not intended as an endorsement for any company or product. *Figure 5.1* shows the experimental setup. Pulser-receiver and PCDAS settings are shown in *Table 5.1*. *Appendix 2* describes in some detail the PCDAS software that was used for data manipulation in this experiment.

Probe Characteristics

The characteristics of the two probes used in the experiment are shown in *Table 5.2*. To obtain a subtle, repeatable change in pulse energy, the circuit damping was set to 50 Ω for Probe 1 and 500 Ω for Probe 2, where the lower value indicates a greater damping in the circuit. The net effect was a slightly greater amount of pulse voltage applied to Probe 2.

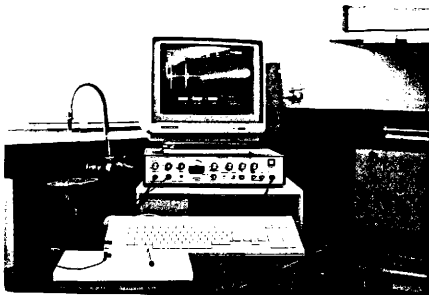


Figure 5.1 Experimental test setup showing computer display screen (top), pulser-receiver unit (middle), and computer keyboard (bottom)

Table 5.1 Pulser-receiver and PCDAS settings

Pulser-Receiver Settings	
Repetition Rate:	500 Hz
Circuit Damping:	50 Ω or 500 Ω
Pulse Energy:	200 volts
Attenuation:	none
Filtering:	1.0 MHz high pass filter
Gain:	40 dB
Pulse-Echo Mode	
Internal Triggering	

PCDAS Settings	
Sampling Rate:	10 MHz
Averaged Waveforms:	1
Display:	Full RF

Table 5.2 Probe characteristics

	Probe 1		Probe 2	
Nominal Frequency:	2.25 MHz		5.0 MHz	
Diameter:	0.635 cm 0.25 inch		0.635 cm 0.25 inch	
Spectral Parameters				
Load Material: Annealed Cast Iron Block				
(n=10)	Average	S.D.	Average	S.D.
Peak Frequency:	2.478 MHz	0.021	3.871 MHz	0.043
Center Frequency:	2.469 MHz	0.020	3.787 MHz	0.047
Half-Power Frequencies				
High:	2.786 MHz	0.059	4.496 MHz	0.039
Low:	2.153 MHz	0.057	3.078 MHz	0.071
% Bandwidth:	25.66	4.364	37.46	1.997
Skewness:	1.069	0.088	1.282	0.170

The frequency characteristics of the two probes were determined with an annealed cast iron block 3.81 x 3.81 x 6.35 cm (1.5 x 1.5 x 2.5 inches) and using the same power settings as those chosen for the *in vitro* evaluation. The displayed signal was attenuated 20 dB for Probe 1 and 40 dB for Probe 2. Probes were tested by placing them onto the center of the block with a viscous couplant and gating the first back echo with PCIDAS. Fourier analysis was performed on the gate and repeated a total of ten times for each probe. The averaged values and standard deviations obtained from this procedure are listed in Table 5.2 along with the nominal probe frequencies. Note that the true peak frequency differs significantly from the manufacturer's nominal frequency. For Probe 1 the true frequency is higher by about 0.23 MHz. For Probe 2 the true frequency is lower by about 1.13 MHz. This indicates the actual difference in frequency between the two probes is about 1.39 MHz, or half the difference which is suggested by the nominal values. This understanding is significant to the overall results of the experiment.

Probe Holder

The two ultrasonic probes were mounted in a specially-made plexiglas block designed to position the probes onto the pins in a repeatable fashion (*Figure 5.2, Appendix 3*). Tests were performed to establish the location and magnitude

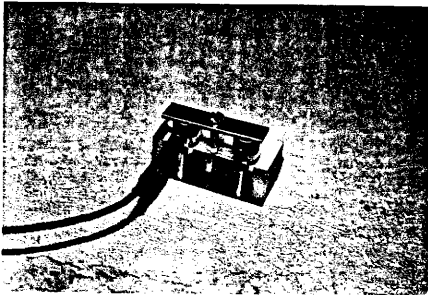


Figure 5.2 Plexiglas probe holder with probes mounted inside and connecting cable attached to Probe 1

of reflections occurring within the block.

Axial Extraction

An Instron tensile testing machine with a 900 N (200 pound) load cell provided axial pin extraction force measurements. To adapt the machine for pin pullouts, the load cell was fitted with a 0.95 cm (0.375 inch) drill chuck for gripping the exposed end of the pin, and a slotted steel hook was used to transfer crosshead loads to the bone. The lower end of the hook was held in crosshead clamping jaws while the load cell and drill chuck were held stationary (Figure 5.3). Bone specimens were not cut into individual sections prior to testing. The hook design allowed application of crosshead forces immediately adjacent to the pin so that bending stresses were not imposed in the bone. However, the hook could apply loads only to the surface of the near (lateral) cortex during extraction.

Crosshead displacement rate was set to 1.27 mm/min (0.05 inch/min) and a strip chart recorded force vs displacement at the rate of 127 mm/min (5 inch/min). The test was run until crosshead displacement reached approximately 7.6 mm (0.3 inch, about 6 minutes of loading).

Pin Preparation

Four Kirschner nonthreaded 316L stainless steel fixation pins were used. Each pin measured 2.78 by

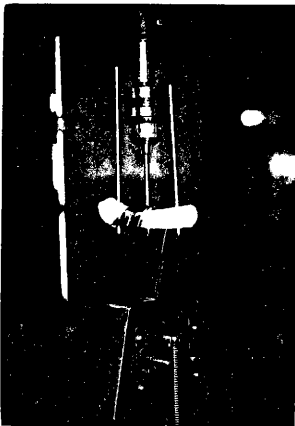


Figure 5.3 Axial extraction jig. Above is the drill chuck for gripping pins; below is the steel hook held with Instron clamping jaws

approximately 102 mm (0.1094 by 4 inches). The pins were used repeatedly, with each pin contributing 5-6 pullout measurements and at least 40 ultrasonic readings.

The individual pins were produced in pairs from a 200 mm (8 inch) double-trochar-tipped intramedullary pin by cutting the pin at its midpoint with a hand saw. The cut surfaces were polished using 100 grit and 240 grit sandpaper by placing the sandpaper on a flat surface and rubbing the pin briskly across it. The surfaces were visually inspected for roughness, unevenness and alignment. When necessary, the polishing step was repeated. After polishing, pin lengths and diameters were measured (Table 5.3).

Bone Specimens

Seven femora were collected from five adult mixed breed canines having a mass of 15 to 25 kg. Following removal of soft tissues, the femora were wrapped with saline-moistened towels and stored for 7 to 14 days at -90°C. Femora were removed from storage one or two at a time and thawed, without unwrapping, at room temperature for 6 hours prior to testing. Once exposed to open air, the specimens were kept moist by intermittent spraying with a 0.9% saline solution to preserve the properties of the bone. The wetting procedure was maintained until the completion of all testing.

Table 5.3 Pin dimension data

Pin ID#	Length, mm (inch)	Avg. Diam., mm (inch)
1	100.05 (3.939)	2.74 (0.108)
2	100.20 (3.945)	2.74 (0.108)
3	100.05 (3.939)	2.77 (0.109)
4	99.75 (3.927)	2.77 (0.109)

Pin Insertion

Pins were placed from the lateral to medial aspect along the diaphyseal region of the femur at right angles to the longitudinal and craniocaudal axes using a Kirschner 150 rpm low speed surgery drill. Four approximate implantation sites were used (proximal to distal) depending on the size of the bone and the number of pins. In all cases adjacent pins were spaced a minimum of 2.2 cm (0.87 inch) apart. Either two or four pins were implanted per bone. The joint areas were avoided to prevent penetration through cancellous bone and to take advantage of the relatively uniform cylindrical geometry of the diaphysis. The pins were implanted far enough to allow full penetration of the trochar tip through the far (medial) cortex. Drilling beyond the point of full penetration was avoided to prevent disruption of the bone-pin interface.

Experimental Design

Since this *in vitro* study could not make use of the normal tendency of a pin to loosen over a period of time, an alternative procedure had to be devised to allow a low-strength bond to be simulated. A supposition was made that near-zero strength would result by drilling a pilot hole identical in size to the pin. Likewise, a 50% reduction in holding power was expected to result from drilling the hole only through the near cortex.

A total of four implantation methods were used. Pins inserted into an individual bone were inserted according to one of the following methods:

- Method 1. Direct implantation without predrilling a pilot hole
- Method 2. Predrilling a 1.98 mm (0.0781 inch) pilot hole through both cortices
- Method 3. Predrilling a 2.78 mm (0.1094 inch) pilot hole through only the near (lateral) cortex
- Method 4. Predrilling a 2.78 mm (0.1094 inch) pilot hole through both cortices

Implantation method was varied from trial to trial. To minimize unwanted effects of the insertion procedure, drill speed and drilling force were maintained as nearly constant as possible for all implantations.

Data Collection

Once several pins had been implanted into a femur, the pulser-receiver and PCDAS were set as described earlier. To obtain an ultrasonic reading, a small drop of glycerin was placed onto the flat end of the pin and the probe holder was seated over the pin. The probe holder was free to rotate around the long axis of the pin. Once in position, the probe holder was gently rotated back and forth to ensure that any small bubbles of air trapped between the probe face and the pin could escape, thereby maximizing the transmission coefficient of the pin-probe interface. A waveform signal was then captured and saved on disk, after which the probe

holder was removed from the pin. An additional drop of couplant was added to the pin and the probe holder was repositioned. Again the waveform was saved. This process was repeated about ten times. Once a set of data had been taken with Probe 1, Probe 2 was connected and the process was repeated. This produced two sets of ultrasonic data which were measured independently of each other.

Immediately following ultrasonic evaluation, the pins underwent axial extraction. The outer femoral diameter was measured across the implantation site on both sides of the pins following extraction tests.

After completion of 22 trials, the four fixation pins were sectioned longitudinally and transversely and mounted in phenolic resin for microstructural analysis and hardness testing.

In choosing waveform files for detailed experimental analysis, each file on disk was visually inspected and four which showed the highest signal strength were selected from each set. Four files were chosen to provide a basis for calculating repeatability of the ultrasonic measurements.

Due to minor difficulties with data digitization, it would have been inappropriate to randomly select the waveform files (not all of the saved waveforms represented the best possible signal). The author's judgment was used in selecting four files which would represent the data had a digitization problem not been present. A total of 176

waveform files were selected for analysis.

Ultrasonic Attenuation Parameter

An attenuation parameter was chosen to represent the amount of energy contained in the displayed waveform. This was termed the Pulse Energy Cutoff Point. It was obtained by taking Fourier transformations at regular intervals along the time domain of the pulse display. Using this process, a point was identified where the frequency content of the signal began to fall toward zero, indicating a progressive loss of pulse energy. The Fourier transformation variable chosen to identify the Pulse Energy Cutoff Point was center frequency (F_{cen}) and the Pulse Energy Cutoff Point was arbitrarily selected as the first observed drop in F_{cen} below a value of 500 kHz. In the extreme case, an F_{cen} value of zero would imply a value of zero pulse energy. This method is similar to measuring changes in the pulse signal amplitude, but is much more accurate.

The 176 wave files underwent Fourier transformation at 1 μ s intervals using the smallest allowable gate size of 3.2 μ s. For each wave file evaluated, a total of 395 datapoints were collected. *Table 5.4* shows the first 35 such datapoints of an arbitrarily selected FFT file. The 395 values of F_{cen} were subsequently averaged in sets of 5 to reduce the total number of datapoints to 79. *Table 5.5* shows the reduction of the data found in *Table 5.4*. Lastly, the 79 datapoints were

Table 5.4 Sample of FFT data before primary reduction

(1)	(2)	(3)	(4)	(5)	(6)	(7)	(8)
0.000	32	1.172	1.504	1.348	1.338	24.818	1.125
1.000	32	2.324	2.617	2.480	2.471	11.858	1.143
2.000	32	2.227	2.734	2.520	2.480	20.472	1.364
3.000	32	1.953	2.656	2.109	2.305	30.508	0.286
4.000	32	1.035	1.426	1.250	1.230	31.746	1.222
5.000	32	2.168	2.539	2.363	2.354	15.768	1.111
6.000	32	2.246	2.520	2.383	2.383	11.475	1.000
7.000	32	3.223	3.535	3.359	3.379	9.249	0.778
8.000	32	3.184	3.477	3.340	3.330	8.798	1.143
9.000	32	3.301	3.750	3.477	3.525	12.742	0.643
10.000	32	3.281	3.574	3.418	3.428	8.547	0.875
11.000	32	1.895	2.246	2.070	2.070	16.981	1.000
12.000	32	2.969	3.262	3.105	3.115	9.404	0.875
13.000	32	2.813	3.301	3.066	3.057	15.974	1.083
14.000	32	2.559	2.852	2.695	2.705	10.830	0.875
15.000	32	2.988	3.281	3.145	3.135	9.346	1.143
16.000	32	3.027	3.359	3.203	3.193	10.398	1.125
17.000	32	3.066	3.340	3.203	3.203	8.537	1.000
18.000	32	2.832	3.359	3.047	3.096	17.035	0.688
19.000	32	3.125	3.438	3.281	3.281	9.524	1.000
20.000	32	3.027	4.141	3.555	3.584	31.063	0.900
21.000	32	3.398	4.063	3.828	3.730	17.801	1.833
22.000	32	3.379	4.102	3.750	3.740	19.321	1.056
23.000	32	3.613	4.238	3.770	3.926	15.920	0.333
24.000	32	2.129	2.461	2.285	2.295	14.468	0.889
25.000	32	1.953	2.363	2.168	2.158	19.005	1.100
26.000	32	1.777	2.031	1.895	1.904	13.333	0.857
27.000	32	2.207	2.559	2.383	2.383	14.754	1.000
28.000	32	2.012	2.363	2.188	2.188	16.071	1.000
29.000	32	3.184	3.477	3.359	3.330	8.798	1.500
30.000	32	3.379	3.691	3.535	3.535	8.840	1.000
31.000	32	3.496	3.770	3.633	3.633	7.527	1.000
32.000	32	4.102	4.434	4.277	4.268	7.780	1.125
33.000	32	4.844	5.000	5.000	4.922	3.175	8.000
34.000	32	4.648	4.941	4.805	4.795	6.110	1.143

(1) Time, microseconds (5) Peak Frequency, MHz
(2) Gate Width, number of points (6) Center Frequency, MHz
(3) Lower Half-Power Frequency, MHz (7) Bandwidth, percent
(4) Upper Half-Power Frequency, MHz (8) Skewness, nondimensional

Table 5.5 Sample of FFT data after primary reduction

(1)	(6*)
0.000	1.965
5.000	2.994
10.000	2.875
15.000	3.182
20.000	3.455
25.000	2.393
30.000	4.231

(1) Time, microseconds
(6*) Center Frequency, forward-averaged, MHz

plotted (time vs avg. center frequency) for visual identification of the Pulse Energy Cutoff Point.

Reference Values

To account for differences in the response of each pin to an acoustic pulse, the pins were tested while unimplanted (unstressed). Data collection procedures were identical to those described earlier except that the probe holder was inverted to provide support for the pins.

Additional Ultrasonic Parameters

The reference values of Pulse Energy Cutoff Point were used to calculate two additional attenuation parameters. The first calculation involved taking the difference between the reference value and those values obtained during testing of an implanted pin. This difference is termed the Pulse Energy Time Shift and is expressed in μs :

$$\text{Pulse Energy Time Shift} = \text{Baseline Reference Cutoff} \\ - \text{Pulse Energy Cutoff Point}$$

The second calculation involved taking the Pulse Energy Time Shift and dividing it by the reference value to produce a nondimensional Percent Time Shift:

$$\text{Percent Time Shift} = \frac{\text{Pulse Energy Time Shift}}{\text{Reference Cutoff}}$$

All ultrasonic parameters described in this chapter were used for statistical modeling.

Statistical Analysis

Statistical analysis was used to identify and quantify the strength of relationships between input variables (pin number, bone number, attenuation parameters, etc.) and the response variable (extraction force). This in turn pointed to experimental factors which singularly, or in combination with other factors, resulted in a strong predictive relationship.

Scatter plots were produced to gain a qualitative understanding of the relationships between variables, strength of trends, and variability. The following factors were plotted against extraction force: Pulse Energy Cutoff Point, Pulse Energy Time Shift, Percent Time Shift, Implantation Method, Bone Number, Bone Diameter, Implantation Site, and Pin Number.

The general linear model (GLM) and analysis of variance (ANOVA) was utilized to determine how well each variable could predict extraction force, alone and in combination with other variables. A total of 133 models were tested.

In limiting the number of regression models tested, two guidelines were followed. Ultrasonic data were used by pairing data from the two probes. Further, different ultrasonic attenuation parameters were not combined (for example, Cutoff Point was not combined with Time Shift).

Four class variables appeared in the experiment. Specifically, there were (1) four pins, (2) four

implantation methods, (3) four implantation sites, and (4) seven bone specimens. Analysis of variance was used to determine what effects could be attributed to the different levels of these classes. Duncan's multiple range test (level of significance $\alpha = 0.05$) was performed on the extraction force data to test for differences due to individual pins, methods, sites, or bones.

A predictor model was chosen based on the minimum mean squared error (MSE) of the residual force terms. After selecting a prediction model, the residual force values were computed and used in subsequent residual plots to check for trends.

CHAPTER VI

RESULTS

Ultrasonic Data

Figures 6.1 through 6.6 show the 6 ultrasonic parameters plotted against extraction force. Each figure is plotted along with a linear least-squares curve fit. Data tables are given in Appendix 5. Figure 6.1 and Figure 6.2 show an inverse relationship between ultrasonic measurements and extraction forces, while Figure 6.3 through Figure 6.6 show a direct relationship.

Although several of the figures show broad trends with considerable scatter, Figure 6.4 and Figure 6.6 show stronger trends with reduced scatter. Figure 6.6 in particular appears to have the lowest scatter of data points lying in the low extraction force range. The figures show that in these two cases, using a fixed zero-stress reference value for each pin reduced the data scatter considerably.

Other Experimental Factors

Figure 6.7 through Figure 6.11 show the remaining (non-ultrasonic) experimental factors plotted against extraction force. Figure 6.7 reveals a tendency for Implantation Methods 1, 2, and 3 to produce similar extraction forces with only Method 4 resulting in a considerably lower extraction force. Bone Number (Figure 6.8) does not appear

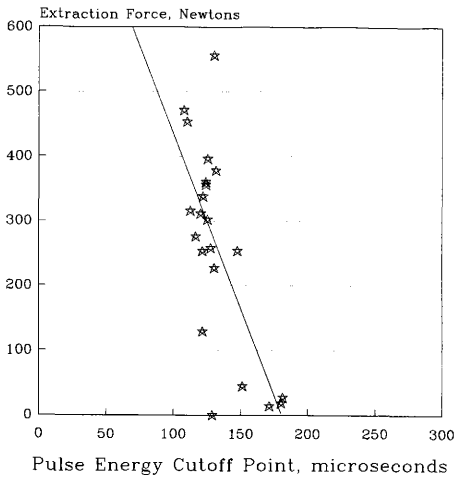


Figure 6.1 Probe 1 Pulse Energy Cutoff Point vs Extraction Force

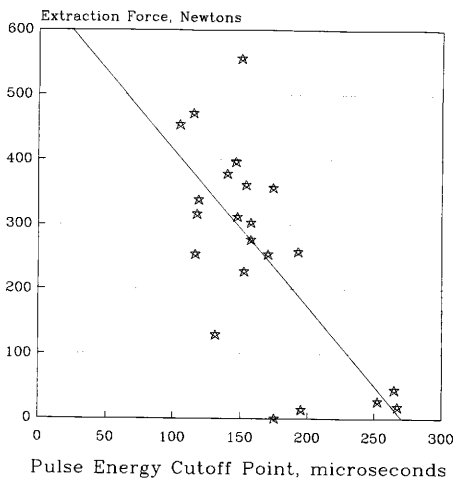


Figure 6.2 Probe 2 Pulse Energy Cutoff Point vs Extraction Force

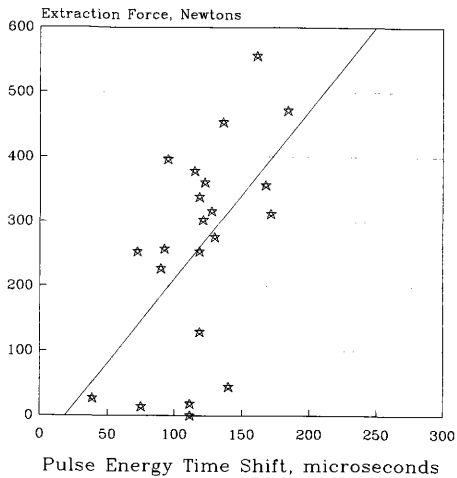


Figure 6.3 Probe 1 Pulse Energy Time Shift vs Extraction Force

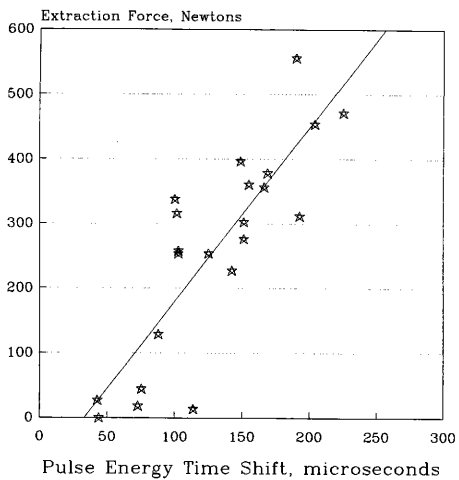


Figure 6.4 Probe 2 Pulse Energy Time Shift vs Extraction Force

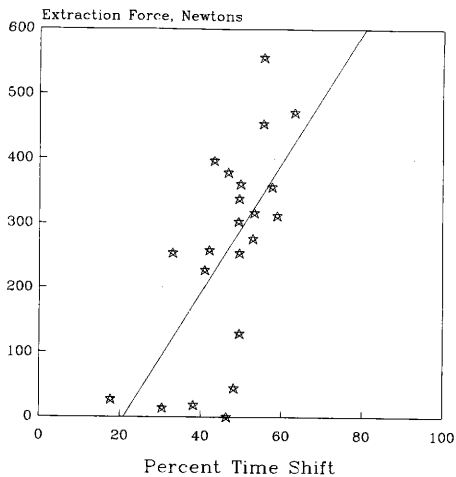


Figure 6.5 Probe 1 Percent Time Shift vs Extraction Force

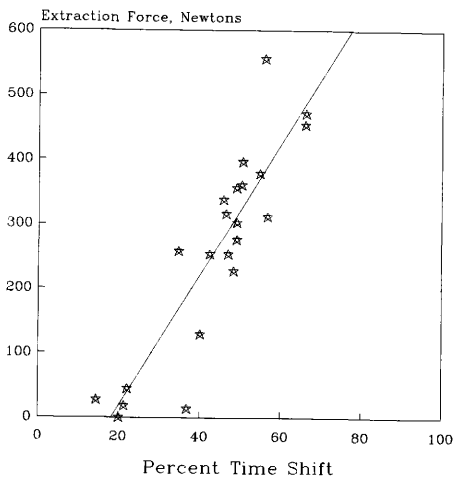


Figure 6.6 Probe 2 Percent Time Shift vs Extraction Force

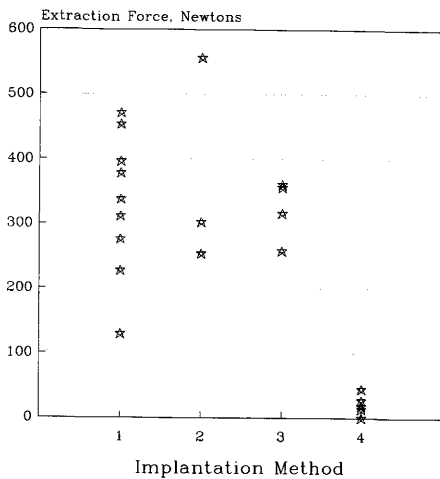


Figure 6.7 Implantation Method vs Extraction Force

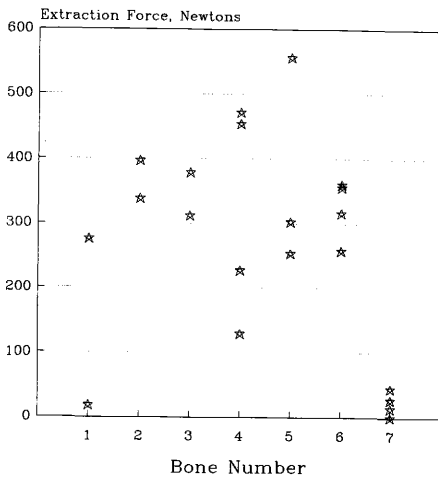


Figure 6.8 Bone Number vs Extraction Force

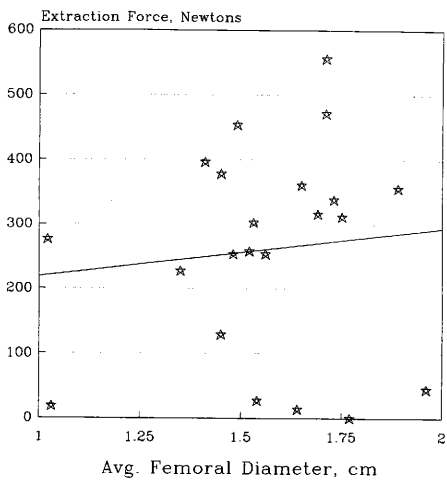


Figure 6.9A Averaged Femoral Diameter vs Extraction Force

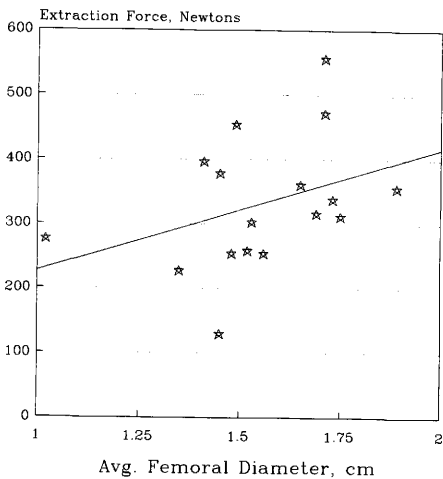


Figure 6.9B Averaged Femoral Diameter vs Extraction Force, excluding data for Implantation Method 4

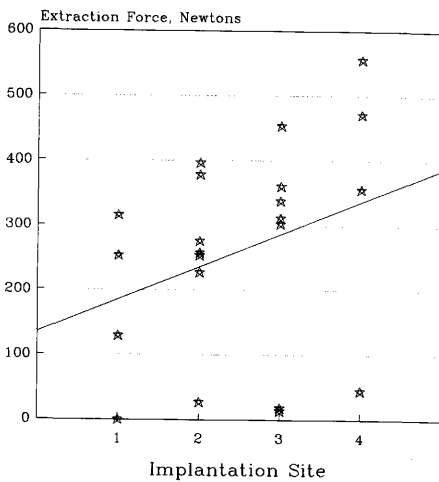


Figure 6.10A Implantation Site vs Extraction Force

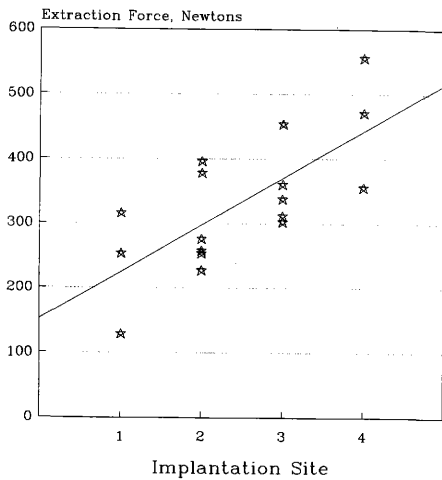


Figure 6.10B Implantation Site vs Extraction Force, excluding data for Implantation Method 4

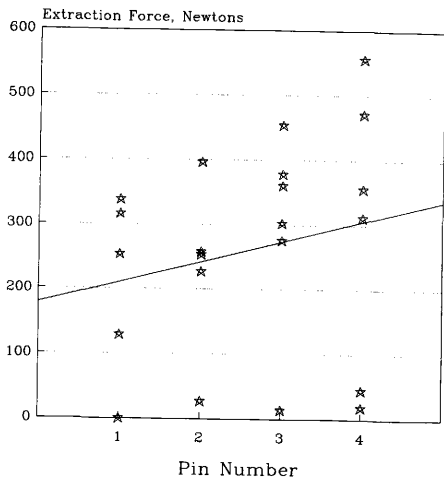


Figure 6.11A Pin Number vs Extraction Force

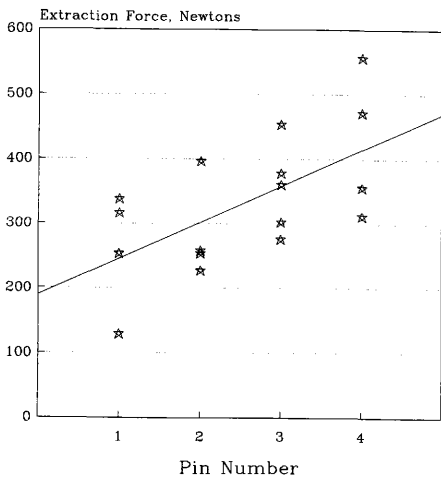


Figure 6.11B Pin Number vs Extraction Force, excluding data for Implantation Method 4

to reveal a trend. From this plot one can get an idea of the amount of scatter often associated with extraction forces. With the exception of Bone 1, each pin in a given bone was treated with the same implantation method. *Figures 6.9A and 6.9B* show Averaged Femoral Diameter plotted against extraction force. Noting that bones subjected to Implantation Method 4 (having almost zero extraction force) are not representative of the potential holding power of the bone, these data are omitted from *Figure 6.9B*. In this way the trend for greater extraction force with greater bone diameter is more apparent. The same modification holds for Implantation Site (*Figures 6.10A and 6.10B*) and Pin Number (*Figures 6.11A and 6.11B*). A stronger trend is seen without Implantation Method 4 data.

Statistical Analysis

Once scatter plots were produced, statistical analysis was used to quantify relationships between input and response variables. Each of the available factors was used to construct linear regression models for predicting extraction forces. 133 models were evaluated, none using more than 7 inputs. *Tables 6.1 and 6.2* show a summary of modeling, while *Appendix 5* lists data for all models.

At the top of *Table 6.1*, five experimental factors are listed along with the three paired sets of ultrasonic data. This is the recorded information available for predicting

Table 6.1 Individual variables and paired ultrasonic data

Individual Variables

PIN	BONE	SITE	METH	DIAM	CUT1	CUT2	SFT1	SFT2	PCT1	PCT2	R ²	p>F	MSE
+	-	-	-	-	-	-	-	-	-	-	.0512	.3112	1298.9
-	+	-	-	-	-	-	-	-	-	-	.0924	.1691	1242.6
-	-	+	-	-	-	-	-	-	-	-	.1011	.1492	1230.6
-	-	-	+	-	-	-	-	-	-	-	.4509	.0006	751.8
-	-	-	-	+	-	-	-	-	-	-	.0118	.6299	1352.9
-	-	-	-	-	+	-	-	-	-	-	.5016	.0002	682.3
-	-	-	-	-	-	+	-	-	-	-	.5021	.0002	681.7
-	-	-	-	-	-	-	+	-	-	-	.3095	.0072	945.3
-	-	-	-	-	-	-	-	+	-	-	.7123	.0001	393.9
-	-	-	-	-	-	-	-	-	+	-	.4179	.0012	796.9
-	-	-	-	-	-	-	-	-	-	+	.7944	.0001	281.5

Paired Ultrasonic Data

PIN	BONE	SITE	METH	DIAM	CUT1	CUT2	SFT1	SFT2	PCT1	PCT2	R ²	p>F	MSE
-	-	-	-	-	+	+	-	-	-	-	.5412	.0006	661.2
-	-	-	-	-	-	-	+	+	-	-	.7135	.0001	412.8
-	-	-	-	-	-	-	-	-	+	+	.7964	.0001	293.4

Table 6.2 Worst and best in each category

PIN	BONE	SITE	METH	DIAM	CUT1	CUT2	SFT1	SFT2	PCT1	PCT2	R ²	p>F	MSE
<u>Single Ultrasonic Data</u>													
-	-	-	-	-	-	-	+	-	-	-	.3095	.0072	945.3
-	-	-	-	-	-	-	-	-	-	+	.7944	.0001	281.5
<u>Paired Ultrasonic Data</u>													
-	-	-	-	-	+	+	-	-	-	-	.5412	.0006	661.2
-	-	-	-	-	-	-	-	-	+	+	.7964	.0001	293.4
<u>No Ultrasonic Data and One Factor</u>													
-	-	-	-	+	-	-	-	-	-	-	.0118	.6299	1352.9
-	-	-	+	-	-	-	-	-	-	-	.4509	.0006	751.8
<u>No Ultrasonic Data and Two Factors</u>													
+	-	-	-	+	-	-	-	-	-	-	.0601	.5549	1354.5
-	-	+	+	-	-	-	-	-	-	-	.5784	.0003	607.6
<u>No Ultrasonic Data and Three Factors</u>													
+	-	+	-	+	-	-	-	-	-	-	.1093	.5441	1355.0
-	+	+	+	-	-	-	-	-	-	-	.6151	.0005	585.5
<u>No Ultrasonic Data and Four Factors</u>													
+	+	+	-	+	-	-	-	-	-	-	.2815	.2043	1157.3
-	+	+	+	+	-	-	-	-	-	-	.6164	.0018	617.9
<u>No Ultrasonic Data and Five Factors</u>													
+	+	+	+	+	-	-	-	-	-	-	.6168	.0053	655.7

Table 6.2 Continued

PIN	BONE	SITE	METH	DIAM	CUT1	CUT2	SFT1	SFT2	PCT1	PCT2	R ²	p>F	MSE
<u>One Pair of Ultrasonic Data plus One Other Factor</u>													
-	-	-	-	+	+	+	-	-	-	-	.5413	.0024	697.8
-	-	+	-	-	-	-	-	-	+	+	.8044	.0001	297.5
<u>One Pair of Ultrasonic Data plus Two Other Factors</u>													
-	+	-	+	-	+	+	-	-	-	-	.5775	.0039	680.5
+	-	+	-	-	-	-	+	+	-	-	.8270	.0001	278.6
<u>One Pair of Ultrasonic Data plus Three Other Factors</u>													
-	+	-	+	+	+	+	-	-	-	-	.5973	.0075	689.2
+	+	+	-	-	-	-	+	+	-	-	.8293	.0001	292.2
<u>One Pair of Ultrasonic Data plus Four Other Factors</u>													
+	+	-	+	+	+	+	-	-	-	-	.7459	.0008	463.9
+	+	+	+	-	-	-	+	+	-	-	.8373	.0001	297.0
<u>One Pair of Ultrasonic Data plus Five Other Factors</u>													
+	+	+	+	+	+	+	-	-	-	-	.7777	.0011	434.8
+	+	+	+	+	-	-	+	+	-	-	.8374	.0001	318.0

extraction forces. The heading names represent the following:

PIN = Pin Number
 BONE = Bone Number
 SITE = Implantation Site
 METH = Implantation Method
 DIAM = Bone Diameter
 CUT1, CUT2 = Pulse Energy Cutoff Point data for Probe 1 and Probe 2 respectively
 SFT1, SFT2 = Pulse Energy Time Shift data for Probe 1 and Probe 2 respectively
 PCT1, PCT2 = Percent Time Shift data for Probe 1 and Probe 2 respectively

Each row in the table represents an individual statistical model which includes one or more inputs. Each column represents a variable which can be included in the model. The "+" under a column heading indicates a variable which was included in the model, while a "-" indicates a variable which was excluded from the model. In each model there is an intercept term which does appear on this chart. The intercept term is not directly referenced in subsequent discussion, but is understood to be present in all cases.

On the far right side of the table, three statistical quantities are listed for each model. R^2 is the fraction of variation in response (extraction force) which is explained by the input ($0 \leq R^2 \leq 1$, where zero means no relationship and one means a perfect relationship. It is also the square of the correlation coefficient between observed and

predicted responses). The quantity $p>F$ shows whether a relationship between input variables and the response variable is significant (it is the probability that all model slope parameters are zero. A value of less than 0.05 is considered statistically significant). Finally, MSE is the mean squared error of residual force terms in the regression model (the square of the average error between observed and predicted responses). A good model contains the fewest number of input variables that achieves high R^2 , low $p>F$, and low MSE . Under these conditions one may conclude with confidence that a strong relationship exists between input variables and the response variable^{41,42}. Note that for these regression data, analysis was performed using units of pounds and that MSE has units of pounds squared.

The top portion of *Table 6.1* shows each of the input variables modeled alone. By scanning the right-hand columns, it becomes clear that among non-ultrasonic data, only Implantation Method achieves significance ($p>F = 0.0006$) and explains a sizable portion of extraction forces ($R^2 = 0.4509$). Pulse Energy Cutoff Point data for both probes accounts for about the same R^2 and MSE . When Baseline Reference Cutoff is used to compute Pulse Energy Time Shift, Probe 1 predicts less well while Probe 2 prediction improves. When Percent Time Shift is computed, Probe 1 still predicts poorly but Probe 2 shows a further improvement. By comparing the upper and lower portions of *Table 6.1*, it is

clear that Probe 1 did not account for a notable improvement in R^2 when modeled in combination with Probe 2. Nevertheless, Probe 1 and Probe 2 were used in combination to reduce the number of regression analyses.

Table 6.2 shows the best and worst model for each category based on the lowest *MSE*. One ultrasonic parameter (PCT2) singularly resulted in an R^2 of 0.7944 with an *MSE* of 281.5. Combining all five non-ultrasonic factors (PIN, BONE, SITE, METH, DIAM) produced an R^2 of 0.6168 with an *MSE* of 655.7. Removing only METH from this model results in a drop in R^2 to 0.2815 and an increase in *MSE* to 1157.3 (not shown on this table). From these observations it becomes clear that ultrasonic data accounts for most of the variation in extraction forces. The non-ultrasonic data may lend support to the model but cannot account for extraction forces nearly as well as ultrasonic data.

Using the available regression data, a model was selected for predicting extraction forces. The lowest observed *MSE* was 278.6 (Table 6.2 and Appendix 5). This model included PIN, SITE, SFT1 and SFT2 and showed an R^2 of 0.8270. The model equation, in standard regression form, is

$$Y_i = \beta_0 + \beta_1 x_{1i} + \beta_2 x_{2i} + \beta_3 x_{3i} + \beta_4 x_{4i} + e_i$$

$$\begin{aligned} \text{Force (N)} = & 749.42 - 84.64(\text{PIN}) + 45.66(\text{SITE}) \\ & + 0.5905(\text{SFT1}) + 3.019(\text{SFT2}) \end{aligned}$$

Scatter plots of residual force variables show reasonably random data patterns for this model. Calculation of confidence intervals show that extraction forces can be predicted to within about ± 180 N (± 40 lb) from the indicated data with 95% confidence. *Figure 6.12* shows observed forces plotted against predicted forces. Note the linearity and constant scatter about the regression line indicating a good fit.

Table 6.3 summarizes the results of means testing. Note that neighboring means with the same symbol beside them (*, & or #) are not found to be significantly different ($\alpha = 0.05$). The value *N* is the number of observations per level (the sum of the *N* values is the total number of observations, 22). The last column is the level number for that variable (1, 2, 3, etc.). The first test (PIN) shows that a difference of 90 N (20 lb) was obtained between the lowest and highest extraction forces. However, due to high variance, the means are not significantly different. The second test (BONE) shows Bone 1 and Bone 7 had significantly lower mean extraction forces compared to all others, but that Bones 1, 4, and 6 were similar. The third test (METH) shows that Implantation Method 4 was significantly different from the other three methods. The final test (SITE) shows that a factor of two was observed between Implantation Site 1 and 4 and was found to be significantly different.

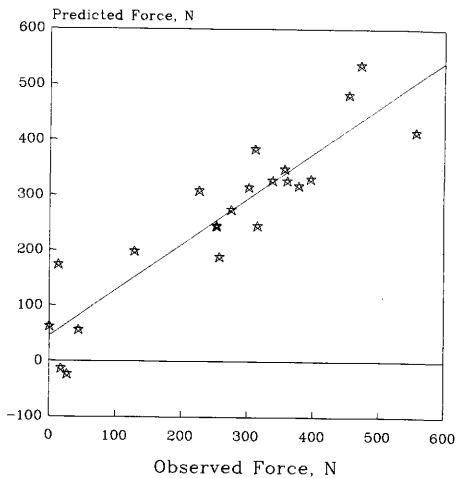


Figure 6.12 Observed Force vs Predicted Force

Table 6.3 Results of means testing (d.f. = 9, α = 0.05)

Group	Mean Extraction Force, N (lb)	N	PIN
*	297.3 (66.83)	6	3
*	292.8 (65.83)	6	4
*	232.2 (52.20)	5	2
*	207.3 (46.60)	5	1
Group	Mean Extraction Force, N (lb)	N	BONE
*	367.0 (82.50)	2	2
*	344.7 (77.50)	2	3
*	341.4 (76.75)	4	5
& *	322.5 (72.50)	4	6
& *	320.3 (72.00)	4	4
& #	146.8 (33.00)	2	1
#	21.1 (4.75)	4	7
Group	Mean Extraction Force, N (lb)	N	METH
*	341.4 (76.75)	4	2
*	331.1 (74.44)	9	1
*	322.5 (72.50)	4	3
#	20.5 (4.60)	5	4
Group	Mean Extraction Force, N (lb)	N	SITE
*	357.0 (80.25)	4	4
# *	265.0 (59.57)	7	3
# *	251.0 (56.43)	7	2
#	174.6 (39.25)	4	1

Repeatability

A set of repeated measurements were taken for each pin during ultrasonic testing. Subsequently, a sample of four measurements was chosen in order to calculate an average value of Pulse Energy Cutoff Point. The standard deviation was also calculated for each set of four measurements and divided by the mean to produce a percent error relative to the mean of the observations (known as the coefficient of variance, or C.V.). The error values (all pins combined) are plotted against extraction forces in *Figure 6.13* and *Figure 6.14* for Probe 1 and Probe 2 respectively. From the graphs it appears that variability does not depend on extraction force, but is fairly evenly distributed over the entire range of forces. Furthermore, Probe 1 shows lower error than Probe 2. The maximum variability associated with Probe 1 is less than 14% with only 3 out of 22 values (13.6%) being greater than 10% and an average error of 4.8%. The maximum variability associated with Probe 2 is over 20% with 8 out of 22 values (36.4%) being greater than 10% and an average error of 8.73%. These results indicate Probe 1 produced results which were more easily repeated than Probe 2.

In the previous paragraph the variability was seen to be independent of extraction force. However, variability is not necessarily independent of the individual pins. The ultrasonic measurement error data were broken down according to pin and are given in *Table 6.4*. For Probe 1, the average

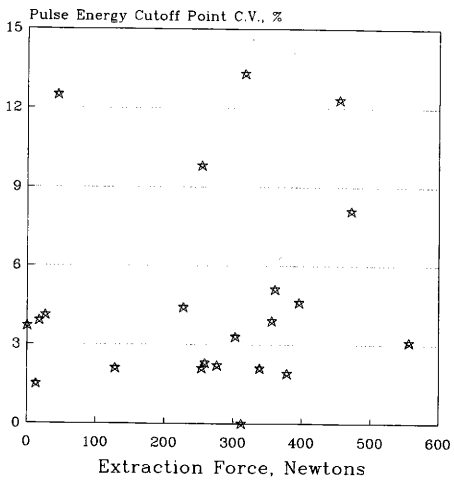


Figure 6.13 Extraction Force vs Probe 1 Coefficient of Variance

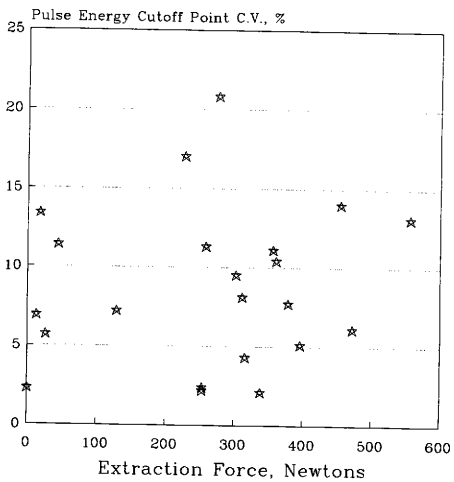


Figure 6.14 Extraction Force vs Probe 2 Coefficient of Variance

Table 6.4 Error in Pulse Energy Cutoff Point, by Pin

	Probe 1 Error, C.V.%	Probe 2, Error, C.V.%
Pin 1:	2.1	2.1
	2.1	2.2
	2.1	2.3
	3.7	4.3
	13.3	7.2
	AVG: 4.7	3.6
Pin 2:	2.3	2.4
	4.1	5.1
	4.4	5.7
	4.6	11.3
	9.8	17.0
	AVG: 5.0	8.3
Pin 3:	1.5	6.9
	1.9	7.7
	2.2	9.5
	3.3	10.4
	5.1	14.0
	12.3	20.8
AVG: 4.4	11.6	
Pin 4:	0.0	6.1
	3.1	8.1
	3.9	11.1
	3.9	11.4
	8.1	13.1
	12.5	13.4
AVG: 5.3	10.5	

errors for each pin are very similar ($\approx 5\%$). However, Probe 2 shows low error for Pin 1 while the highest error is associated with Pins 2, 3, and 4.

In addition to the *in vitro* error values, there is error associated with ultrasonic measurements taken when the pin is not implanted (in the stress-free condition). In this case, the average error for Probe 1 is 6.8% while the average error for Probe 2 is 5.5%. Note that only four data points are associated with each of these error values.

Error associated with the extraction force measurements could not be assessed due to the unrepeatable nature of this test. Extraction forces are assumed to have been measured without error, but any error which is present will be absorbed into the model error term e_i .

Microstructure

No differences in pin microstructure were found nor were any defects or inclusions detected (*Appendix 4* gives methods and micrographs). The grain orientation clearly ran in the longitudinal direction of the pin, indicating that pins were probably manufactured by an extrusion or drawing process. Owing to the degree of deformation during manufacture, individual grain boundaries could not be observed nor could the grain size be determined. There was no evidence of grain recrystallization. Grains appeared identical throughout the cross section.

Hardness Testing

Pin hardness data is given in *Table 6.5* (methods are briefly described in *Appendix 4*). Note that only one measurement was possible on the transverse cut while four readings were taken on each of the longitudinal cuts. The transverse hardness is somewhat lower than the longitudinal hardness and varies over a wider range. The longitudinal hardness shows better consistency although Pin 4 appears to have a slightly lower value. Small C.V. indicates that measurements were quite repeatable.

Table 6.5 Hardness data (Rockwell C scale)

Pin Number	Transverse Plane	Longitudinal Plane, avg. (C.V.)
1	25.8	36.4 (1.7%)
2	28.3	36.3 (0.8%)
3	29.9	36.2 (1.0%)
4	30.6	34.1 (1.9%)

CHAPTER VII

DISCUSSION

Ultrasonic Data

As seen in *Chapter 6*, all ultrasonic data (*Figures 6.1-6.6*) were found to be statistically significant in predicting extraction forces. The best single predictor of extraction forces was Percent Time Shift for Probe 2, where 79% of the variation in extraction force was accounted for.

Data taken with Probe 1 showed a marked decrease in R^2 when the Baseline Reference value was taken into account. The reason for this is not known. Intuitively one would have expected the data to improve its prediction capability, as in the case of Probe 2 data. The R^2 value for Probe 2 improved by almost 60% over its original value, while Probe 1 showed an overall drop of 20%. Considering how the original values of R^2 were identical for Probe 1 and Probe 2, this discrepancy in prediction strength is even more perplexing. Perhaps the explanation is related to the difference in the original Pulse Energy Cutoff Values. Probe 1 data ranged from 107 to 181 μs , while Probe 2 data ranged from 105 to 267 μs . From this observation it appears that some characteristic of Probe 2 was intrinsically more sensitive to pin stability, although this was not immediately apparent based on observation of the R^2 value.

The relationship between Percent Pulse Energy Cutoff

Point (Probe 2) and extraction force is probably about as strong as one could reasonably expect to get. Although it should be possible to reduce data scatter further, a perfect correlation should never be anticipated. This is due to the fact that physical characteristics of the bone-pin interface which affect extraction force do not necessarily affect ultrasonic attenuation, and vice versa. The two tests are in fact fundamentally different evaluations of a complex phenomenon referred to as pin stability. Initially one might be put off by this statement, but two points should be considered. First, the ultrasonic tests were quite repeatable, indicating that interfacial characteristics affecting ultrasonic attenuation could be measured repeatably. Second, extraction force is not necessarily the best method of quantitating pin stability. The fact seems to be that at present there are simply no alternatives.

Figures 6.3-6.6 have a common feature which should be briefly mentioned. In each case, the regression curve does not have a (0,0) intercept. Even when interfacial stresses are so low that no extraction force is registered, the slightest contact between bone and pin will produce measurable attenuation. This is an example of how attenuation demonstrates sensitivity to interfacial conditions which cannot be characterized with axial extraction.

Other Experimental Factors

Implantation Methods did not achieve the intended results, with the exception of Method 4. Methods 1-3 produced the same average extraction forces. Ironically, the method expected to show the least variability in fact had the highest (Method 1, *Figure 6.7*). This points to the difficulty in obtaining repeatable results even with a standardized implantation method. For Method 3, a 2.78 mm pilot hole was drilled through the near cortex to reduce extraction forces by about 50%. However, the average extraction force was no different than for Methods 1 and 2, suggesting that the far cortex accounted for a larger share of the pin holding power than the near cortex.

Another problem with Implantation Method was that only one data point appeared between 45 and 225 N (10 and 50 lbs). No observations can be made with regard to scatter and fit in this range of extraction forces.

Bone Number (*Figure 6.8*) did not play a significant role in the prediction model since each bone resulted in about the same extraction forces. This suggests that bone properties affecting extraction force, including diameter, were similar. Bone 7 appears to be quite different from the rest, but this is due to the effect of Implantation Method 4. The highest data scatter is associated with Bone 4 and cannot be accounted for by known factors.

Knowledge of bone diameter played a minimal role in

prediction of extraction forces. This is presumed to be for two reasons. As contrasted between *Figure 6.9A* and *6.9B*, data resulting from Implantation Method 4 tended to eliminate a natural trend for larger bones to show higher extraction forces. In addition, the bone sizes did not vary over a wide range. It is not known how much variation in extraction force would be observed with bones of assorted sizes. This has the potential to produce significant effects in future studies.

Figures 6.10A,B and *6.11A,B* should be considered as a group for the following reason. In the majority of cases (16/22), each level of Implantation Site corresponds to the equivalent level of Pin Number. That is, Pin 1 was implanted in Site 1, Pin 2 was implanted in Site 2, and so on. This presents a complication referred to as *confounding*. When the level of two or more predictor variables does not change with respect to one another, any trends which appear between these data cannot be separated. As seen in the figures, both Implantation Site and Pin Number show a marked upward trend. However, the source cannot be inferred. The trend may be due either to Site or Pin, or both. Intuitively, one might look for a relationship between some other variables to help explain this trend. *Figure 7.1* shows Pin Number plotted against Bone Diameter. This figure shows the same basic trend of *Figures 6.10A,B* and *6.11A,B*. Pin 4 was implanted through the largest diameter of bone and showed the highest

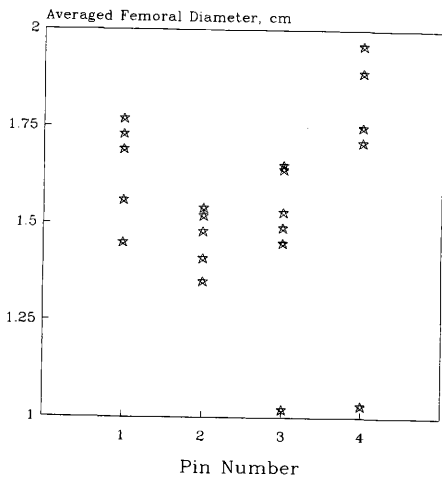


Figure 7.1 Pin Number vs Averaged Femoral Diameter

extraction forces. This might suggest that implantation site, by virtue of the differences in bone diameter, was responsible for the trend. Otherwise, there may be some difference in the pins which caused a trend. In either case, no conclusions are possible from the available data.

Statistical Analysis

As described in *Chapters 5 and 6*, the best prediction model was chosen based on lowest mean squared error (MSE). This process does not normally result in selection of the model having highest R^2 . In fact, several models had slightly higher R^2 , but they contained a greater number of inputs. In modeling, it is desirable to use the minimum number of variables needed to adequately describe the response. Unfortunately, a selection procedure based simply on R^2 will always choose the model having the maximum number of inputs.

As seen in *Appendix 5*, 40/133 of the models (30%) resulted in an R^2 of 0.8000 or higher, while 50/133 (38%) resulted in an R^2 of 0.7000 to 0.7999. The number of models having R^2 lower than 0.7000 was 43/133 (32%). Most of these (24/43, 56%) did not contain ultrasonic data. The models having R^2 greater than 0.7000 (90/133, 68%) all contained ultrasonic data, a further indication of the importance of this data to prediction strength. As expected, the highest R^2 (0.8374) was associated with a model having 7 inputs, but

this value was only slightly higher than for the 4 variable model having lowest MSE.

A further examination of the selected model is in order. It has already been shown that Pin Number and Implantation Site were confounded and thus are highly correlated ($\rho = 0.85$). These variables both appear in the model. Likewise, the ultrasonic data from Probe 1 and Probe 2 are moderately correlated ($\rho = 0.63$). The regression analysis of variance suggests rejecting either Implantation Site or Probe 1 Time Shift from the model. If Probe 1 data is rejected and the resulting 3 variable model tested, analysis of variance still suggests rejecting Implantation Site, but not strongly. The result of rejecting Probe 1 data is a slight drop in MSE and R^2 . Based on the original criterion, this 3 variable model is fractionally better than the 4 variable model. Further rejecting Implantation Site results in a 2 variable model with higher MSE and much lower R^2 than either the 3 or 4 variable models (Table 7.1). This discussion points to the much higher strength of Probe 2 data compared to Probe 1 data.

Note how the predictive usefulness of this model is strictly limited to the parameters unique to this experiment. This includes pins, bones, implantation methods, and so on. The model has been used primarily to show that a fixed set of materials and methods can adequately account for pin extraction forces.

Table 7.1 Results of analysis of variance testing for the optimal prediction model

Input Variables	MSE	R ²	Reject from model
PIN SITE SFT1 SFT2	278.6	0.8270	SFT1 ¹ or SITE ²
PIN SITE SFT2	276.5	0.8182	SITE ²
PIN SFT2	301.8	0.7906	----

¹Strong rejection criterion

²Borderline rejection criterion

Variable interactions have shown to be quite unpredictable. Referring back to Table 6.1, notice that Pin Number and Implantation Site would have been rejected out of hand based on the single-variable model prediction strength, yet somehow both ended up in the best prediction model. As a further example, Pin Number has an R^2 value of 0.0512 and the Pulse Energy Cutoff Point data for Probes 1 and 2 combined has an R^2 value of 0.5412. When these three are combined in a model, R^2 increases to 0.7937. Implantation Method has an R^2 value of 0.4509, while Percent Time Shift data for Probes 1 and 2 combined has an R^2 value of 0.7964. When these three are combined in a model the resulting R^2 barely changes, to 0.7982. These examples illustrate how interaction effects may be completely contrary to what one would conclude by looking at statistics for the individual factors.

Means testing showed that Bones 1 and 7 had significantly different mean extraction forces. This difference is not, however, attributable to a difference in the bones. Bones 1 and 7 were subjected to Implantation Method 4, resulting in near-zero extraction forces. This effect can be seen clearly in the next test (METH). The means test on SITE shows that some differences exist with respect to implantation sites. Recall, however, that Pin Number was confounded with Implantation Site. The differences might arise due to either factor.

Repeatability

The level of repeatability obtained with ultrasonic parameters appears to be within a reasonable range, though improvement should be an objective of future studies. This problem can be avoided in part by taking more data, when practical, to obtain a better estimate of the mean value.

For unknown reasons, Probe 2 demonstrated lower repeatability than Probe 1. A natural tendency might be to assume the difference is due to frequency characteristics, but this might not be the case. There may be some aspect of pin-probe coupling that Probe 2 was more sensitive to than Probe 1 (for example, probe contact force). It is also possible that error was caused by an alignment deficiency induced by the plexiglas probe holder.

Mechanism of Pulse Attenuation

Guided waves are induced by the proximity of exterior boundaries in the test medium and are strongly influenced by conditions along these boundaries. External influences acting on the boundary will alter wave behavior within the test material. In the present investigation, this influence takes the form of a compressive force against the fixation pin, while wave influence primarily takes the form of heavy attenuation. If the pin is firmly anchored, high interfacial stresses will provide strong acoustic coupling for absorption of ultrasonic energy into the bone.

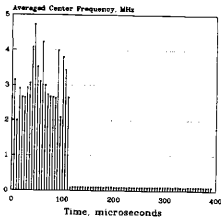
Attenuation Parameter

In the experimental methods, a criterion was selected for identification of the Pulse Energy Cutoff Point. This was to be the first observed drop in frequency below 500 kHz, under the assumption that frequency declines gradually. In actuality, the frequency showed a sharp and sudden drop from moderate levels (2-4 MHz) down to zero. In retrospect it is clear this sudden drop was due to the use of a high pass signal filter. Low frequency components of the signal had been eliminated. The cutoff criterion was changed to locate the first point along the time scale of a zero frequency value (*Figure 7.2A and 7.2B*). In *Figure 7.2A* the drop occurs quite abruptly at 115 μ s. *Figure 7.2B* shows a more gradual drop with some circuit noise appearing to the far right of the graph (300-400 μ s).

Figure 7.3A shows a more dramatic illustration of the possible effects of circuit noise, with *Figure 7.3B* showing a signal without noise for comparison. Most of the cutoff plots showed small amounts of noise, while others showed none at all. *Figure 7.3A* shows an extreme situation which was not representative, but demonstrates a phenomenon that must be guarded against.

Figures 7.4A and 7.4B are a comparison of the baseline response of Pins 2 and 1 respectively. The difference between the two is clear. Pin 2 shows a strong response while Pin 1 shows a rather weak response. Based simply on

Pin 3
Datafile #081



Pin 3
Datafile #134

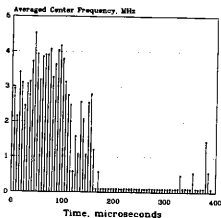
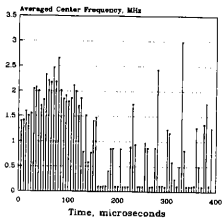


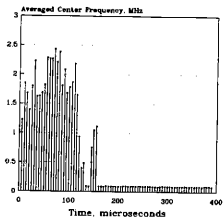
Figure 7.2 Plots of Averaged Center Frequency as a function of position along the time-domain scale. (a) Sharp cutoff observed at 115 μs ; (b) gradual drop in frequency with cutoff at 165 μs and noise artifacts at the far right of the time scale

Pin 2
Datafile #064



(a)

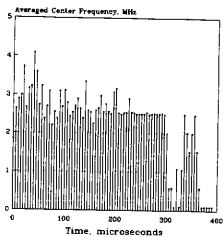
Pin 2
Datafile #074



(b)

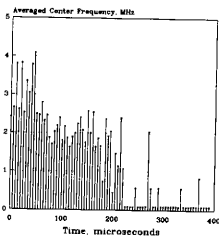
Figure 7.3 Illustration of the extreme effects of circuit noise.
(a) Cutoff at 160 μ s followed by strong noise spikes; (b) cutoff at 135 μ s followed by a brief signal recovery and no noise

Baseline File #082



(a)

Baseline File #094



(b)

Figure 7.4 Comparison of the baseline response of two pins tested with Probe 2. (a) Pin 2, showing strong response; (b) Pin 1, showing weak response

this figure, Pin 2 would be expected to show more sensitivity to bonding than Pin 1 since Pin 1 already appears to be under the influence of some attenuating factor.

Recall that center frequency was selected from the available FFT parameters to identify the cutoff point. A brief look at the remaining parameters will show that each shows an abrupt change similar to center frequency. All frequency parameters (center, peak, and half-power frequencies) behave identically, while bandwidth becomes large and skewness goes to zero. Although the selection of center frequency was somewhat arbitrary, it appears that any one of the FFT parameters could have provided the same information.

Effect of Probe Frequency

There was a marked difference in the response of the two probes, possibly due to frequency. Probe 2 showed a wider range of cutoff values, lower repeatability, and a stronger relationship with extraction forces. The greater sensitivity is suggested by guided wave principles. As wave frequency increases, higher-order modes are induced and a greater fraction of pulse energy travels along the exterior boundary. Thus a greater fraction of pulse energy is affected by the bone-pin interface.

Probe Holder

Several reflections from within the probe holder were clearly apparent, but the high attenuation of plexiglas (380 dB/m compared to 110 dB/m for stainless steel²³) absorbed the pulse energy within about 36 μ s. In contrast, the initial pulse returns from the pins were not observed until about 40-45 μ s, well after the last block reflections were observed. Therefore, block reflections could not have caused any interference with the pin reflections. However, shorter pins could have indeed presented an interference problem.

Axial Extraction

A low crosshead displacement rate (1.27 mm/min or 0.05 inch/min) was chosen in order to obtain the maximum static holding power of the pins. In some cases, the force rose in a steep linear manner, reached a peak, and then dropped suddenly. In other cases, the force increased more gradually in a linear manner until bending away while still continuing to increase somewhat. In the first case, maximum extraction force was taken at the peak. In the second case, maximum extraction force was taken as the point where the linear relationship between force and displacement ended. The bone specimens were not sectioned prior to testing due to the unlikelihood of disturbing an adjacent implant during extraction of a nonthreaded pin.

Pulse Velocity and Arrival Times

Figures 4.2 and 4.3 can be used to find the wave modes present in the pin, in addition to the velocities of the major components, by multiplying the actual probe peak frequency and the thickness (diameter) of the pin. Although these curves represent waves traveling in a carbon steel plate, no significant difference is expected for waves traveling in a stainless steel bar. For Probe 1, the $f \times t$ value is 6.9 MHz mm, while the value for Probe 2 is 10.8 MHz mm. If the probes had been close to their nominal frequencies, the $f \times t$ values would have been 6.3 MHz mm for Probe 1 and 13.9 MHz mm for Probe 2.

Figure 7.5 shows the group speed curves with points corresponding to the $f \times t$ values for Probe 1 and Probe 2 highlighted. Although purely a matter of luck, it is probably fortunate that both probes (in combination with the 2.78 mm pins) produced a mode near the peak of two of the curves. This figure shows that Probe 1 produced a strong pulse of L_{13} energy and that Probe 2 produced a strong pulse of L_{14} energy, where both modes are of the symmetric type.

Since the points highlighted on Figure 7.5 are the result of a frequency multiplied by a thickness, it follows that a change in either of those parameters would change the location of the points. Simply using a different sized pin would shift the points either to the left or right. Similarly, changing to a different frequency probe would

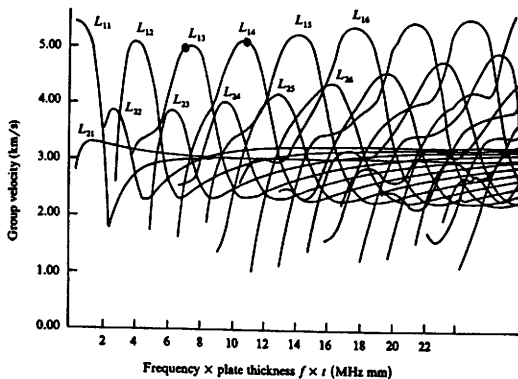


Figure 7.5 Group speed curves for Lamb waves traveling in a steel plate and showing points corresponding to Probe 1 (6.9 MHz mm) and Probe 2 (10.8 MHz mm) [Adapted from Egle, D.M, and Bray, D.E. Nondestructive Measurement of Longitudinal Rail Stresses Federal Railroad Administration FRA-ORD-76-270 (1975)]

shift the points. If the highlighted points had fallen away from the peak of these curves, the result would have been greater dispersion and, perhaps, more difficulty in producing conclusive results. Instead, the pulse energy remained fairly coherent which allowed individual pulse reflections to be observed. If dispersion is allowed to dominate, pulse attenuation may be harder to measure.

The major group velocities can be read directly from this figure. For Probe 1, the value is about 5.00 km/s (5000 m/s or 197000 in/s), and for Probe 2, about 5.125 km/s (5125 m/s or 202000 in/s). With an average pin length of about 100 mm (3.94 inch), the predicted pulse arrival times for Probe 1 and Probe 2 would be integer multiples of 40 μ s and 39 μ s respectively. The observed arrival times for the first pulse echo ranged from about 40 to 45 μ s. Due to the complexity of the pulse signal and limitations of the display equipment, the arrival time could not be precisely determined. However, multiple reflections were distinctly observed in the unimplanted pins at approximately integer multiples of the first pulse arrival time.

Based on a comparison of the theoretical and observed results, there seems to be a good correspondence. First, the observed and predicted arrival times are similar. Second, the observation of distinct pulses of energy is suggested by *Figure 7.5*. Third, the stronger relationship observed with Probe 2 is suggested by the fact that a higher order wave

mode concentrates a greater portion of the pulse energy at the bone-pin interface.

Microstructure

Microstructural analysis was utilized to check for material irregularities since ultrasonic pulses are significantly affected by properties of the material through which they travel. When wavelength approaches the grain size, increased scattering and absorption of the ultrasonic pulse occurs. If material inhomogeneities such as inclusions or voids are present, these will also affect an ultrasonic pulse²³.

Pin microstructure did not reveal anything which might account for variation in the ultrasonic data.

Sources for Experimental Error

Unfortunately, this type of experiment is likely to have many sources of variability. In most cases, the variability cannot be observed or eliminated and the experiment must be carried out with a degree of confidence that overall effects will not be detrimental. Some sources for error fall under the control of the experimenter, and these will be mentioned as well. The present discussion is not meant to be comprehensive, but is intended to introduce potential sources for error. Variability affecting ultrasonics and extraction will be considered separately.

Ultrasonic tests are expected to be affected the most by: (1) pin/probe alignment and acoustic coupling, (2) circuit noise, (3) the waveform selection and evaluation process, (4) moisture content in the bone, and (5) cortical thickness.

Extraction forces are expected to be affected the most by: (1) cortical thickness, (2) fluid, tissue, or bone debris at the bone-pin interface, (3) surface roughness of the pins, (4) cutting ability of the trochar tip, and (5) alignment of pins with the loading direction during extraction.

CHAPTER VIII
SUMMARY AND CONCLUSIONS

Strengths and Limitations

The ultrasonic technique applied in this study shows promise for development into a clinically applicable method of evaluating bone-pin interface stability. Considerable refinement is still needed, however. This section will describe the strengths and limitations of the technique and indicates areas for future research.

The present evaluation technique satisfies several of the most important requirements for any clinically applicable testing procedure. First, it is noninvasive and would be painless if applied to a living patient. Further, when care is taken in placement of the probe, loads imposed on the pins during testing are negligible and will not disrupt the pins.

On a trial-to-trial basis, the measured ultrasonic parameter is repeatable within 10-15% of its mean value. For this particular experiment, extraction forces can be predicted with an accuracy of about ± 180 N (± 40 lbs) with 95% confidence by utilizing prior knowledge of the implantation site and pin number. The functional relationship between ultrasonic data and extraction forces can be presented in a way to eliminate much of the variations observed with different pins.

Data collection is fairly straightforward and can be completed in a matter of a few minutes for each pin. The method of data reduction should be easily repeatable.

Limitations of the present method are related primarily to the pins. Data in the present study are not directly applicable to nonthreaded pins having diameter or length dimensions different from the pins in this experiment, nor are these data applicable to the myriad of threaded pin designs. As yet, the behavior of ultrasonic waves in threaded pins is unknown, and is likely to depend on the type of threads. Extraction measurements may not be an appropriate correlate for threaded pins since holding power is determined more by the ultimate shearing stress of bone than interfacial contact stresses. Maximum twist-out force may be a more appropriate correlate when threaded pins are studied.

The response of a pin to an ultrasonic stress wave will be affected by the consistency of grain structure and the frequency of the wave. Wave frequency determines the type of wave modes present and the degree of scattering from grain effects and dispersion. Wave mode will affect the sensitivity, while scattering will cause the pulse energy to be dissipated more rapidly. Higher frequencies had a tendency for lower repeatability.

Considerable preparation and planning is required prior to implanting the pins. The unstressed acoustic response of

each pin should be studied in order to establish a reference value of the measured attenuation parameter. This requires cutting each pin to its final length before implantation and providing a flat and well-polished probe contact surface. After preparing the contact surface, care must be taken to avoid any damage that would alter the acoustic coupling. Otherwise, subsequent measurements would be meaningless. In order to pool data from different pins mounted in the same fixator frame, each of the pins must be identical in type, diameter, and preparation.

Before ultrasonic tests can be made on an implanted pin, the fixator clamp must be disconnected and moved clear of the pin. A minimum of about one inch of pin should be available for performing ultrasonic tests.

Presently, data analysis is the limiting factor in determining how quickly results are obtained and how many trials are evaluated. The data files take up considerable computer memory storage space in addition to demanding a great deal of computational processing. With more powerful equipment, the waveform evaluation process can be automated so that one need only place the probe onto a pin and perform a single keystroke. In this fashion it may be possible to obtain near-real-time analysis where the ultrasonic attenuation parameter is calculated within a minute or so of the actual test rather than several days later.

A final point to bear in mind is that subtle electronic

noise in the pulser circuitry could have detrimental effects on identifying a signal cutoff point. Operator vigilance will be required to prevent this from occurring.

Areas for Future Research

Since many unanswered questions remain about the use of this technique in a clinical setting, the next phase of research should concentrate on three areas.

First, the results obtained from this study should be applied to an *in vivo* test to investigate differences in response between cadaveric and living bone, the effects of soft tissue contact, and the feasibility of monitoring pin stability over a period of weeks. The experimenter can observe how changes in the ultrasonic measurements relate to changes in the condition of the patient, and gain a better understanding of the trend of pin stability over time. Extraction tests would again provide a guideline for estimating pin stability and comparing results between pins.

Second, the basic response characteristics and correlational strength of commonly used threaded pins should be investigated with an *in vitro* study similar to this one. Nonthreaded pins having an outer diameter larger or smaller than 2.78 mm (7/64 inch) could be used to establish how changes in the pin diameter affect ultrasonic response. Estimates of pin stability could be obtained by extraction tests for nonthreaded pins and twist-out tests for threaded

pins.

Third and lastly, the feasibility of applying a travel-time measurement technique should be investigated. Due to noise and precision limitations, the present study was unable to contribute any understanding of possible travel-time changes. Unfortunately, the complexity and occasional variability of the arriving pulse signal may hinder attempts to measure travel times accurately.

Future Application

Given good repeatability of the ultrasonic test and the uncertainty which is introduced by extraction measurements, it may be more appropriate to record only ultrasonic data over a period of time. In fact, this is the only clinical option. This research and considerable prior research suggest that ultrasonic tests can detect subtle changes in the condition of an interface. These measurements, though not quantified in terms of force, can be related to changes in the condition of the patient or the development of complications. Excluding extraction forces from the analysis does not appear to represent a loss of valuable information since no specific extraction force is known to result in the development of fixation pin complications.

In most cases the maximum pin stability is obtained at the moment of implantation and tends to diminish over time. An ultrasonic test would establish the initial level of

bonding, and afterwards would show how bonding had changed with respect to that initial state. This same methodology applies for any size patient. Comparisons to extraction data are completely eliminated.

Improving Accuracy and Sensitivity

Bearing in mind that the difference in actual peak frequencies of the two probes was only 1.39 MHz, a substantial difference in response was still observed. This suggests that increasing probe frequency an additional 2-3 MHz might produce a higher level of sensitivity than the one for Probe 2. A warning should be attached to this statement. Probe 2 exhibited greater difficulty in repeating ultrasonic measurements. Therefore, higher frequency probes may tend to be more sensitive to factors like acoustic coupling. The experimenter will have to determine whether any additional error can be eliminated or if it is allowable when weighed against gains in sensitivity.

A greater amount of pulse energy can be obtained by increasing the pulse voltage. This may subsequently improve the sensitivity of the test, and may reduce scatter of the attenuation parameter at near-zero extraction forces. A stronger pulse should be somewhat less sensitive to subtle differences in the interface at low stress.

Signal filtering may assist in eliminating parts of the signal which are unwanted or are of no practical use. Most

of the available pulse signal is either not used or is converted into a more useful form. Far too much information is contained within a typical pulse. Once the essential information has been identified, the remaining signal can be eliminated or ignored.

One of the most important goals should be to obtain a high-quality coupling between the probe and the pin. This ensures that acoustic energy can pass freely between the probe and the pin. Consistent coupling will result in consistent measurement of ultrasonic parameters. No loss of coupling can be allowed.

Conclusions

A strong relationship has been observed between the extraction forces of fixation pins implanted in cadaveric femur and an ultrasonic attenuation parameter obtained from a simple pulsed-wave excitation technique. Nevertheless, a great deal of scatter is present in the data. There were many potential sources of variability which could not be precisely controlled. In most cases, the source of error was not identifiable. A fundamental problem with the relationship between extraction and ultrasonic attenuation is that each detects slightly different physical features of the bone-pin interface and can therefore never produce a perfect correlation. The data scatter may be due to random error, but most of it is probably due to the difference

between the ultrasonic and extraction tests.

Extraction force data was inexplicably scattered. Implantation methods did not model degrees of pin fixation as expected, and as a result, there is a large gap in the data between 45 and 225 N (10 and 50 pounds). Prediction strength based on an individual bone or an individual pin was in some cases weak or zero, while combining all data tended to reveal the strongest relationship.

The ultrasonic data appeared to be quite repeatable, while no assessment of the repeatability of extraction forces was possible. An individual probe took repeated measurements with low error. In addition, two different probes show similar data patterns. Differences in response between pins appears to be largely eliminated by utilizing a zero-stress reference attenuation value measured for each pin individually.

The physical principles of wave propagation support the findings of this research, and further imply ways to improve the test. In theory, higher frequency wave modes should show a stronger relationship since more pulse energy is concentrated at the outer surface of the pin. Experimental results clearly demonstrate a difference in sensitivity.

Two instances of inadvertent confounding were created. Pin Number was confounded with Implantation Site, while Bone Number was confounded with Implantation Method. A trend in the scatter plots of Pin Number and Implantation Site

suggests either a difference in the pins or a difference in the sites.

REFERENCES

- 1 **Brinker, W.O., and Flo, G.L.** Principles and application of external skeletal fixation *Vet Clin N Am* (1975) 5 197-208
- 2 **Gahring, D.R.** Use of external fixation devices in management of fractures and osteotomies *Calif Vet* (1980) 9 19-21
- 3 **Fox, S.M.** *Proceedings of a Course in Fractures and External Fixation* Veterinary Continuing Education, Massey University, Palmerston North, New Zealand (1989)
- 4 **Palmer, R.H., Hulse, D.A., Hyman, W.A., and Palmer, D.R.** Principles of bone healing and biomechanics of external skeletal fixation *Vet Clin N Am* (1992) 22 45-68
- 5 **Wagenknecht, M., Andrianne, Y., Burny, F., and Donkerwolcke, M.** Study of the mechanical characteristics of external fixation pin anchorage *Orthopedics* (1984) 7 629-632
- 6 **Palmer, R.H., Hulse, D.A., Pollo, F.E., Hyman, W.A., Palmer, D.R., Rastegar, S., and Longnecker, M.T.** Pin loosening in external skeletal fixation: The effects of pin design and implantation site *Proc Vet Ortho Soc* (1991) 18 50
- 7 **Gumbs, J.M., Brinker, W.O., DeCamp, C.E., Schaeffer, R., Kaneene, J.B., and Soutas-Little, R.W.** Comparison of acute and chronic pull-out resistance of pins used with the external fixator (Kirschner splint) *J Am An Hosp Assoc* (1988) 24 231-234
- 8 **McGrath, T.J.** *The Stability of the Bone-External Splintage Pin Interface as Affected by Pin Insertion Method and Biomaterial* Doctoral Dissertation, Texas A&M University (1987)
- 9 **Schatzker, J., Sanderson, R., and Murnaghan, J.P.** The holding power of orthopedic screws *in vivo* *Clin Ortho Rel Res* (1975) 108 115-126
- 10 **Behrens, F.** General theory and principles of external fixation *Clin Ortho Rel Res* (1989) 241 15-23

- 11 **Ling, R.S.M.** Observations on the fixation of implants to the bony skeleton *Clin Ortho Rel Res* (1986) **210** 80-96
- 12 **Egger, E.L., Histand, M.B., Blass, C.E., and Powers, B.E.** Effect of fixation pin insertion on the bone-pin interface *Vet Surg* (1986) **15** 246-252
- 13 **Matthews, L.S., Green, C.A., and Goldstein, S.A.** The thermal effects of skeletal fixation-pin insertion in bone *J Bone Joint Surg* (1984) **66A** 1077-1082
- 14 **Yovich, J.W., Turner, A.S., Smith, F.W., and Davis, D.M.** Holding power of orthopedic screws: Comparison of self-tapped and pre-tapped screws in foal bone *Vet Surg* (1986) **15** 55-59
- 15 **Vangsness, C.T., Carter, D.R., and Frankel, V.H.** *In vitro* evaluation of the loosening characteristics of self-tapped and non-self-tapped cortical bone screws *Clin Ortho Rel Res* (1981) **157** 279-286
- 16 **Bennett, R.A., Egger, E.L., Histand, M.B., and Ellis, A.B.** Comparison of the strength and holding power of 4 pin designs for use with half pin (Type I) external skeletal fixation *Vet Surg* (1987) **16** 207-211
- 17 **DeCamp, C.E., Brinker, W.O., and Soutas-Little, R.W.** Porous titanium-surfaced pins for external skeletal fixation *J Am An Hosp Assoc* (1988) **24** 295-300
- 18 **McDonald, D.E., Palmer, R.H., Hulse, D.A., Neigut, J.S., Hyman, W.A., and Slater, M.R.** Pin loosening in external skeletal fixation: A biomechanical and microstructural comparison of the near and far cortex pin-bone interfaces *Proc Vet Ortho Soc* (1992) **19** 3
- 19 **Uhthoff, H.K.** Mechanical factors influencing the holding power of screws in compact bone *J Bone Joint Surg* (1973) **55B** 633-639
- 20 **Uhthoff, H.K., and Germain, J.-P.** The reversal of tissue differentiation around screws *Clin Ortho Rel Res* (1977) **123** 248-252

- 21 **Green, S.A.** Complications in external fixation in: *Current Concepts in External Fixation of Fractures* (Ed Uhthoff, H.K.) Springer-Verlag, Berlin (1982) 43-52
- 22 **Bar-Cohen, Y., and Mal, A.K.** Ultrasonic inspection in: *Metals Handbook Volume 17: Nondestructive Evaluation and Quality Control* ASM International, Metals Park, Ohio (1989) 231-277
- 23 **Bray, D.E., and Stanley, R.K.** *Nondestructive Evaluation: A Tool for Design, Manufacturing, and Service* McGraw-Hill, New York (1989) 45-172
- 24 **Kinsler, L.E., Frey, A.R., Coppens, A.B., and Sanders, J.V.** *Fundamentals of Acoustics* John Wiley & Sons, New York (1982)
- 25 **Rose, J.L. and Meyer, P.A.** Ultrasonic procedures for predicting adhesive bond strength *Mat Eval* (1973) 31 109-114
- 26 **Chang, F.H., Flynn, P.L., Gordon, D.E., and Bell, J.R.** Principles and application of ultrasonic spectroscopy in NDE of adhesive bonds *IEEE Trans Sonics Ultrasonics* (1976) 23 334-338
- 27 **Pilarski, A.** Ultrasonic evaluation of the adhesion degree in layered joints *Mat Eval* (1985) 43 765-770
- 28 **Alers, G.A., Flynn, P.L., and Buckley, M.J.** Ultrasonic techniques for measuring the strength of adhesive bonds *Mat Eval* (1977) 35 77-84
- 29 **Guyott, C.C.H., and Cawley, P.** Evaluation of the cohesive properties of adhesive joints using ultrasonic spectroscopy *NDT Intl* (1988) 21 233-240
- 30 **Rose, J.L., Avioli Jr., M.J., and Bilgram, R.** A feasibility study on the nondestructive evaluation of an adhesively bonded metal to metal bond: an ultrasonic pulse echo approach *Brit J NDT* (1983) 25 67-71
- 31 **Pilarski, A. and Rose, J.L.** A transverse-wave ultrasonic oblique-incidence technique for interfacial weakness detection in adhesive bonds *J App Phys* (1988) 63 300-307

- 32 **Mal, A.K.** Guided waves in layered solids with interface zones *Intl J Eng Sci* (1988) **26** 873-881
- 33 **Mal, A.K., Bar-Cohen, Y., and Xu, P.-C.** Analysis of leaky Lamb waves in bonded plates *Intl J Eng Sci* (1989) **27** 779-791
- 34 **Mal, A.K., Bar-Cohen, Y., and Xu, P.-C.** Leaky Lamb waves for the ultrasonic nondestructive evaluation of adhesive bonds *J Eng Mat Tech* (1990) **112** 255-259
- 35 **Kaneko, T., Nagai, Y., Ogino, M., Futami, T., and Ichimura, T.** Acoustoelectric technique for assessing the mechanical state of the dental implant-bone interface *J Biomedical Mat Res* (1986) **20** 169-176
- 36 **Kaneko, T.** Assessment of the interfacial rigidity of bone implants from vibrational signals *J Mat Sci* (1987) **22** 3495-3502
- 37 **Kaneko, T.** Comparison between acoustic and mechanical tapping methods for assessing the interfacial states of bone implants *J Mat Sci* (1989) **24** 2820-2824
- 38 **Kaneko, T.** Assessment of the dental implant-bone interface from a pulsed microvibration *J Mat Sci Lett* (1991) **10** 185-187
- 39 **Redwood, M.** *Mechanical Waveguides* Pergamon Press, London, England (1960) 117-173
- 40 **Bray, D.E., and Finch, R.D.** *Flaw Detection in Model Railway Wheels* Federal Railroad Administration FRA-RT-71-75 (1971) 28-65
- 41 **Milton, J.S., and Arnold, J.C.** *Introduction to Probability and Statistics* McGraw-Hill, New York (1990)
- 42 **Weisberg, S.** *Applied Linear Regression* John Wiley and Sons, New York (1985)
- 43 *Dorland's Illustrated Medical Dictionary, 26th ed.* W.B. Saunders Company, Philadelphia (1981)
- 44 **McGannon, H.E.** Iron and steel in: *Mark's Standard Handbook for Mechanical Engineers* (Eds Avallone, E.A., and Baumeister III, T.) McGraw-Hill, New York (1978) Ch 6 36-38

- 45 **Smith, W.F.** *Structure and Properties of Engineering Alloys* McGraw-Hill, New York (1981) 270-311
- 46 **Davison, R.M., DeBold, T., and Johnson, M.J.** Corrosion of stainless steels in: *Metals Handbook Vol. 13, Corrosion* ASM International, Metals Park, Ohio (1987) 547-550
- 47 **Shigley, J.E., and Mischke, C.R.** *Mechanical Engineering Design* McGraw-Hill, New York (1989)
- 48 **Washko, S.D., and Aggen, G.** Wrought stainless steels in: *Metals Handbook Vol. 1, Properties and Selection: Irons, Steels, and High-Performance Alloys* ASM International, Materials Park, Ohio (1990) 855

APPENDIX I

GLOSSARY OF MEDICAL TERMINOLOGY

Several definitions are taken either in whole or in part from Reference 43. In addition, the contributions of Dr. Ross Palmer to this Appendix are acknowledged.

acute study a study in which the patient is euthanized within a few hours or days of an operative procedure; used to determine short-term effects

aseptic free of pathogenic organisms; sterile

atrophy a wasting away; diminution in size of a cell, tissue, organ, or part

cancellous bone reticular, spongy, or lattice-like bone; in long bones cancellous tissue is found in the end sections

chronic study a study in which the subject is euthanized several weeks after an operative procedure; used to determine long-term effects

closed reduction (see **fracture reduction**) reducing the fracture without surgically exposing it

comminuted fracture a fracture in which the bone is broken or crushed into small pieces; often a result of a high-energy injury such as impact

cortical bone the outer layer of dense compact bone

craniocaudal axis the axis intersecting the front and back portions of the bone

delayed union union of fracture taking longer than expected, but progressing toward successful union

diaphysis the elongated cylindrical portion of a long bone, between the ends or extremities; it consists of a tube of compact bone enclosing the medullary canal

direct implantation pin insertion which does not involve predrilling a hole

distal extremity of bone toward the feet

ethanasia humane death of an experimental animal for the purpose of studying its body

femur the long bone of the upper leg; thighbone

fracture reduction putting the bone pieces back together

hematoma a localized collection of clotted blood

implantation (see **insertion**) surgical placement of a device into the skeleton

implantation site (see **pin position**) location of pin insertion

insertion (see **implantation**) surgical placement of a device into the skeleton

internal fixation fracture repair method in which all implants are completely within the body; often utilizes bone plates, intramedullary nails, lag screws, and cerclage wire

in vitro in an artificial environment

in vivo within the living body

lateral aspect bone surface away from the midline of the body

limb lengthening surgical method to lengthen limbs as a treatment for traumatically or congenitally shortened limbs

medial aspect bone surface closest to the midline of the body

morbidity diseased; afflicted

necropsy examination of a body after death; may involve removal of tissues

necrosis tissue death

nonunion incomplete union of bony fracture

oblique fracture fracture line is not perpendicular to the longitudinal bone axis

open fracture fracture exposed to outside environment via associated skin perforation

open reduction (see **fracture reduction**) reducing the fracture via open surgical means; the fracture is exposed surgically

osteomyelitis infection of bone tissue

osteosynthesis mechanical fastening of the ends of a fractured bone

osteotomy surgical cutting of bone; may be used to produce an artificial fracture environment; may be used to correct a length or alignment deficit; may be used to provide access to interior parts without disrupting surrounding soft tissues

patella small bone of the knee joint; kneecap

percutaneous (see **transcutaneous**) penetrating through the skin

pin angling insertion of pins at oblique angles to the longitudinal bone axis; inserting pins so they are not parallel to one another

pin position (see **implantation site**) location of pin insertion

predrilling drilling a pilot hole prior to inserting the pin

pretapping cutting threads into the bone prior to inserting the pin; usually follows predrilling

proximal extremity of bone away from the feet

ring sequestra a ring of dead bone that has become separated during the process of necrosis from sound bone; often associated with high-speed pin insertion

self-tapping a pin which cuts its own threads during insertion; no pretapping is required

sepsis infection

spiral fracture fracture usually resulting from torsional impact of the limb

tibia the larger of the two bones in the lower part of the leg; shinbone

trabeculae cells associated with cancellous bone

transcutaneous (see **percutaneous**) penetrating through the skin

transverse fracture fracture along a plane perpendicular to the longitudinal bone axis

trochar sharp and pointed; trochar pins usually have a triangular (three-sided) tip ending in a sharp point

APPENDIX II
PCDAS SIGNAL ANALYSIS SOFTWARE

PCDAS Features

The PCDAS Signal Analysis software is designed to work in conjunction with a PCTR-160 analog-to-digital converter board installed in the Texas Instruments Professional Computer. PCDAS is the means by which waveform data was displayed and manipulated for this research. The main features of PCDAS are listed below.

- Time scale expansion allows the user to select how much of the waveform to display on the screen
- Waveform freezing temporarily stores the displayed waveform in a data buffer. The frozen waveform can be analyzed, stored in a binary output file, or sent to the line printer for hardcopy output
- Waveform averaging determines how many sampled waveforms are averaged prior to on-screen display
- Sampling rate controls how fast the A/D board samples incoming wave information
- Time delay adjusts the starting position of the displayed waveform
- Gating allows the user to select a portion of the displayed waveform for evaluation or output
- Input and output saves and retrieves waveform files on disk
- Rectification allows the user to display the waveform in either non-rectified or full-wave rectified mode
- Fast Fourier Transformation (FFT) and Power Spectrum Display provides graphical as well as parametric information about the gated portion of the waveform

Main Program and Subroutines

As shown in *Table A-2.1*, the intertwining of subroutines is rather complex. In each table heading, NAME indicates the FORTRAN source code file name, followed by the name(s) referenced in the CALL statement; SUBROUTINES indicate which FORTRAN and OBJECT subroutines the file calls; and CALLED FROM indicates which of the source code files the subroutine is called from.

Flowchart

A flowchart schematically represents a simplified structure of the computer code in order to show the tasks subroutines perform and how they branch from one to another. For example, if one were interested in the subroutine OUTWAVE (for outputting a waveform), a flowchart would show how the program branches through PCDAS, SETMD, and MMI before arriving at the OUTWAVE subroutine. Given this information and a listing of the source codes, the process of tracing the flow of operation becomes considerably easier.

The flowchart shown here is simplified in three important respects. First, multiple calls to the same subroutine are omitted. Second, the order in which the subroutines are called is not specified. And third, the subroutines having no source code available are omitted (*Table A-2.2*). In making this omission, it has been assumed

that no further branching occurs from within these subroutines.

The program flowchart is shown in *Figures A-2.1* through *A-2.4* while *Table A-2.3* describes the task of each subroutine. *Figure A-2.1* is the most simplified schematic of PCDAS showing the main program and several key subroutines. Note that input, output, and Fourier transformation all take place from the MMI subroutine.

Figure A-2.2 shows the PCDAS main program and its associated subroutines. The functions of the main program are to set the initial system parameters, monitor the keyboard for a user keystroke, and to collect data from the A/D board. If a keystroke occurs, PCDAS calls SETMD; otherwise, it continues to input data from the A/D board.

Figure A-2.3 shows the SETMD subroutine and its associated subroutines. The function of SETMD is to set the mode of the system based on a keyboard entry by the operator. For instance, if the user presses 'E' for gate evaluation, the SETMD subroutine activates the gate evaluation mode, and the user can now change the size or location of the gate as desired. A carriage return is the keystroke command which performs Fourier transformation on the gate once the gate evaluation mode has been set.

Figure A-2.4 shows the MMI subroutine and its associated subroutines. The chief function of MMI is to determine which operation is desired based on the system

mode and keystroke input, and to call the appropriate block of code which performs that operation. Whereas SETMD only changes the current system mode, MMI performs the indicated action. From this standpoint, MMI is the decision-making subroutine which dictates the overall flow of the program. One would be remiss in assuming the PCDAS main program controls conditional branching; this is the case only to a limited extent.

PCDAS Operation

PCDAS is an interactive program; it requires the user to monitor and interact on a continuous basis. The program does not have any intrinsic iterative capabilities; it performs one task at a time based on the user's command input. In addition, only one command at a time may be entered. Although the program allows a time-domain waveform to be digitized for disk storage, it does not allow the user to save parameters associated with FFT analysis. Any such data must be recorded by hand.

When performing FFT analysis, the user selects a gate size, manually places the gate over the area to be evaluated, selects gate evaluation mode, and presses the return key to calculate FFT parameters. A display shows the power spectrum curve and lists the FFT parameters (described in *Chapter 3*). At this point the user views the displayed information, manually records data, and presses the return

key to exit FFT evaluation. Now the user must move the gate to the next position and press the return key which begins the process over again. Done in this way, evaluating and recording 400 individual FFT data points requires 3 to 4 hours. For reduction, all 400 datapoints must be key-entered into a spreadsheet. Following this procedure, the reduced data is key-entered from spreadsheet to graphics software to produce the final product. This process is tedious and time-consuming, in addition to resulting in a high potential for data entry errors.

Modifications

The process just described required identical repetition for all waveform files in the investigation. To perform the process interactively would have taken weeks or months; instead the PCDAS program was modified to do the analysis iteratively. The time needed to evaluate one waveform file was reduced from several hours to 15 minutes. In addition, the FFT parameters were transferred into a file to avoid the necessity of key-entering data for subsequent reduction and graphing. With the aid of a modified program, complete analysis of all waveform files was accomplished in about one week.

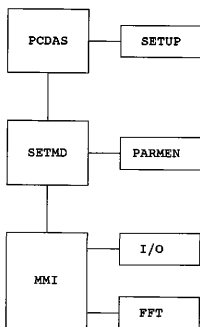


Figure A-2.1 Simplified schematic of PCDAS program

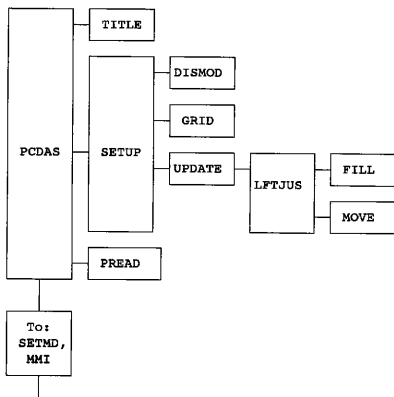


Figure A-2.2 PCDAS main program and subroutine calls

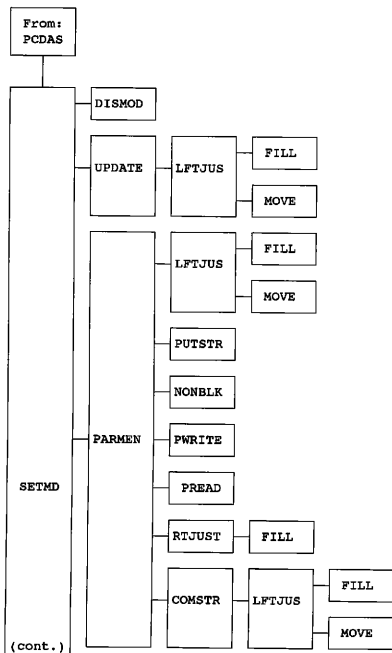


Figure A-2.3 SETMD subroutine. Follows PCDAS; followed by MMI

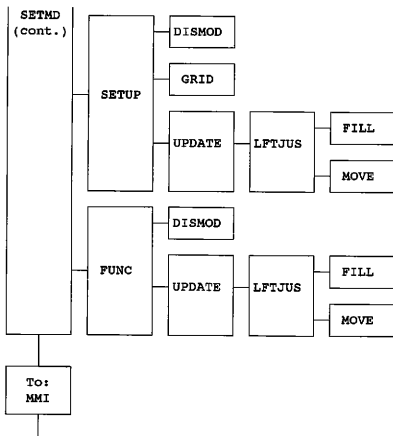


Figure A-2.3 Continued

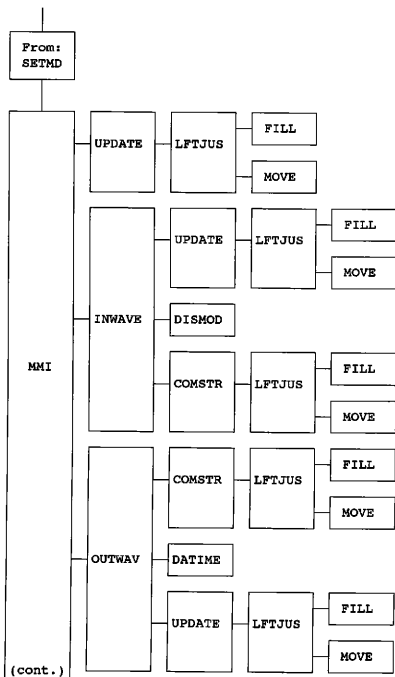


Figure A-2.4 MMI subroutine showing UPDATE, INWAVE, and OUTWAVE

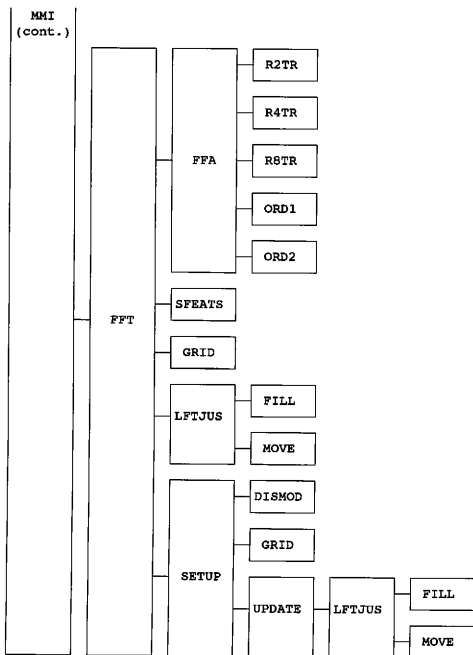


Figure A-2.4

Continued

Table A-2.1 Listing of subroutines

SOURCE FILE NAME	FORTRAN SUBROUTINES	OBJECT SUBROUTINES	CALLED FROM
PCDAS.FOR program pcdas	title pread setup setmd	setint keybd adcnew wplot envel gate	-----
COMSTR.FOR subroutine comstr	lftjus move	-----	parmen inwave outwav
DISMOD.FOR subroutine dismod	dsplay	-----	setmd setup func inwave
FFA.FOR subroutine ffa	r4tr r2tr r8tr ord1 ord2	-----	fft
FFT.FOR subroutine fft	ffa sfeats grid lftjus setup	wplot gatepl wave savbuf cls setpt bufill dsplay datime verlin keybd	mmi
FUNC.FOR subroutine func	update dismod	color dsplay beep	setmd

Table A-2.1 Continued

SOURCE FILE NAME	FORTRAN SUBROUTINES	OBJECT SUBROUTINES	CALLED FROM
FUTILS.FOR			
subroutine lftjus	move fill	-----	update parmen comstr fft
subroutine rtjus	fill	-----	parmen
subroutine move	-----	-----	lftjus
subroutine fill	-----	-----	lftjus rtjust
subroutine datime	-----	dattim	outwav
subroutine nonblk	-----	-----	parmen
GRID.FOR			
subroutine grid	-----	setpt	setup fft
INWAVE.FOR			
subroutine inwave	dismod update comstr	zerbuf display bufil2 beep	mmi
MMI.FOR			
subroutine mmi	update inwave outwave fft	and movit gatepl	setmd
ORD1.FOR			
subroutine ord1	-----	-----	ffa
ORD2.FOR			
subroutine ord2	-----	-----	ffa
OUTWAV.FOR			
subroutine outwav	comstr datime update	nonblk wave2 display beep	mmi

Table A-2.1 Continued

SOURCE FILE NAME	FORTRAN SUBROUTINES	OBJECT SUBROUTINES	CALLED FROM
PARMON.FOR subroutine parmen	lftjus putstr nonblk pwrite pread rtjust cometr	cls color display	setmd
PREAD.FOR subroutine pread	-----	-----	pcdas
PUTSTG.FOR subroutine putstr	-----	display cursor keybd	parmen
PWRITE.FOR subroutine pwrite	-----	-----	parmen
R2TR.FOR subroutine r2tr	-----	-----	ffa
R4TR.FOR subroutine r4tr	-----	-----	ffa
R8TR.FOR subroutine r8tr	-----	-----	ffa
SETMOD2.FOR subroutine setmd	func mmi dismod update parmen setup	wplot gatepl dsplay color cls	pcdas
SETUP.FOR subroutine setup	dismod grid update	cls display	pcdas setmd fft
SFEATS.FOR subroutine sfeats	-----	cursor	fft

Table A-2.1 Continued

SOURCE FILE NAME	FORTRAN SUBROUTINES	OBJECT SUBROUTINES	CALLED FROM
TITLE.FOR subroutine title	-----	cls dsplay keybd color	pcdas
UPDATE.FOR subroutine update	lftjus	dsplay cursor gatepl	setup setmd func mni inwave outwav

Table A-2.2 Function subroutines with no available source code

adcnew	gatepl
beep	keybd
bufil2	keyscr
bufill	plotnew2
cls	savbuf
color	setint
cursor	setpt
dsply	verlin
envel2	wave2
gate	zerbuf

Table A-2.3 Subroutines with available source codes and their respective tasks

COMSTR	is used for putting together the input and output file names by combining separate string information into a single string
DISMOD	displays the available keystroke options
FFA	performs a Fourier analysis on the gated portion of the waveform residing in the data buffer
FFT	displays the power spectrum
FUNC	sets or records parameters using the 10 function keys
FUTILS	contains five utilities for performing string manipulation; also contains a time/date utility
GRID	creates the waveform display grid
INWAVE	retrieves a saved waveform from disk and places it into the program's data buffer
MMI	determines which operation is required based on the system mode and keystroke input, and calls the appropriate block of code which performs that operation
ORD1	performs array reordering
ORD2	performs array reordering
OUTWAV	creates an output file containing the waveform currently residing in the program's data buffer and marked by the gate
PARMEN	displays the screen used for modifying system parameters and reading/writing a parameter file
PREAD	reads the parameter file residing on disk, thereby setting the default values for sampling rate, gate size, screen delay, and so on
PUTSTR	used for positioning and modifying string information on the parameter screen
PWRITE	write a parameter file to disk

Table A-2.3 Continued

R2TR	performs array processing
R4TR	performs array processing
R8TR	performs array processing
SETMD	sets the mode of the system based on a keyboard entry by the operator
SETUP	creates the screen display area for showing a waveform
TITLE	displays a screen showing the name of the program and the company who produces it
UPDATE	updates the waveform display area

APPENDIX III

PROBE HOLDER

A plexiglas block was constructed for holding the probes and aligning them with the pins to ensure consistent positioning and repeatability. *Figure 5.2* is a close-up of both probes mounted in the block. The block has round slots drilled into it for holding the probes, and each slot opens into a cylindrical channel which guides the pin up to the probe face. A metal bar spans the top of the block to hold the probes firmly in place. The probe seen on the left side of the block is the 2.48 MHz probe (Probe 1, shown in the figure with cable connected), while the probe seen on the right side of the block is the 3.87 MHz probe (Probe 2). As a matter of convenience, the block was designed to hold both probes at once. However, they were used one at a time for taking ultrasonic measurements. Once measurements had been taken with one probe, the microdot connecting cable was removed and placed on the other probe.

Figure A-3.1 shows the block as it appears when positioned on a fixation pin. The pin is shown inserted into a plastic pipe. Note that about one-half-inch of the pin extends into the block.

To ensure alignment of the fixation pin and the probe, the probe slot as well as the pin channel were drilled on a press, with the same side of the block facing up in both cases. The probe slot was cut with a one-half-inch mill bit

so that a flat-bottomed hole would be produced. The pin channel was drilled centrally in the probe slot with a standard 2.78 mm (0.1094 inch) twist drill bit. Drilling speeds were kept to a minimum (300-400 rpm) to avoid excessive frictional heating which melts the plexiglas. The 2.78 mm (0.1094 inch) pin channels had adequate radial clearance without reaming, while the probe slots were enlarged slightly to account for differences in the outer diameter of the probes. A fastener hole was drilled in the top of the block between the probe slots to provide firm anchorage for the metal bar.

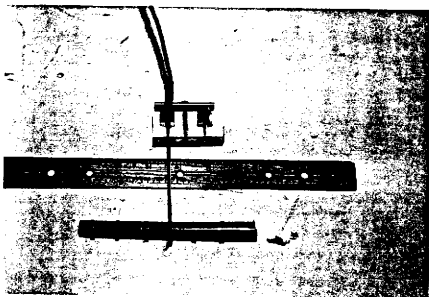


Figure A-3.1 Plexiglas probe holder placed onto a fixation pin inserted through a plastic pipe. 12 inch ruler indicates scale

APPENDIX IV
PROPERTIES AND MICROSTRUCTURE
OF 316L STAINLESS STEEL

Introduction

Stainless steels are used in many common applications which require a material to have excellent corrosion resistance and good mechanical properties over a wide range of temperatures⁴⁴. Corrosion resistance is achieved primarily through the addition of chromium to the iron-carbon system, while small amounts of other elements can be added to refine material properties. The addition of at least 12% chromium to steel results in the formation a film which is passive in the presence of oxidizing agents. This film subsequently protects the underlying material from further attack⁴⁵.

Alloying Elements

Stainless steels can be composed of as many as ten to fifteen individual elements with the range of corrosion resistance determined by the amounts of each element in the material. Chromium always is the essential alloying element, while several other commonly used elements are nickel, manganese, molybdenum, carbon, and nitrogen.

A brief review of the effect of each of these elements, summarized from Reference 46, is given in the following. Chromium in the amount of about 18% must be present to cause

a steel to become stainless. The passive film begins to form once about 10.5% chromium is present, but larger quantities must be used to provide corrosion resistance in aggressive environments. Amounts of chromium greater than 18% are usually avoided due to the possible detrimental effects on mechanical properties and manufacturability. Instead, additional corrosion resistance is achieved by adding small amounts of other elements. The addition of 10-20% nickel enhances the mechanical properties of stainless steel by stabilizing the austenitic grain structure and promoting repassivation in the event a break occurs in the protective film. Manganese is used in moderate quantities (about 2%) along with nickel and performs many of the same functions, but complete replacement of nickel with manganese is impractical. The addition of up to 6% molybdenum helps stabilize the passive film when chlorides are present in the environment in addition to providing increased resistance to pitting and crevice corrosion.

Small amounts of carbon (0.25% or less) are used in order to retain good mechanical properties at high temperatures and to allow for hardenability by heat treatment. Apart from these functions, carbon's presence has a negative effect on the corrosion resistance of the steel due to its tendency to form carbide precipitates in the grain boundaries. This results in a localized region where chromium is depleted below 12%, causing the steel to become

vulnerable to oxidation.

The addition of fractional amounts of nitrogen can improve resistance to pitting while increasing strength. Nitrogen also helps in controlling the amount and type of phases present in the microstructure. However, like carbon, its presence can have detrimental effects on mechanical properties and must be used in limited amounts, usually less than 0.40%.

Austenitic Stainless Steels

When about 10% nickel is added to the iron-chromium system, the austenitic structure is retained at all normal heat treatment temperatures and results in improved ductility and formability (recall that austenite is a solid solution of carbon in FCC iron). This family of stainless steels is known as the austenitic stainless steels, and they are essentially a ternary iron-chromium-nickel alloy. Small amounts of manganese, carbon, and nitrogen also contribute to the stabilization of the austenitic structure. Austenitic stainless steels hold a dominant position in domestic production due to their high corrosion resistance and manufacturability. They possess excellent properties at room temperature and at elevated temperatures and thus are suited to a wide range of applications. These stainless steels are considered to have the best overall corrosion resistance, particularly when in contact with industrial environments or

acids⁴⁵.

Since austenitic stainless steels maintain their austenitic structure at room temperature, they are not hardenable by heat treatment, although considerable strengthening can be accomplished with cold working. Machining is made more difficult by the fact that austenitic stainless steels are easily work hardened⁴⁷.

Austenitic stainless steels may become vulnerable to intergranular corrosion when chromium carbides form in the grain boundaries. This can occur with extended exposure to temperatures between 425°C and 870°C. Reheating the steel above 925°C and quenching will restore normal corrosion resistance. To minimize carbide precipitation, two low-carbon grades, 304L and 316L, have been developed. The carbon content in these steels does not exceed 0.03% and makes them suitable for welding operations where post-weld annealing is not possible⁴⁴.

Applications

Stainless steels possess excellent corrosion resistance characteristics, good mechanical properties, and an attractive surface finish. They find many uses ranging from architectural and structural applications to aggressive high temperature high stress environments, and cryogenic uses that require good low-temperature resistance to crack propagation. Some of the specific applications are cookware,

cutlery, appliances, chemical and food-processing equipment, storage tanks, cryogenic vessels, heat-treatment equipment, heat exchangers, combustion chambers, steam turbine and jet engine parts, ball bearings, valves parts, and surgical instruments⁴⁵.

In addition to widespread industrial application, stainless steel has become a popular choice in the medical profession for the manufacture of orthopedic implants, screws, plates, and wires. Stainless steel offers high strength, ductility, and good biocompatibility, all at an affordable cost to the practitioner.

Composition

Table A-4.1 shows the composition which is most commonly used in the production of an AISI grade of 316L stainless steel. Some flexibility of the classification system is seen by the manner in which several chemical elements are represented. In order to know the exact composition, mechanical properties and corrosion resistance of a stainless steel, a comprehensive volume should be consulted. The AISI designations provide a general guideline, but a specification such as those established by ASTM provides all pertinent information needed in the selection of a specific grade and composition of a stainless steel. The ASTM specs will give detailed information about the compositional limits in addition to manufacturing and

Table A-4.1 Composition of 316L stainless steel

Element	Percent by weight
Chromium	16.00-18.00
Nickel	10.00-14.00
Carbon	0.03 max
Molybdenum	2.00-3.00
Manganese	2.00
Phosphorus	0.045
Sulfur	0.03
Silicon	1.00
Iron	balance (62-69)

testing requirements⁴⁶.

Mechanical Properties

An annealed sample of 316L stainless steel at room temperature will have a yield stress of about 42 ksi. Ultimate strength is reached at roughly twice the yield stress, and elongation in a 2-inch specimen is 50%. The tensile properties compare well to those of annealed plain low-carbon steels, with stainless steel exhibiting superior ductility in all cases⁴⁵.

Microstructure Analysis Procedure

Using a diamond cutoff saw, three cuts were made on each pin. The flat end of the pin was removed and saved, then two additional cuts produced longitudinal (1 inch) and transverse ($\frac{1}{4}$ inch) sections. Each metallographic specimen was deburred with 240 grit sandpaper and placed in an ultrasonic cleaning device for 30 seconds. 1.25 inch phenolic resin (bakelite) mounts were utilized; each specimen was cured at 300°F and 4.2 ksi for 9 minutes and engraved with the corresponding pin ID number. An initial grind was performed to expose the inner core on the longitudinal mount. Afterwards sanding was performed with 240, 320, 400, and 600 grit wheels, followed by 5 μm diamond polishing and 0.05 μm aluminum oxide polishing. Specimens were subjected to about 5 pounds of pressure during each of

the 5 minute grinding steps.

An etchant containing 45 ml of HCl, 15 ml of NH_3 , and 20 ml of methanol was prepared. Each specimen was maintained in the etchant for 1 minute, followed by water rinsing and methanol drying. The specimens were then photographed under 400 \times magnification.

Photomicrographs revealed a hazy grain structure which was distinctly oriented in the direction of the longitudinal plane (Figure A-4.1). No evidence of large inhomogeneities or recrystallization of the grain structure was observed. However, the specimens had a tendency to produce dark splotches, so much so in the transverse cut that it was not photographed.

Hardness Testing

A Brale indenter under 150 kgf load was used to determine hardnesses of the pin sections. Mounted specimens were placed directly into the testing machine. The transverse section had only enough surface area to perform a single test, while longitudinal sections were tested repeatedly along the midline of the pin (Table 6.5).

Hardness data were compared to tabulated values for wrought 316L stainless steel⁴⁸. The maximum hardness of an annealed specimen of 316L is about 95 HRB. A value of 36 HRC (Table 6.5) corresponds to about 112 HRB, indicating a much higher hardness than 316L in the annealed condition. This is

supported by the observation of highly anisotropic grain structure. An annealed steel would have shown lower hardness and equiaxed grains.

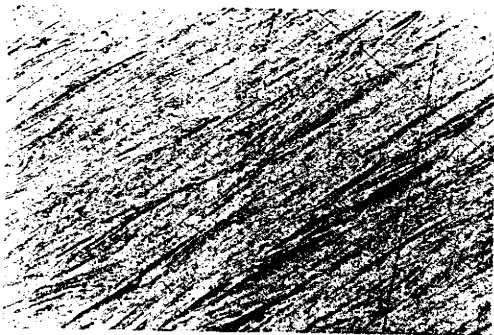


Figure A-4.1 Photomicrograph of Pin 2 at a magnification of 400 times. Grains run parallel to the long axis of the pin

APPENDIX V
DATA TABLES

Table A-5.1 Individual variables and paired ultrasonic data

Individual Variables

PIN	BONE	SITE	METH	DIAM	CUT1	CUT2	SFT1	SFT2	PCT1	PCT2	R ²	p>F	MSE
+	-	-	-	-	-	-	-	-	-	-	.0512	.3112	1298.9
-	+	-	-	-	-	-	-	-	-	-	.0924	.1691	1242.6
-	-	+	-	-	-	-	-	-	-	-	.1011	.1492	1230.6
-	-	-	+	-	-	-	-	-	-	-	.4509	.0006	751.8
-	-	-	-	+	-	-	-	-	-	-	.0118	.6299	1352.9
-	-	-	-	-	+	-	-	-	-	-	.5016	.0002	682.3
-	-	-	-	-	-	+	-	-	-	-	.5021	.0002	681.7
-	-	-	-	-	-	-	+	-	-	-	.3095	.0072	945.3
-	-	-	-	-	-	-	-	+	-	-	.7123	.0001	393.9
-	-	-	-	-	-	-	-	-	+	-	.4179	.0012	796.9
-	-	-	-	-	-	-	-	-	-	+	.7944	.0001	281.5

Paired Ultrasonic Data

PIN	BONE	SITE	METH	DIAM	CUT1	CUT2	SFT1	SFT2	PCT1	PCT2	R ²	p>F	MSE
-	-	-	-	-	+	+	-	-	-	-	.5412	.0006	661.2
-	-	-	-	-	-	-	+	+	-	-	.7135	.0001	412.8
-	-	-	-	-	-	-	-	-	+	+	.7964	.0001	293.4

Table A-5.2 Models containing no ultrasonic data

Two Factors

PIN	BONE	SITE	METH	DIAM	CUT1	CUT2	SFT1	SFT2	PCT1	PCT2	R ²	p>F	MSE
+	+	-	-	-	-	-	-	-	-	-	.1300	.2664	1253.8
+	-	+	-	-	-	-	-	-	-	-	.1075	.3393	1286.1
+	-	-	+	-	-	-	-	-	-	-	.5257	.0008	683.6
+	-	-	-	+	-	-	-	-	-	-	.0601	.5549	1354.5
-	+	+	-	-	-	-	-	-	-	-	.1935	.1296	1162.2
-	+	-	+	-	-	-	-	-	-	-	.4811	.0020	747.8
-	+	-	-	+	-	-	-	-	-	-	.2593	.0577	1067.4
-	-	+	+	-	-	-	-	-	-	-	.5784	.0003	607.6
-	-	+	-	+	-	-	-	-	-	-	.1101	.3632	1295.4
-	-	-	+	+	-	-	-	-	-	-	.5279	.0008	680.3

Table A-5.2 Continued

Three Factors

PIN	BONE	SITE	METH	DIAM	CUT1	CUT2	SFT1	SFT2	PCT1	PCT2	R ²	p>F	MSE
+	+	+	-	-	-	-	-	-	-	-	.2149	.2149	1194.2
+	+	-	+	-	-	-	-	-	-	-	.5810	.0011	637.4
+	+	-	-	+	-	-	-	-	-	-	.2740	.1158	1104.4
+	-	+	+	-	-	-	-	-	-	-	.5812	.0011	637.1
+	-	+	-	+	-	-	-	-	-	-	.1093	.5441	1355.0
+	-	-	+	+	-	-	-	-	-	-	.5955	.0008	615.3
-	+	+	+	-	-	-	-	-	-	-	.6151	.0005	585.5
-	+	+	-	+	-	-	-	-	-	-	.2812	.1069	1093.5
-	+	-	+	+	-	-	-	-	-	-	.5283	.0031	717.6
-	-	+	+	+	-	-	-	-	-	-	.6058	.0007	599.6

More Than Three Factors

PIN	BONE	SITE	METH	DIAM	CUT1	CUT2	SFT1	SFT2	PCT1	PCT2	R ²	p>F	MSE
+	+	+	+	-	-	-	-	-	-	-	.6152	.0019	619.9
+	+	+	-	+	-	-	-	-	-	-	.2815	.2043	1157.3
+	+	-	+	+	-	-	-	-	-	-	.6003	.0025	643.8
+	-	+	+	+	-	-	-	-	-	-	.6067	.0022	633.5
-	+	+	+	+	-	-	-	-	-	-	.6164	.0018	617.9
+	+	+	+	+	-	-	-	-	-	-	.6168	.0053	655.7

Table A-5.3 Paired ultrasonic data with one other factor

PIN	BONE	SITE	METH	DIAM	CUT1	CUT2	SFT1	SFT2	PCT1	PCT2	R ²	p>F	MSE
+	-	-	-	-	+	+	-	-	-	-	.7397	.0001	396.0
+	-	-	-	-	-	-	+	+	-	-	.8041	.0001	298.0
+	-	-	-	-	-	-	-	-	+	+	.7966	.0001	309.4
-	+	-	-	-	+	+	-	-	-	-	.5586	.0017	671.4
-	+	-	-	-	-	-	+	+	-	-	.7150	.0001	433.6
-	+	-	-	-	-	-	-	-	+	+	.7969	.0001	308.9
-	-	+	-	-	+	+	-	-	-	-	.7453	.0001	387.5
-	-	+	-	-	-	-	+	+	-	-	.7320	.0001	407.7
-	-	+	-	-	-	-	-	-	+	+	.8044	.0001	297.5
-	-	-	+	-	+	+	-	-	-	-	.5774	.0012	642.8
-	-	-	+	-	-	-	+	+	-	-	.7416	.0001	393.1
-	-	-	+	-	-	-	-	-	+	+	.7982	.0001	307.0
-	-	-	-	+	+	+	-	-	-	-	.5413	.0024	697.8
-	-	-	-	+	-	-	+	+	-	-	.7177	.0001	429.4
-	-	-	-	+	-	-	-	-	+	+	.8014	.0001	302.1

Table A-5.4 Paired ultrasonic data with two other factors

PIN	BONE	SITE	METH	DIAM	CUT1	CUT2	SFT1	SFT2	PCT1	PCT2	R ²	p>F	MSE
+	+	-	-	-	+	+	-	-	-	-	.7409	.0001	417.3
+	+	-	-	-	-	-	+	+	-	-	.8043	.0001	315.2
+	+	-	-	-	-	-	-	-	+	+	.7971	.0001	326.8
+	-	+	-	-	+	+	-	-	-	-	.7608	.0001	385.3
+	-	+	-	-	-	-	+	+	-	-	.8270	.0001	278.6
+	-	+	-	-	-	-	-	-	+	+	.8165	.0001	295.6
+	-	-	+	-	+	+	-	-	-	-	.7449	.0001	410.8
+	-	-	+	-	-	-	+	+	-	-	.8059	.0001	312.6
+	-	-	+	-	-	-	-	-	+	+	.7982	.0001	325.0
+	-	-	-	+	+	+	-	-	-	-	.7398	.0001	419.1
+	-	-	-	+	-	-	+	+	-	-	.8059	.0001	312.6
+	-	-	-	+	-	-	-	-	+	+	.8016	.0001	319.6
-	+	+	-	-	+	+	-	-	-	-	.7563	.0001	392.6
-	+	+	-	-	-	-	+	+	-	-	.7321	.0001	431.5
-	+	+	-	-	-	-	-	-	+	+	.8046	.0001	314.8
-	+	-	+	-	+	+	-	-	-	-	.5775	.0039	680.5
-	+	-	+	-	-	-	+	+	-	-	.7487	.0001	404.8
-	+	-	+	-	-	-	-	-	+	+	.7983	.0001	324.9

Table A-5.4 Continued

PIN	BONE	SITE	METH	DIAM	CUT1	CUT2	SFT1	SFT2	PCT1	PCT2	R ²	p>F	MSE
-	+	-	-	+	+	+	-	-	-	-	.5806	.0037	675.4
-	+	-	-	+	-	-	+	+	-	-	.7377	.0001	422.5
-	+	-	-	+	-	-	-	-	+	+	.8039	.0001	315.8
-	-	+	+	-	+	+	-	-	-	-	.7605	.0001	385.8
-	-	+	+	-	-	-	+	+	-	-	.7440	.0001	412.4
-	-	+	+	-	-	-	-	-	+	+	.8044	.0001	315.0
-	-	+	-	+	+	+	-	-	-	-	.7699	.0001	370.5
-	-	+	-	+	-	-	+	+	-	-	.7437	.0001	412.8
-	-	+	-	+	-	-	-	-	+	+	.8064	.0001	311.7
-	-	-	+	+	+	+	-	-	-	-	.5915	.0030	657.9
-	-	-	+	+	-	-	+	+	-	-	.7576	.0001	390.5
-	-	-	+	+	-	-	-	-	+	+	.8016	.0001	319.5

Table A-5.5 Paired ultrasonic data with three other factors

PIN	BONE	SITE	METH	DIAM	CUT1	CUT2	SFT1	SFT2	PCT1	PCT2	R ²	p>F	MSE
+	+	+	-	-	+	+	-	-	-	-	.7657	.0001	400.9
+	+	+	-	-	-	-	+	+	-	-	.8293	.0001	292.2
+	+	+	-	-	-	-	-	-	+	+	.8166	.0001	313.9
+	+	-	+	-	+	+	-	-	-	-	.7455	.0003	435.5
+	+	-	+	-	-	-	+	+	-	-	.8107	.0001	324.0
+	+	-	+	-	-	-	-	-	+	+	.7983	.0001	345.2
+	+	-	-	+	+	+	-	-	-	-	.7413	.0003	442.7
+	+	-	-	+	-	-	+	+	-	-	.8118	.0001	322.1
+	+	-	-	+	-	-	-	-	+	+	.8041	.0001	335.3
+	-	+	+	-	+	+	-	-	-	-	.7696	.0001	394.3
+	-	+	+	-	-	-	+	+	-	-	.8276	.0001	295.1
+	-	+	+	-	-	-	-	-	+	+	.8168	.0001	313.5
+	-	+	-	+	+	+	-	-	-	-	.7734	.0001	387.8
+	-	+	-	+	-	-	+	+	-	-	.8292	.0001	292.3
+	-	+	-	+	-	-	-	-	+	+	.8166	.0001	313.9
+	-	-	+	+	+	+	-	-	-	-	.7458	.0003	434.9
+	-	-	+	+	-	-	+	+	-	-	.8065	.0001	331.1
+	-	-	+	+	-	-	-	-	+	+	.8017	.0001	339.4

Table A-5.5 Continued

PIN	BONE	SITE	METH	DIAM	CUT1	CUT2	SFT1	SFT2	PCT1	PCT2	R ²	p>F	MSE
-	+	+	+	-	+	+	-	-	-	-	.7610	.0002	409.1
-	+	+	+	-	-	-	+	+	-	-	.7496	.0002	428.6
-	+	+	+	-	-	-	-	-	+	+	.8046	.0001	334.4
-	+	+	-	+	+	+	-	-	-	-	.7709	.0001	392.1
-	+	+	-	+	-	-	+	+	-	-	.7653	.0001	401.6
-	+	+	-	+	-	-	-	-	+	+	.8077	.0001	329.0
-	+	-	+	+	+	+	-	-	-	-	.5973	.0075	689.2
-	+	-	+	+	-	-	+	+	-	-	.7581	.0002	414.0
-	+	-	+	+	-	-	-	-	+	+	.8065	.0001	331.1
-	-	+	+	+	+	+	-	-	-	-	.7714	.0001	391.2
-	-	+	+	+	-	-	+	+	-	-	.7619	.0002	407.5
-	-	+	+	+	-	-	-	-	+	+	.8065	.0001	331.1

Table A-5.6 Paired ultrasonic data with more than three other factors

PIN	BONE	SITE	METH	DIAM	CUT1	CUT2	SPT1	SPT2	PCT1	PCT2	R ²	p>F	MSE
+	+	+	+	-	+	+	-	-	-	-	.7696	.0004	420.5
+	+	+	+	-	-	-	+	+	-	-	.8373	.0001	297.0
+	+	+	+	-	-	-	-	-	+	+	.8179	.0001	332.4
+	+	+	-	+	+	+	-	-	-	-	.7740	.0004	412.6
+	+	+	-	+	-	-	+	+	-	-	.8295	.0001	311.3
+	+	+	-	+	-	-	-	-	+	+	.8166	.0001	334.8
+	+	-	+	+	+	+	-	-	-	-	.7459	.0008	463.9
+	+	-	+	+	-	-	+	+	-	-	.8226	.0001	323.9
+	+	-	+	+	-	-	-	-	+	+	.8069	.0001	352.4
+	-	+	+	+	+	+	-	-	-	-	.7749	.0004	410.9
+	-	+	+	+	-	-	+	+	-	-	.8323	.0001	306.1
+	-	+	+	+	-	-	-	-	+	+	.8173	.0001	333.6
-	+	+	+	+	+	+	-	-	-	-	.7750	.0004	410.8
-	+	+	+	+	-	-	+	+	-	-	.7667	.0005	425.9
-	+	+	+	+	-	-	-	-	+	+	.8081	.0001	350.3
+	+	+	+	+	+	+	-	-	-	-	.7777	.0011	434.8
+	+	+	+	+	-	-	+	+	-	-	.8374	.0001	318.0
+	+	+	+	+	-	-	-	-	+	+	.8180	.0003	356.0

Table A-5.7 Baseline reference values

Pin/Probe	File #	Cutoff Point	Avg	S.D.	C.V. %
Pin 1 Probe 1	047	240	240.00	0.00	0.0
	048	240			
	050	240			
	055	240			
Pin 1 Probe 2	091	225	218.75	12.50	5.7
	094	225			
	095	225			
	097	200			
Pin 2 Probe 1	058	230	220.00	21.60	9.8
	061	240			
	063	190			
	064	220			
Pin 2 Probe 2	081	305	295.00	27.08	9.2
	082	315			
	084	305			
	085	255			
Pin 3 Probe 1	034	230	246.25	29.83	12.1
	036	290			
	038	225			
	041	240			
Pin 3 Probe 2	002	305	308.75	4.79	1.6
	003	305			
	005	315			
	006	310			
Pin 4 Probe 1	017	295	291.25	14.93	5.1
	019	295			
	021	305			
	027	270			
Pin 4 Probe 2	007	335	340.00	16.83	5.0
	008	330			
	015	330			
	016	365			

Table A-5.8 Summary data sheet

Force is given in newtons and diameter is given in centimeters

Bone #	Pin #	Impl. Site	Impl. Meth.	Extr. Force	Fem. Diam.	Avg. Diam.	Force DIAM.	Probe 1 Cutoff	Probe 1 Ref.	Probe 2 Cutoff
1	3	2	1	275.8	1.03 1.01	1.02	271.1	116.25	246.25	157.50
1	4	3	4	17.8	0.99 1.06	1.02	17.4	180.00	291.25	267.50
2	1	3	1	338.1	1.79 1.67	1.73	195.3	121.50	240.00	118.75
2	2	2	1	395.9	1.43 1.39	1.41	281.1	125.00	220.00	146.25
3	3	3	1	378.1	1.48 1.43	1.45	260.5	131.25	246.25	140.00
3	4	2	1	311.4	1.78 1.72	1.75	178.1	120.00	291.25	147.50
4	1	1	1	129.0	1.49 1.41	1.45	88.9	121.25	240.00	131.25
4	2	2	1	226.9	1.34 1.36	1.35	167.6	130.00	220.00	152.50
4	3	3	1	453.7	1.47 1.51	1.49	304.8	110.00	246.25	105.00
4	4	4	1	471.5	1.66 1.76	1.71	276.4	107.50	291.25	115.00
5	1	1	2	253.5	1.58 1.55	1.56	162.0	121.25	240.00	116.25
5	2	2	2	253.5	1.49 1.48	1.48	170.9	147.50	220.00	170.00
5	3	3	2	302.5	1.50 1.55	1.53	198.3	125.00	246.25	157.50
5	4	4	2	556.0	1.68 1.74	1.71	325.0	130.00	291.25	150.00
6	1	1	3	315.8	1.73 1.64	1.69	187.3	112.50	240.00	117.50
6	2	2	3	258.0	1.52 1.51	1.52	170.1	127.50	220.00	192.50
6	3	3	3	360.3	1.61 1.68	1.64	219.1	123.75	246.25	153.75
6	4	4	3	355.9	1.84 1.93	1.89	188.7	123.75	291.25	173.75
7	1	1	4	0.0	1.82 1.72	1.77	0.0	128.75	240.00	175.00
7	2	2	4	26.7	1.56 1.52	1.54	17.3	181.25	220.00	252.50
7	3	3	4	13.3	1.60 1.68	1.64	8.1	171.25	246.25	195.00
7	4	4	4	44.5	1.91 2.00	1.95	22.8	151.25	291.25	265.00

Table A-5.8 Continued, left to right

Probe 2 Ref.	Probe 1 Shift	Probe 2 Shift	Probe 1 %Shift	Probe 2 %Shift
308.75	130.00	151.25	0.528	0.490
340.00	111.25	72.50	0.382	0.213
218.75	118.50	100.00	0.494	0.457
295.00	95.00	148.75	0.432	0.504
308.75	115.00	168.75	0.467	0.547
340.00	171.25	192.50	0.588	0.566
218.75	118.75	87.50	0.495	0.400
295.00	90.00	142.50	0.409	0.483
308.75	136.25	203.75	0.553	0.660
340.00	183.75	225.00	0.631	0.662
218.75	118.75	102.50	0.495	0.469
295.00	72.50	125.00	0.330	0.424
308.75	121.25	151.25	0.492	0.490
340.00	161.25	190.00	0.554	0.559
218.75	127.50	101.25	0.531	0.463
295.00	92.50	102.50	0.420	0.347
308.75	122.50	155.00	0.497	0.502
340.00	167.50	166.25	0.575	0.489
218.75	111.25	43.75	0.464	0.200
295.00	38.75	42.50	0.176	0.144
308.75	75.00	113.75	0.305	0.368
340.00	140.00	75.00	0.481	0.221

VITA

Name: James Robert Dickens

Date of Birth: January 10, 1966

Place of Birth: Anaheim, California

Parents: Ferman Atlas Dickens

Doris Jo Coan Dickens

Sisters: Kristie Lynn Dickens Knoll

Kathy Lou Dickens Haines

Karol Lea Dickens Whitlow

Kimmie Lane Dickens Browning

Education: North Harris County College, Houston, TX

Associate of Arts, 1986

Engineering

Texas A&M University, College Station, TX

Bachelor of Science, 1990

Mechanical Engineering

Texas A&M University, College Station, TX

Master of Science, 1992

Mechanical Engineering

Current Address: 512 Imperial Valley Apt. B

Bryan, TX 77803